UiT
THE ARCTIC UNIVERSITY OF NORWAY

Faculty of Science and Technology

Department of Geology

Caledonian nappe emplacement: an example from Uløya, Northern Norway

—

Katrin Kraus

GEO-3900 Master's Thesis in Geology
June 2016

University of Tromsø
Faculty of Science and Technology
Department of Geology

Caledonian nappe emplacement: an example from Uløya, Northern Norway

Master thesis in Hard Rock Geology

Submitted by: Katrin Kraus

First supervisor: Prof. Holger Stünitz

Second supervisor: Carly Faber

Third supervisor: Prof. Jiří Konopásek

Tromsø, June 2016

Abstract

On Uløya, an island located east of the Lyngen peninsula in northern Troms, Norway, four Caledonian nappes are exposed. These are from bottom to top: part of the Kalak Nappe Complex (KNC), the Vaddas, the Kåfjord and the Nordmannvik nappe. In the present study the geology of these nappes is described, macroscopic and microscopic deformation structures are analyzed, and phase equilibrium modeling is presented to define Caledonian deformation and emplacement of the nappes.

A penetrative foliation dipping at an angle of 20-40° to the SW displays a pervasive stretching lineation plunging NW or SE. Nappe emplacement took place by thrusting to the SE as indicated by the dominant sense of shear observed in the field and in thin section. Thrusting was accompanied by strong shearing documented by the penetrative foliation and various mylonites. Two Caledonian fold generations were identified, a first generation of isoclinal to tight folds and a second generation of closed to open folds, which refold the first generation folds. Both generations have fold axes parallel to the Caledonian stretching lineation trending NW-SE, indicating a typical Caledonian orientation.

Metamorphic conditions estimated in the KNC, the Vaddas, the Kåfjord and the Nordmannvik nappe are in accordance with metamorphic conditions of a subduction and collision environment as reconstructed for the Caledonian orogeny. Parts of Baltica were subducted beneath Laurentia followed by collision of the two continents. The nappes show increasing metamorphic conditions (pressure and temperature) with the exception of the Vaddas nappe, which shows much higher pressures than the overlying Kåfjord and Nordmannvik nappes. A different subduction mechanism or out-of-sequence-thrusting may have been active to transport the Vaddas nappe to greater depth than the overlying nappes.

Gneisses of the KNC and the Nordmannvik nappe itself show migmatization which in the Nordmannvik nappe was overprinted by subsequent Caledonian solid-state shearing. P-T estimates of 8.8-9.8 kbar and 760-775°C from Gasser et al. (2015) for Neoproterozoic migmatization in meta-sedimentary rocks of the KNC are very similar to conditions of migmatization estimated for the Nordmannvik nappe in the present work (∼8.5-10 kbar and ∼750-780°C), possibly indicating a common previous tectonometamorphic history of the KNC and the Nordmannvik nappe. Caledonian solid state shearing occurred at higher pressures and lower temperatures than migmatization.

Contents

1. Introduction

Orogenic belts are an expression of large-scale plate movements and influence a number of processes on earth for example oceanic and atmospheric cycles. Complex tectonic forces lead to oceanic closure, subduction and collision of plates. One of these collisional mountain belts are the Caledonides, that are despite intensive research associated with many uncertainties. Numerous thrust sheets with diverse tectonic origins and a wide variety of metamorphic grades as well as discontinuous tectonic units are the reason for the complex geology of the Caledonides. These are also the reasons why the Caledonides are subject of a number of studies including the present one. In the following introduction, first the Caledonian orogeny is described then an overview of the Caledonian tectonic units in northern Norway is given. Subsequently the objectives of this work are pointed out and the local geology and Caledonian deformation structures in the study area are presented.

1.1. Caledonian Orogeny

The closure of the Iapetus Ocean and the oblique convergence of Baltica and Laurentia in the Early Paleozoic lead to the subduction of parts of the Baltica continent beneath the Laurentia continent during the collision and mountain building processes of the Caledonides. Today these mountains are found on both sides of the North Atlantic Ocean, in Greenland, Svalbard, Scandinavia and Great Britain as the consequence of the opening of the Atlantic in the Mesozoic.

The Caledonides are the result of the amalgamation of rock units from various tectonic settings (Corfu et al., 2014b). Slivers of both continental and oceanic crust occur. There is evidence of thrust tectonics, syn-collisional metamorphism and magmatism as well as post-collisional uplift and extension (Corfu et al., 2014b).

The Scandinavian Caledonides extend along the whole coast of Norway from the southern tip to the Barents Sea in the north, forming part of a mountain range ∼1500 km long. Below the Caledonides, exposed to the east, basement rocks of Archaen to Neoproterozoic age of the Fennoscandian shield are present (Gee and Sturt, 1985). The (par)autochthonous basement is variably influenced by the Caledonian deformation, metamorphism and thrusting (Gee, 1978). It is unconformably overlain by a thin cover of

Neoproterozoic to Early Palaeozoic autochthonous sedimentary rocks (Roberts and Gee, 1985). These rocks are in turn overlain by a variety of allochthonous tectonic units separated into Lower, Middle, Upper and Uppermost Allochthon (see fig. 1.1; Roberts and Gee, 1985).

The Lower Allochthon comprises low-grade Neoproterozoic and Early Palaeozoic sedimentary rocks while the Middle Allochthon is composed of both pre-Caledonian Fennoscandian basement and unconformably overlying Late Neoproterozoic shelf and continental rise successions (Stephens and Gee, 1985; Andresen and Steltenpohl, 1994). Many thrust sheets of the Middle Allochthon are intruded by pre-orogenic rift-related mafic dyke swarms (Stephens and Gee, 1985). Both the Lower and Middle Allochthon are interpreted to originate from the Baltoscandian margin (Gayer and Roberts, 1973). The Upper Allochthon composes of metamorphic rocks (the Seve nappe complex) representing the Baltica-Iapetus continent-ocean transition (Stephens and Gee, 1985) as well as ophiolites and island arc terranes (the Køli nappe complex) representing the Iapetus ocean (Andresen and Steltenpohl, 1994). Structurally higher tectonic units within the Upper Allochthon are interpreted to originate from the peri-Laurentian margin (e.g., Bergström, 1979). The Uppermost Allochthon was formed in a continental margin setting (Roberts and Gee, 1985; Stephens and Gee, 1989; Roberts et al., 2007) at the Laurentia continent. However, assignment of rocks to the different allochthons has been difficult and is still under discussion, therefore the Caledonian nappes described in chapter 1.2 Regional Geology are not assigned to the different allochthons. Major thrusts, extensional faults, or strike-slip faults separate the allochthonous units (Corfu et al., 2014a). Younger Palaeozoic to Cenozoic sedimentary rocks deposited before and during the opening of the North Atlantic Ocean cover the Caledonides in the north and the west (Corfu et al., 2014a).

The traditional view dividing the Caledonian orogeny into a Finnmarkian (540-490 Ma) and a Scandian (425-400 Ma) event has been challenged by recent research (e.g., Kirkland et al., 2006b; Corfu et al., 2007). The main collision event where Baltica and Laurentia collided obliquely forming the Scandinavian Caledonides in Early Paleozoic time remains undisputed although age dates vary along strike of the orogen. A westward directed subduction of Baltica beneath Laurentia is generally accepted (e.g., Gee, 1975; Andresen and Steltenpohl, 1994), but recent research argues for a subduction-switch in the final stages of the Iapetus closure towards eastward directed subduction (e.g., Andréasson et al., 2003). Both subduction and exhumation occurred at very fast rates demonstrated by monazite geochronology of (ultra-)high-pressure rocks from the Western Gneiss Region (Terry et al., 2000). After the collision of Baltica and Laurentia late-stage extensional deformation, partly due to the gravitational collapse of the orogen, followed (Gee, 1978).

The overall large-scale structure of the Scandinavian Caledonides is dominated by east-

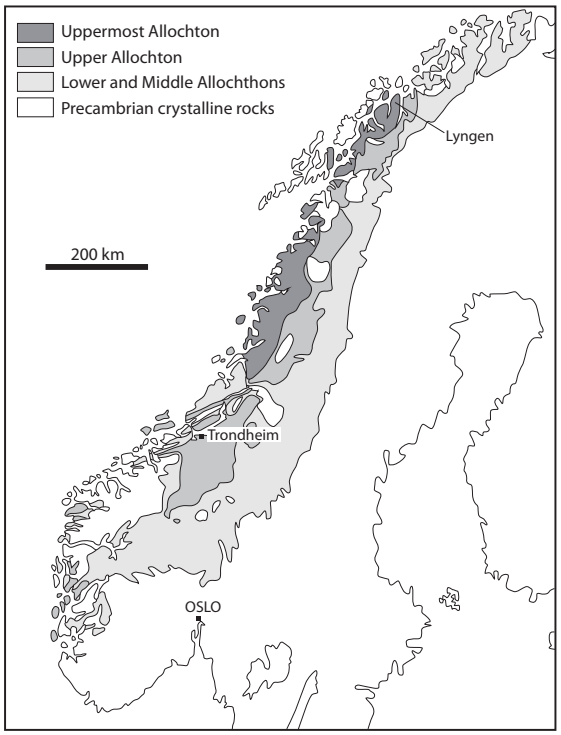

Fig. 1.1.: Simplified tectonostratigraphical subdivisions of the Scandinavian Caledonides after Roberts (2003).

to southeastward emplacement of thrust nappes which is overprinted by west- to northwestward extensional faulting. Large-scale open folding and bending also affected the basement (Corfu et al., 2014a). Along and across the strike of the orogen large variabilities of major tectonic units are observed, such as discontinuities or pinch and swell structures (Gee, 1978). Especially higher in the nappe stack geological units are restricted to local parts of the orogen. Reasons for this variability in the structure of the Caledonides are probably originally discontinuous units with variable initial thicknesses modified during nappe emplacement by thinning or disruption (Corfu et al., 2014a). Furthermore some units contain older (pre-Caledonian) tectonic elements, which complicate the tectonostratigraphy.

1.2. Regional Geology

The northern region of the Scandinavian Caledonides is divided into the following main tectonic units: a wide autochthonous to parautochthonous Neoproterozoic to Palaeozoic sedimentary cover, lying on Archaean to Palaeoproterozoic basement, allochthonous Mesoproterozoic to Early Palaeozoic meta-sedimentary and igneous rocks of the Kalak Nappe Complex (KNC), allochthonous Ordovician-Silurian meta-sedimentary and meta-plutonic

rocks (Corfu et al. (2014a); see fig. 1.2). The autochthonous to parautochthonous sedimentary cover on top of the basement consists of fluvial and shallow marine sediments as well as glacial deposits forming the Tanafjord-Varangerfjord succession (Siedlecka et al., 2004; Nystuen et al., 2008). Overlying these sediments the Geissa nappe as a fold-and-thrust belt composed of similar sediments is found (Rice, 2014). The Laksefjord nappe complex has a base of thin crystalline basement slivers overlain by a thick sequence of clastic sedimentary rocks (Roberts and Gromet, 2009).

The structurally lowest allochthon exposed in the area is the Kalak Nappe Complex as seen in a schematic transect across strike of the Caledonides from Tromsø to Skibotn (see fig. 1.3). The KNC is composed of a number of thrust sheets formed mainly by clastic sedimentary rocks, a small amount of para- and orthogneisses and minor limestones deposited on orthogneiss basement slivers (Gayer et al., 1985; Ramsay et al., 1985). Three meta-sedimentary sequences can be distinguished: the Sværholt succession, the Sørøy succession and the Åfjord pelites and Falkenes limestones (Kirkland et al., 2007a; Slagstad et al., 2006). The Sværholt succession as the oldest sedimentary sequence was deposited at 1073-980 Ma (Kirkland et al., 2007a). Both the Sværholt and Sørøy successions were intruded by a variety of mafic to felsic plutons including the Seiland igneous province with the main event at 570-560 Ma (e.g. Pedersen et al., 1989; Kirkland et al., 2006b; Corfu et al., 2011). The various para- and orthogneisses of older ages in the KNC include the Eidvågeid paragneiss and the Fagervik complex (Corfu et al., 2007; Kirkland et al., 2008b). However, a number of local rock units in the Kalak nappe complex are not reliably assigned to specific formations due to unknown age and origin. It was believed that the KNC derived from the Baltoscandian margin (Ramsay et al., 1985) while recent researchers argue for a Laurentain origin (e.g. Kirkland et al., 2008b). Furthermore the KNC is thought to be the northern equivalent of the Seve Nappe Complex further south in the Caledonides (Lindahl et al., 2005).

Overlying KNC meta-sedimentary rocks of mainly Silurian age are found which are exposed on Magerøy, Hjelmsøy, Porsangerhalvøya and Sørøy as well as east of the Lyngenfjord (Corfu et al., 2014a). Rocks of the latter location are divided into at least three nappes, the Kåfjord, the Vaddas, and the Nordmannvik nappe showing increasing metamorphic grade from the base to the top (Zwaan and Roberts, 1978). The origin and age of these nappes is largely unknown.

According to Lindahl et al. (2005) the Vaddas nappe is divided into two units where the lower unit is formed by a sedimentary and magmatic sequence which is unconformably overlain by the upper unit, a sedimentary succession of Late Ordovician to Silurian age. A conglomerate horizon eroding the underlying unit represents the unconformity between both sequences (Lindahl et al., 2005). The lower unit was interpreted to resemble the

Kalak Nappe Complex while the upper is associated with the Køli Nappe Complex which is located further south in the Caledonides (see fig. 1.2; Ramsay et al., 1985; Lindahl et al., 2005). The Vaddas nappe is thought to have undergone one metamorphic event which generally reached low amphibolite facies conditions (Andersen, 1988) although this is poorly constrained. Granite intrusions at the base of the Vaddas show an U-Pb age of 602±5 Ma which might prove a distinct origin for this unit as the age is significantly older than Silurian, and similar ages have not been recorded in the KNC (Corfu et al., 2007).

The lower part of the Kåfjord nappe is formed by marbles, meta-psammites and garnet mica schists while the upper part is formed by gneisses containing amphibolite layers and and granite bodies (Andersen, 1988). Like the upper unit of the Vaddas nappe the overlying Kåfjord nappe is considered equivalent to the Køli Nappe Complex (Lindahl et al., 2005; Augland et al., 2013). High strain deformation seen as mylonitization and the development of internal thrusts mark the Kåfjord nappe (Andersen, 1988). The metamorphic grade with middle to upper amphibolite facies in the Kåfjord nappe is thought to be slightly higher than in the Vaddas (Andersen, 1988).

A mylonitic high-strain zone forms the boundary between the Kåfjord and the Nordmannvik nappe (Augland et al., 2013). The Nordmannvik nappe is manly composed of mylonitic micaceous gneisses containing garnet amphibolite, marble, dolomitic marble, calc-silicate and ultramafic lenses (Bergh and Andresen, 1985). The general metamorphic grade in the Nordmannvik nappe is amphibolite- to granulite-facies (Andresen and Bergh, 1985; Bergh and Andresen, 1985).

Overlying these nappes the Lyngsfjellet nappe is found, consisting of two distinct units, the Lyngen Magmatic Complex, a large ophiolitic complex, which is unconformably overlain by the Balsfjord group, a sedimentary sequence of Late Ordovician to Early Silurian age (Binns and Matthews, 1981; Minsaas and Sturt, 1985). Both units show lower to middle greenschist facies metamorphism, which increases towards the overlying Nakkedal nappe (Coker-Dewey et al., 2000). Therefore the Nordmannvik and Lyngsfjellet nappe boundary forms probably an out-of-sequence-thrust.

The Nakkedal nappe is composed of three main elements, a quartzo-feldspathic paragneisses of unknown depositional and metamorphic age, granitoid intrusions of unknown crystallization age, and the Skattøra Migmatite Complex (Augland et al., 2013). Eclogite-facies rocks of the Tromsø nappe, which overlies the Nakkedal nappe, underwent three deformational-metamorphic events (Krogh et al., 1990) and constitute the uppermost allochthon in the region.

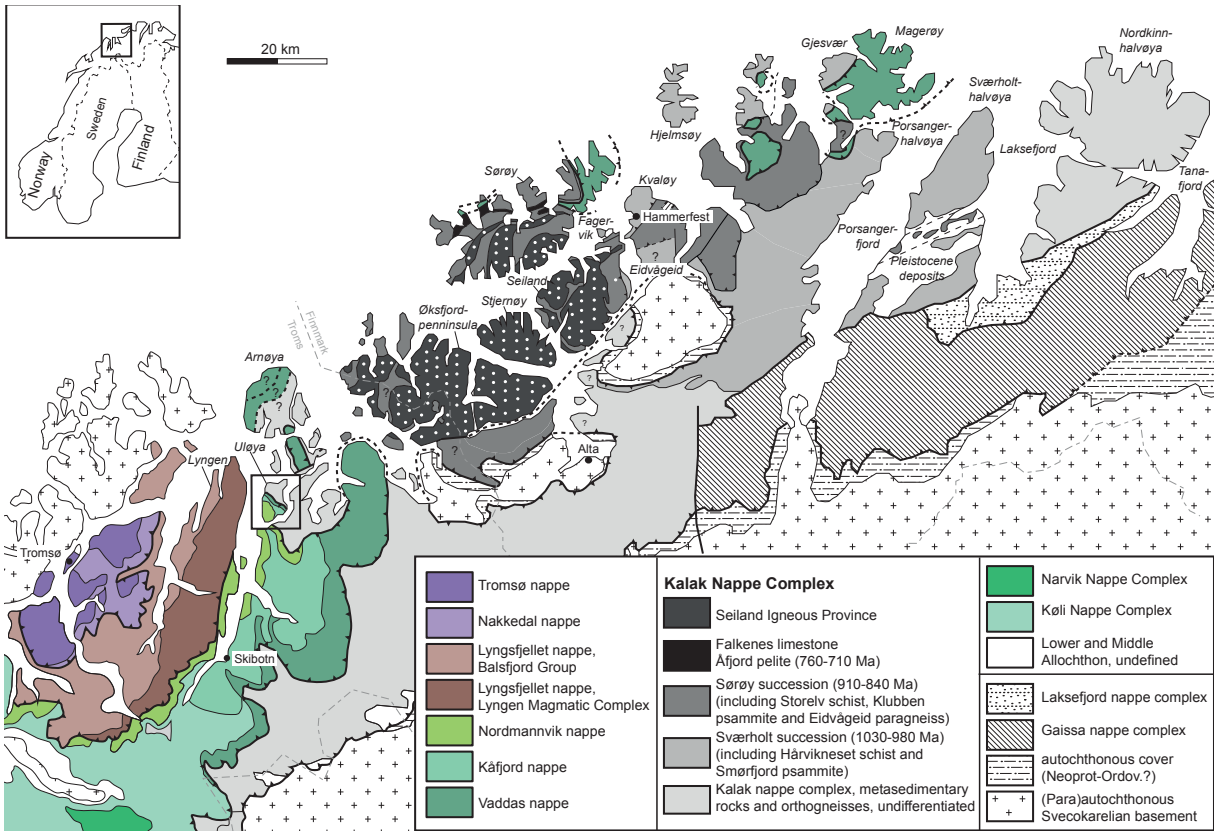

Fig. 1.2.: Tectonostratigraphic map of the Scandinavian Caledonides in northern Norway after Augland et al. (2013) and Gasser (2013). The box marks the study area of the present work.

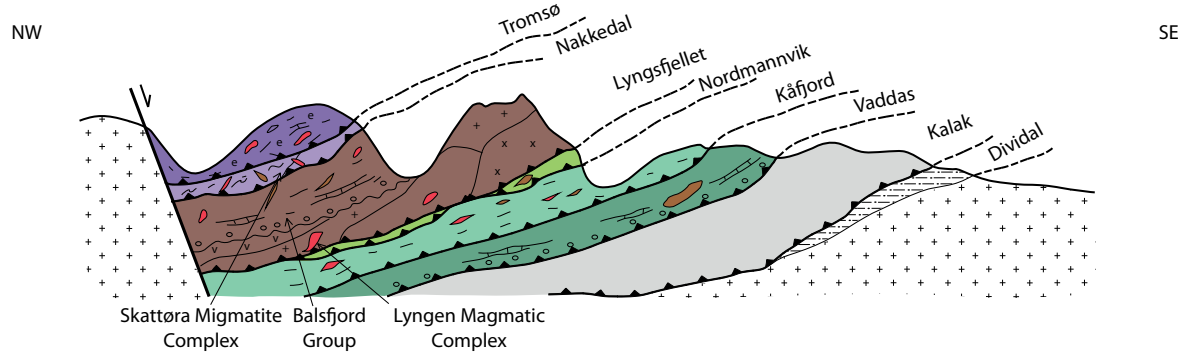

Fig. 1.3.: Schematic cross section of the Caledonian nappe stack along the Tromsø-Skibotn transect after Augland et al. (2013) showing the tectonostratigraphy.

1.3. Objective of this work

The present work focuses on structural analysis from both fieldwork and microscopy as well as on P-T estimates from phase equilibrium modeling of the Caledonian nappes exposed on Uløya, an island in Troms in northern Norway. The island was chosen for investigation because four nappes the KNC, the Vaddas nappe, the Kåfjord nappe and the Nordmannvik nappe are well exposed in a relatively small area where both the nappes themselves and the nappe contacts can be studied in detail. Although a lot of research has been published about the KNC there are still a number of uncertainties concerning the KNC, several local rock units have not been assigned to specific formations and the origin of the KNC still under discussion (e.g. Ramsay et al., 1985; Kirkland et al., 2008a). However only limited research has been conducted on the Vaddas, Kåfjord and Nordmannvik nappes. The base of the Vaddas nappe is considered to resemble the KNC while the top of the Vaddas nappe together with the Kåfjord nappe is assumed equivalent to the Køli Nappe Complex located further south in the Caledonides. Very little is known about the Nordmannvik nappe mostly due to its unique high temperature deformation and the lack of comparable tectonic units in the Caledonides in northern Norway. For all nappes P-T estimates of the metamorphic conditions are missing. Therefore petrological descriptions of the nappes as well as descriptions of Caledonian deformation structures and estimates of the metamorphic conditions are presented and discussed in the present work. The objective is to characterize the Caledonian nappe emplacement on the island Uløya and thereby contribute to a better understanding of the position of KNC, the Vaddas, Kåfjord and Nordmannvik nappe in the Caledonian framework.

1.4. Geology of the nappes exposed on Uløya

The study area consists of the island Uløya and is situated just east of the Lyngen peninsula in the northern Scandinavian Caledonides (see fig. 1.2). On the island, four Caledonian nappes are exposed: part of the KNC as well as the Vaddas, the Kåfjord and the Nordmannvik nappe. In the following the geological units of all four nappes as described on the 1:250 000 map sheet Nordreisa from the Norwegian Geological Survey (NGU - Norges Geologiske Undersøkelse) are introduced as the most suitable description for the area (Zwaan, 1988).

The thrust sheets of the KNC are composed mostly of metamorphosed arkoses and basement rocks. The basement rocks are comprised of Archean to Early Proterozoic granitic to granodioritic gneisses, amphibolitic gneisses, and intrusive rocks with mafic to ultra mafic composition. Furthermore, the basement consists of Early Proterozoic greenschists, several types of mica schists, limestones, dolomites and meta-sandstones.

The upper nappes of the KNC are penetrated by mafic intrusives and dikes which have produced contact metamorphism.

Meta-sedimentary and meta-volcanic rocks of the Vaddas nappe overlie the KNC. The lower base of the Vaddas nappe is formed by 200-300 m thin layers of alternating limestone, sandstone, graphitic schists, conglomerates and meta-basalts which form a shallow marine sequence. The upper part of the nappe is formed by a more than 2000 m thick sequence of meta-graywackes which is variably present along strike of the orogen. Typical for the Vaddas nappe are interlayered light gray-green meta-sandstones and blue-violet garnet mica schists. Some sediments show graded bedding, typical for turbidite deposits. The rocks are intruded by mafic, partially olivine rich and partially layered intrusive rocks.

The lower boundary of the Kåfjord nappe is formed by 400 m thick mylonites. Within the mylonites layers of marble and hornblende-schist, interpreted as metamorphosed basalt, occur. Above the mylonites 2000 m thick deposits of garnet mica schists are found showing increasing quartz content and migmatization upwards. These schists are intruded by granite and pegmatite dikes. Amphibolite occurs in the form of layers and lenses.

The Nordmannvik nappe consists mainly of migmatized garnet mica schists interlayered with 40 m thick marble and dolomite layers. In association with the carbonate rocks, lenses of sagvandit, an ultramafic and metasomatic rock, occur. The rocks do not form a sedimentary sequence but instead are interpreted to be assembled by continuous shear movement during high-grade metamorphism. Along the lower boundary of the Nordmannvik nappe, the mica schist has a mylonitic structure. The upper boundary to the Lyngsfjellet nappe is marked by cataclastic deformation of the mylonitic rocks of the Nordmannvik nappe and by a greenschist metamorphic overprint.

1.4.1. Caledonian Deformation

Numerous Caledonian deformation events have been described by various authors. The most comprehensive deformational description in the framework of the present project was compiled by Zwaan and Roberts (1978). They described a multiphase Caledonian deformation with up to six folding events affected the KNC and the overlying Vaddas, Kåfjord and Nordmannvik nappe in northern Norway. Not all stages of deformation are locally preserved, often only three folding events are observed. Due to subsequent overprinting of the first low-grade D_1 deformation event the structures of this event are not well known. It is associated with an axial planar schistosity to non-cylindrical folds in the Hammerfest area in northwestern Finnmark and large-scale isoclinal folds on western Sørøy. These structures have been affected by a late D_1-flattening event (Zwaan and Roberts, 1978). Lower in the nappe stack towards southeastern Finnmark, in the Nordreisa area, evidence

of the D_1-event is very rare. Here regional homogeneous strong flattening was probably predominant.

A second high-grade amphibolite facies D_2 deformation event overprinted the first event. Syn-kinematic kyanite and sillimanite of this second event is found in the highest nappes in northern Norway. The lower nappes show middle and even lower greenschist-facies metamorphism indicating an increase in metamorphic grade from the base to the top of the nappe stack. The D_2 phase is marked by tight to isoclinal asymmetrical folds at all scales with long upper limbs and restricted hinge zones. These folds are widely preserved especially in the Nordreisa and Tromsø area where they are associated with a well-developed stretching lineation in NW-SE direction. The predominant regional S_2 schistosity which developed parallel to the axial surfaces of the described folds can be traced throughout the whole of northern Norway. Similar to the first deformation event the late-stage D_2 event was dominated by near-vertical flattening (Zwaan and Roberts, 1978). In general a dominant N-S trend of D_2 fold hinges is preserved but in some areas the fold hinges were rotated. In the Nordreisa area the NW-SE trending fold hinges become gradually dominant parallel to the regional stretching lineation. Rotation of the fold hinges in the area of the uppermost nappe of the KNC as well as the Vaddas and the Kåfjord nappe led to the development of structural and metamorphic discordances and produced mylonites along the nappe boundaries. The rotation to the predominant NW-SE orientation was probably related to high internal strains reached during the D_2 deformation in the KNC and the overlying nappes. Vergence of the NW-SE rotated D_2 folds is consistently to the northeast. In the north-eastern area around Laksefjord the D_2 event was less intense. There close to tight N-S trending folds and a penetrative NW-SE lineation restricted to zones close to major thrusts are observed. High strains in the Nordreisa area in the lower part of the complex produced a mylonitic S_2 schistosity while in the N-S trend dominated nappes an equigranular texture with a penetrative axial planar foliation limited to fold hinges is prevailing.

The major structural and metamorphic discordances in the allochthones in northern Norway probably relate to the D_2 deformation event. This includes the main thrusting of the KNC in the late stages of D_2. During the D_2 event but possibly also during the earlier D_1 event slices of basement with or without supracrustal cover were reworked into the deforming basement cover leading to strong mylonitization, sometimes with mylonitic character.

Younger deformation structures in the KNC and the above Vaddas, Kåfjord and Nordmannvik nappe are mainly brittle which does not include initial crenulations and local folding of minor tectonic phases associated with the main thrust zones. A third related D_3 folding event is formed by open, upright to moderately flat folds that variably devel-

oped a crenulation cleavage. Megaimbrication structures and minor thrusts in the highest parts of nappe stack comprising the Vaddas, Kåfjord and Nordmannvik nappe are parallel to the basal thrust of the Lyngsfjellet nappe indicating that the D_3 deformation event is related to thrusting of the Lyngsfjellet nappe during Silurian. The gradual westward thinning of the KNC and the overlying nappes towards the Lyngen thrust supports this relation.

2. Methodology

Uløya was mapped during fieldwork on the basis of the existing geological map from the NGU (Zwaan, 1988). Oriented rock samples of the different lithologies were taken in the field as well as measurements of structural elements like foliation, lineation and folds. A geological compass by FPM Freiberg, Germany, was used to measure the orientation of these structural elements. Further deformation structures observed in the field, for example shear zones, shear sense indicators and indications for migmatitization were noted and documented in pictures. GPS coordinates were taken for all observations with the app GPS Tour © 2012 version 1.2 by AppicDesign. For the lithological descriptions the grain sizes were defined as fine-grained with a grain size of smaller than 0.75 mm, as medium-grained for a grain size of 0.75 to 1 mm, and coarse-grained for grain sizes of 1 to 2 mm.

Representative samples for all nappes and the nappe boundaries were selected to make polished thin section for analysis of mineralogy and microstructures. The thin sections are oriented parallel to the stretching lineation and normal to the foliation. A polarized light microscope LaborLux 11Pol S manufactured by Leitz, Germany, was used for microscopy. Grain sizes are given as the short and the long axes which were determined as the average of ten grains. Volume percent of the minerals were estimated in thin section. Structural measurements taken in the field were plotted and edited with the program Stereoplot © 2011-2016 version 9.5.1 by Richard W. Allmendinger. Abbreviations for rock-forming minerals were used after Whitney and Evans (2010).

Based on the mineralogy five samples UL230, UL234a, UL237, UL248 and UL250 were selected for phase equilibrium modeling to estimate P-T conditions of the four nappes exposed on Uløya. Microprobe analyses of these samples were performed with the Jeol JXA 8900R microprobe at the Department of Geology at the Christian-Albrechts-University in Kiel, Germany. The analyses were done in WDS mode and matrix corrections were carried out according to the CITZAF procedure version 3.5 after Paul Carpenter 1993, implemented in the Joel software. The measurements were conducted with an accelerating voltage of 15 kV, a beam current of 15 nA and a counting time of 15 seconds on the peak as well as 7 seconds on the background. Garnet, biotite and muscovite were measured with a fully focused beam of 1 μm diameter while feldspar was measured with

a 5 μm beam diameter. For garnet maps the area was divided into a grid of measuring points on which counting rates were generated to get relative element concentrations.

X-ray fluorescence analysis to get the bulk rock chemical composition of the same samples was conducted with the Panalytical Axios XRF spectrometer in Cape Town, South Africa. Analyses for eleven major elements (Fe, Mn, Ti, Ca, K, S, P, Si, Al, Mg, and Na) were done using fused disks prepared with lithium borate flux. Loss on ignition (LOI) was determined from weight loss of the samples after 1.5 h ignition at 1050°C. P-T estimates were calculated with the program PerpleX version 6.6.8 by Connolly (2005) last updated 2013 using the following solution models: biotite (Tajčmanová et al., 2009), chlorite, chloritoid, cordierite, garnet, staurolite, ilmenite (Holland and Powell, 1998), melt (Holland and Powell, 2001), ternary feldspar (Fuhrman and Lindsley, 1988) and mica (Coggon and Holland, 2002).

3. Results

In the following chapter the results of this work are presented. First of all the geological map of Uløya and a cross section are introduced. Then the rocks forming the individual nappes are described as observed during fieldwork as well as large-scale deformation structures. Afterwards structural data is presented in the form of stereographic projections. Petrographic descriptions of the individual nappes including micro-structural observations follow. Subsequently the mineral chemistry of the five samples selected for phase equilibrium modeling is presented as well as the results of said modeling.

3.1. Geological map

Mapping was done on the basis of the geological map 1:250 000 map sheet Nordreisa compiled by the NGU (Zwaan, 1988). The geological boundaries were modified according to mapping during fieldwork but in general the previous lithological boundaries and descriptions agree with field observations (see fig. 3.1 and 3.2). The exposed nappes on Uløya from the base to the top are the KNC, the Vaddas nappe, the Kåfjord nappe and the Nordmannvik nappe (see also fig. 3.3). The geological units strike NW-SE and dip relatively shallow towards the SW. The boundaries between the units run in the same orientation as the geological units themselves. An undefined fault runs across the northwestern tip of Uløya in NE-SW orientation leading to a repetition of the Vaddas nappe in northwest of Uløya.

The KNC makes up the largest part of Uløya, constituting the whole northern part of the island. Its top occurs as a NW-SE-trending nappe boundary, approximately across the middle of the island, with the Vaddas nappe in the southwest. The main lithologies of the KNC that were distinguished in the field are meta-arkoses containing layers of garnet mica-schists and hornblende/amphibolite-schists, hornblende-schists/amphibolites and various gneisses of unknown origin. Mafic bodies, layers or lenses are found in all units.

The Vaddas nappe forms a narrow nappe sandwiched between the KNC and the Kåfjord nappe exposed across the middle of the island in NW-SE direction. The thickness of the Vaddas nappe here is much lower than in surrounding areas (e.g. Kåfjord) and a wide va-

riety of rocks is found in a limited area with a steep topography. The units mapped by the NGU were partially merged in the present work because of the variety of rocks in a limited area, the discontinuity of the units as well as the low thickness. The lower boundary of the Vaddas nappe is marked by a distinct mylonized gneiss that displays some migmatization in places. Above that follow meta-arkoses, meta-conglomerates, greenschists, calc-silikates, amphibolites interlayered with garnet mica schists, a distinct marble horizon across the whole island containing amphibolite as well as quartzitic garnet mica schists and zoisite mica schists which form the upper part of the Vaddas nappe. In the northeast of the island, north of the undefined fault, the Vaddas nappe is exposed again showing a similar succession of geological units. In addition prophyroclasitc rocks and meta-basalt were observed. Amphibolite layers and bodies are again found in all units.

The lower boundary of the Kåfjord nappe occurs as a mylonite. The Kåfjord nappe, in contrast to the Vaddas nappe comprises of mostly of one lithology, mica schists that are variably rich in quartz and contains in places garnet, zoisite and sillimanite. The schists are locally interlayered with amphibolites/hornblende-schists. Layers of rust-colored schists/rust-colored quartzites were locally observed along the coast and were mapped by the NGU higher up in the nappe in steep terrain that was not accessed during fieldwork for the present study.

The boundary of the Kåfjord nappe and the Nordmannvik nappe is marked by a distinct change in lithology to a mylonized quartz-rich garnet mica schist that displays migmatization in places. The Nordmannvik nappe composes the whole southwestern tip of the island. Layers and lenses of calc-spar and dolomite marble are found within the migmatized mica schist especially in the lower part of the nappe. Layers and lenses of amphibolite are occasionally observed.

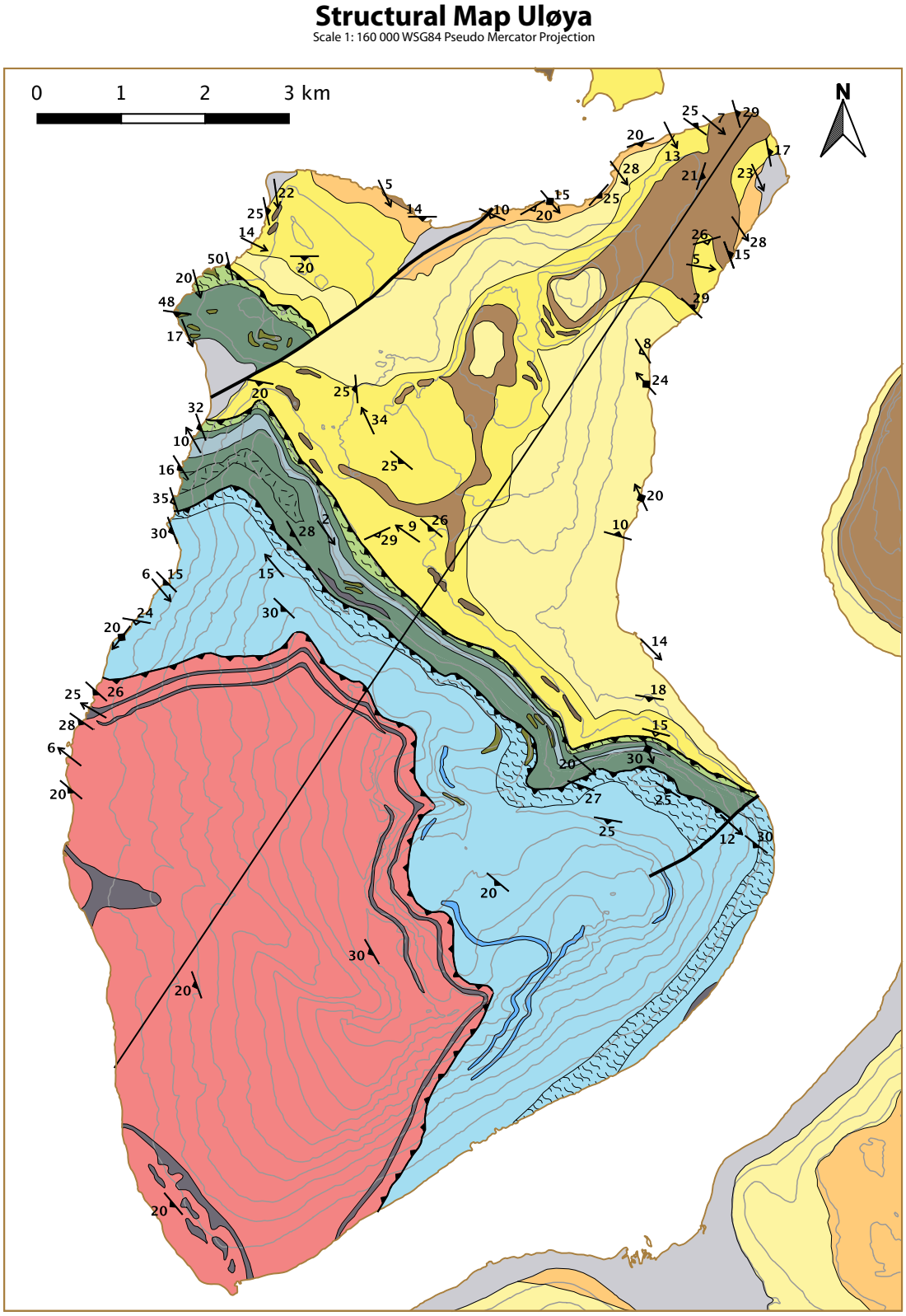

Fig. 3.1.: Geological map on the basis of the 1:50 000 map map sheet Nordreisa from the NGU (Zwaan, 1988). Modifications of the geological boundaries have been made according to fieldwork.

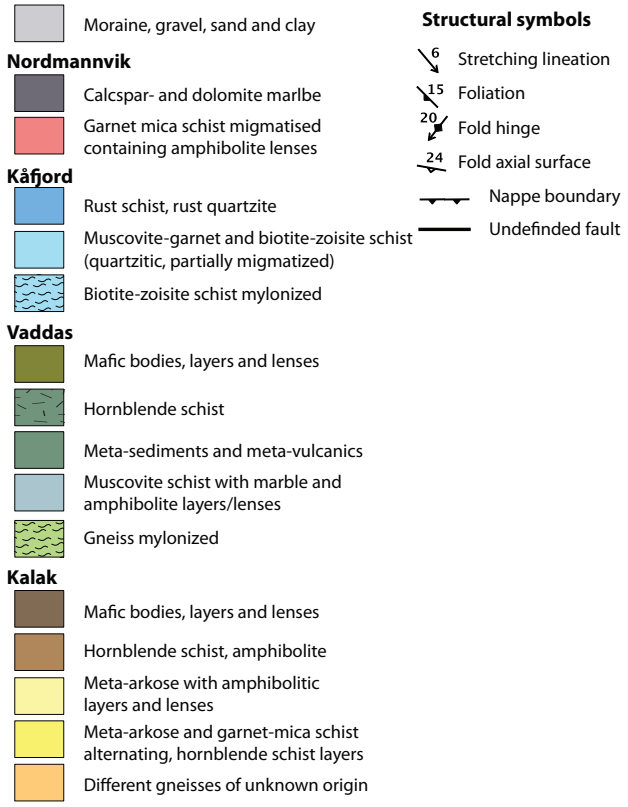

Fig. 3.2: Legend of the geological map explaining the different geological units as well as geological boundaries and symbols.

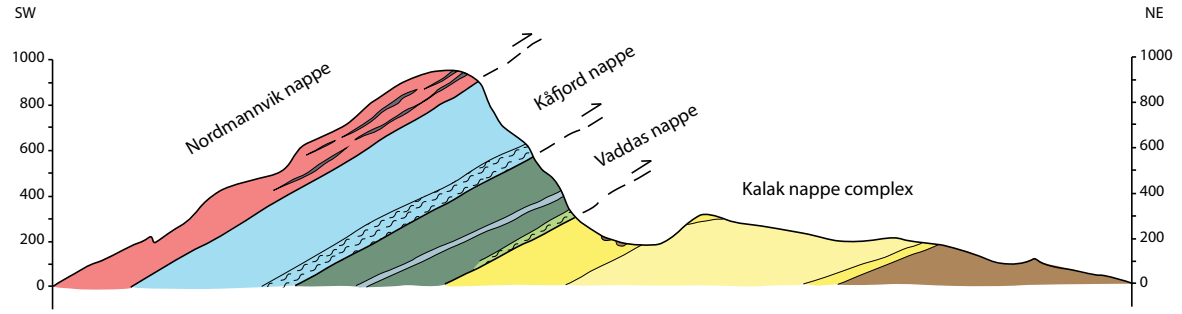

Fig. 3.3.: A geological cross section along the profile seen in the geological map was constructed showing how the nappes are stacked on top of each other dipping to the SW.

3.2. Nappe Descriptions

3.2.1. Kalak Nappe Complex

The largest part of the KNC is composed of **meta-arkoses**. Macroscopically these rocks have a white to beige color, are mostly fine-grained and exhibit a foliation (see fig. 3.4 a)). The light color is due to abundant feldspar and quartz, the latter sometimes with a light pink color. Minor amounts of mica are found as flakes distributed in the foliation but also as thin gray layers. **Garnet mica schists** are found interlayered with the meta-arkoses. These fine- to medium-grained schists, depending on the degree of shearing, of light to dark gray color contain idiomorphic pink garnet grains (up to $5\,mm$, see fig. 3.4 b)). A strong foliation is developed, sometimes emphasized by a layering of quartz- and feldspar-rich versus mica-rich layers. Generally the schists are quartzitic. Parts of the KNC are formed by various **gneisses**. In the north of the island along the coast sheared paragneisses of light gray color containing pink pegmatite lenses are exposed. The gray fine- to medium-grained geneiss is rich in biotite, while the pegmatite lenses are formed by alkali feldspar and quartz. Amphibolite dikes occur within the gneisses. Furthermore strongly sheared beige-colored fine-grained orthogeneisses rich in quartz and feldspar occur in the north of the island (see fig. 3.4 c)). A strong foliation and lineation within these is developed due to intensive shearing. The grain size varies from medium- to fine-grained. These orthogneisses are hard to distinguish from the meta-arksoses of the KNC. **Amphibolites/hornblende schists** have the dark green color typical for hornblende and contain white grains of plagioclase, sometimes forming clasts or layers. The medium-to coarse-grained rocks are mostly foliated due to the parallel alignment of elongate hornblende crystals. Garnet as red idiomorphic crystals of up to $2\,mm$ size are frequently observed in the amphibolites.

3.2.2. Vaddas Nappe

A variety of rocks were observed within the Vaddas nappe. The lower boundary to the KNC is marked by a distinct **gneiss** that is strongly mylonitized. A fine-grained dark gray quartz-rich matrix with biotite contains white feldspar layers and clasts as well as red garnet crystals (see fig. 3.5 a)). Due to mylonitisation a strong foliation is developed. Above the mylonite a variety of sedimentary and volcanic rocks different from the homogeneous meta-arkoses of the KNC occur. **Meta-arkoses** rich in quartz and feldspar are observed. The rocks are light colored, beige, white or gray, with a medium grain-size and a strong foliation. Furthermore **meta-conglomerates** with a strong foliation and a high amount of clasts deflecting the foliation are found (see fig.

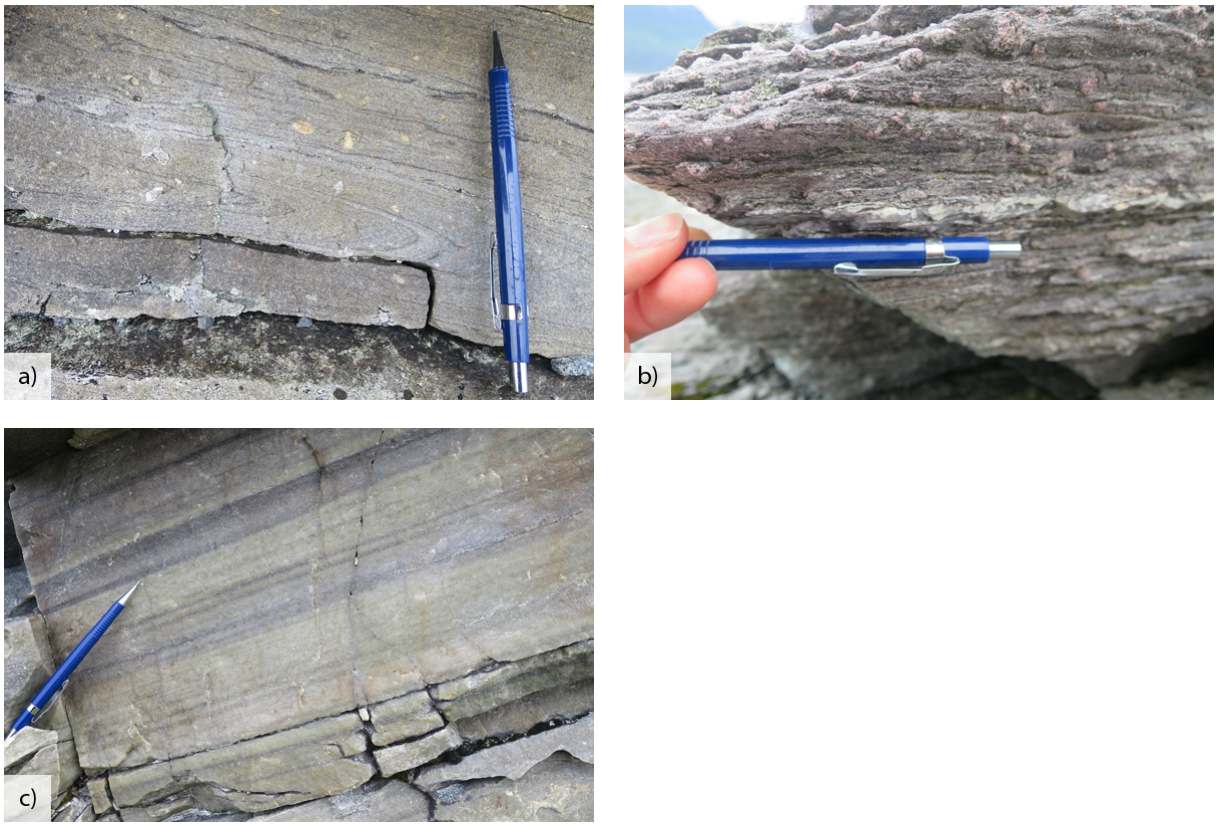

Fig. 3.4.: a) Meta-arkoses compose most of the KNC. The light colored rock is often fine-grained and isoclinal folds are frequently observed (UL298). b) Grey garnet mica schists are interlayered with the meta-arkoses. Idiomorphic garnet grains are embedded in the strongly foliated rock (UL319). c) Fine-grained mylonitized light colored orthogneisses look very similar to the meta-arkoses of the KNC (UL322).

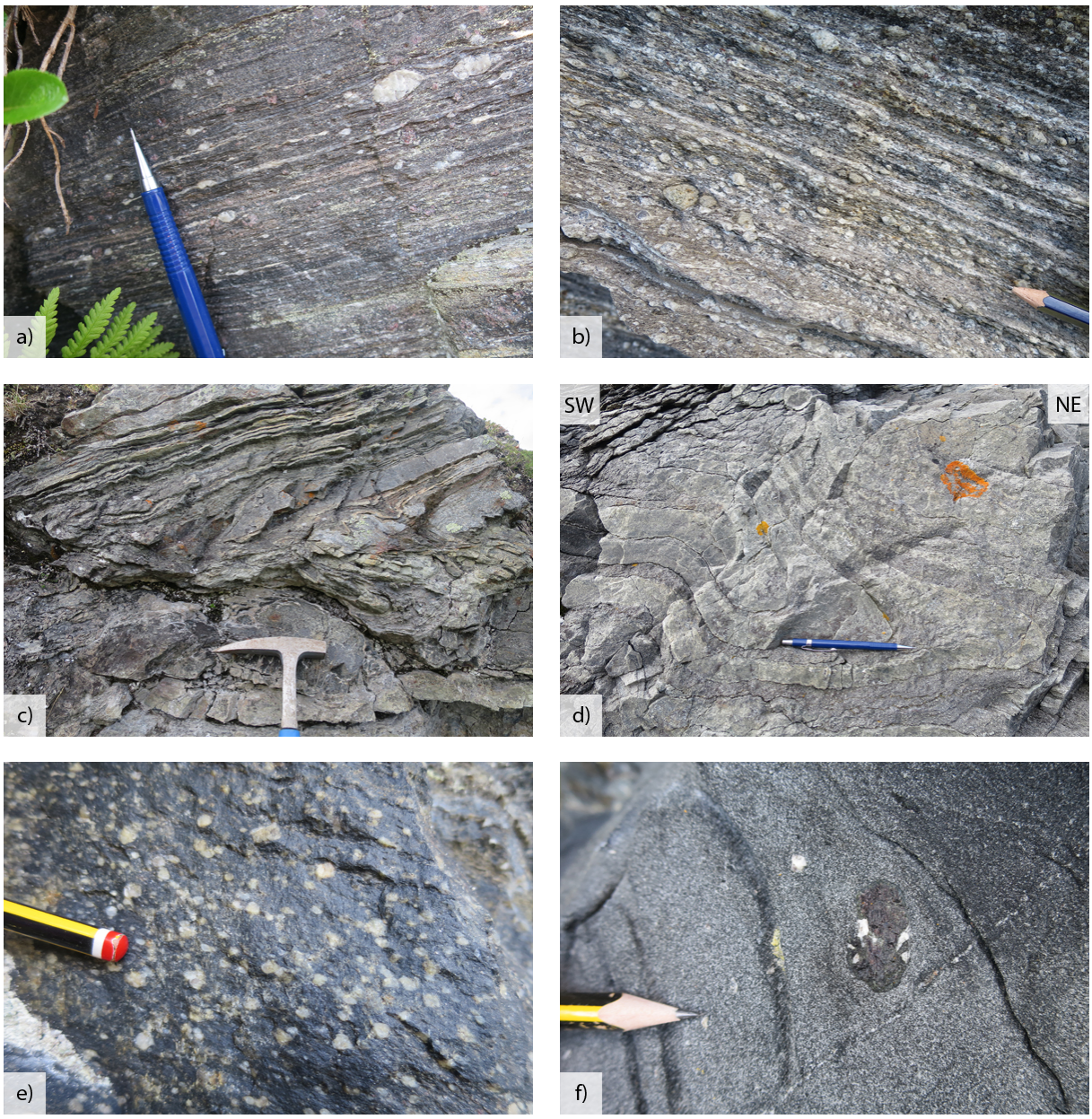

Fig. 3.5.: a) The lower boundary of the Vaddas nappe is formed by a mylonitized migmatitic gneiss (UL330). b) Meta-conglomerates are rich in clasts deflecting the foliation. The round shape of the clasts is the result of shearing (UL466). c) Greenschists show a layering of light green, biotite-, actionolite-rich and white-gray, quartz- and feldspar-rich layers (UL333). d) Within green-gray colored zoisite biotite schists of the Vaddas nappe folds are observed: A tight fold is refolded by an open moderately inclined fold (UL373). e) A very fine-grained almost black matrix contains white feldspar clasts typical for porphyric rocks (UL464). f) Meta-basalts do not show a specific texture. Different crystals, mostly feldspar, are scattered in a fine-grained gray matrix (UL465).

3.5 b)). The matrix of this white- to light gray-colored rock is formed by biotite, quartz and feldspar. The up to 1 cm big clasts are rounded and formed by quartz and feldspar. Higher up in the sequence green-colored **schists** are found showing a layering of green-gray rock with white-gray layers (see fig. 3.5 c)). The greenish rock is rich in biotite and contains actinolite observed as a fibrous green-blue mineral while the white layers are rich in feldspar and quartz. A foliation has developed, thin layers are folded on a small scale forming a crenulation. Furthermore **calc silicate rocks** were observed which are mostly fine-grained and massive or weakly foliated exhibiting a greenish gray color. Locally layering occurs with dark green, gray-green and white quartz-rich layers. Coarse-grained **amphibolites** are abundant in the following sequence. The dark green rock with white feldspar grains is foliated due to parallel alignment of the amphiboles that also form a distinct lineation. Garnet is present in some amphbibolite layers. Interlayered with the amphibolite **garnet mica schists** are found. These rocks show a typical schistosity with crenulated foliation surfaces. Dark red garnet grains were observed on the foliation surfaces. Schists rich in biotite have a brown to golden color while those rich in muscovite have a silvery or when weathered golden color. On top of the described sequence a distinct **marble** horizon is observed across the whole island. The light yellow-orange, beige-colored marble is easily recognized. The orange color is due to weathering, fresh surfaces are beige-colored. Since marble is very weak the rock is strongly deformed and does not show a consistent foliation. Layers of amphibolite and garnet mica schist are found within the marble. The upper part of the Vaddas nappe is marked by a variety of schists, mostly **quartzitic garnet mica schists** with compositional layering of biotite- versus muscovite-rich layers. Due to the high content of fine-grained quartz the schists appear dark gray on a fresh surface perpendicular to the foliation. Since the foliation is mainly formed by biotite surfaces parallel to the foliation have a brown color. Sometimes the schists contain zoisite or tourmaline as small black or white prismatic crystals on the foliation surfaces. Layers of amphibolite of different thicknesses up to 1 m occur within the schists. The uppermost unit in the Vaddas nappe are a green medium-grained **zoisite mica schists** rich in biotite but also containing quartz and feldspar (see fig. 3.5 d)). Prismatic white to light green zoisite crystals up to 1 cm in length are observed on the foliation surfaces of the strongly foliated rock.

In the northwest of the island north of the undefined fault the Vaddas nappe is composed of similar rock units like those described above. One distinct difference is a sequence of porphyroclastic rocks, meta-basalt, amphibolite and marble. The **prohyroclastic rock** shows a fine-grained almost black matrix with angular white clasts of feldspar in different sizes up to $5\,mm$ (see fig. 3.5 e)). On top of this porphyric rock there is a layer of homogeneous **meta-basalt**. In the fine-grained dark gray matrix different porphyroclasts

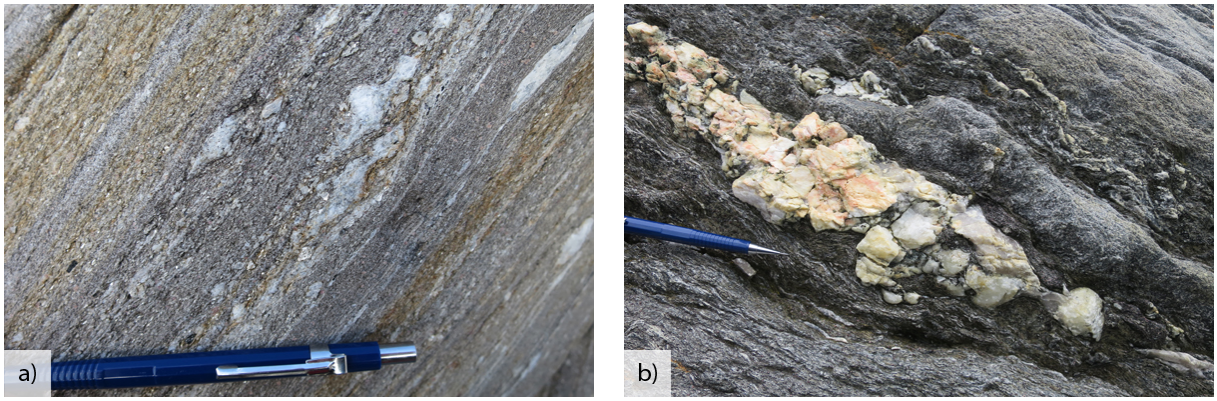

Fig. 3.6.: a) A mylonitized migmatite forms the lower boundary of the Kåfjord nappe. The light brown rock contains muscovite and biotite as well as stretched leucosomes of quartz and feldspar (UL372). b) Dark gray biotite schists from the Kåfjord nappe occasionally contain light pink pegmatite lenses of quartz and alkali feldspar (UL365).

of mostly feldspar with various sizes up to 2 cm are scattered, (see fig. 3.5 f)). No fabric or preferred mineral orientation is developed. The overlying dark green amphibolite is also homogeneous without any fabric. The medium-grained rock is composed of amphibole and plagioclase forming a salt and pepper texture. A fine-grained, homogeneous marble of light gray to beige color without a texture overlies the amphibolite.

3.2.3. Kåfjord Nappe

As typical for the nappe boundaries on Uløya the lower boundary of the Kåfjord nappe with the Vaddas nappe is formed by a **mylonitized migmatite** (see fig. 3.6 a)). This mylonite shows a light brown to white color and is rich in quartz and feldspar. The foliation is formed by biotite and muscovite. Garnet grains of different sizes are abundant. Stretched layers and porphyroclasts of feldspar and quartz, representing deformed leucosomes, as well as garnet crystals deflect the foliation. Above the mylonites a thick sequence of various **mica schists** is exposed. The amounts of muscovite and biotite vary substantially and therefore the schists alter from muscovite to biotite schists. Usually, both minerals are present. Besides these, quartz and feldspar are the main rock-forming minerals. In parts, the schists are rich in quartz turning the rock into a quartzitic mica schist. Quartz occurs also in the form of segregations as layers and stretched lenses. Occasionally, pegmatite lenses of alkali feldspar and quartz occur (see fig. 3.6 b)). Garnet is frequently present as small ($<5\,mm$) idiomorphic dark red grains. Besides garnet, zoisite is in parts very abundant, visible mainly on foliation surfaces. In one location, nests white fibrous sillimanite were observed. Tourmaline as small ($<3\,mm$) prismatic black crystals occur rarely (UL287). Sometimes the foliation is crenulated. The schists are generally

Fig. 3.7.: The Nordmannvik nappe is composed of a migmatised garnet mica schist that is locally sheared. Quartz- and feldspar-rich leucosomes are stretched and sometimes strain gradients like in the picture can be observed where the strain increases from the top of the picture downwards (UL278).

fine- to medium-grained and show a variety of colors from rusty- to golden-brown, dark gray or gray-green depending on the mineral composition, which is usually rich in muscovite, biotite or biotite and zoisite. Amphibolite layers occur occasionally within the schists.

3.2.4. Nordmannvik Nappe

The nappe contact of the Kåfjord to the Nordmannvik nappe is again marked by a mylonite, in this case the **migmatised garnet mica gneiss** of the Nordmannvik nappe. This migmatite forms the dominant lithology of the Nordmannvik nappe and shows a distinct foliation and layering. The gneiss has a dark gray color and contains white quartz- and feldspar-rich layers or lenses (see fig. 3.7). These are interpreted as leucosomes formed during migmatization. The gneiss is rich in both muscovite and biotite. Dark red idiomorphic garnets of 3 mm and bigger in diameter are distributed in the rock. In part, the rock is strongly sheared leading to disappearance of the migmatitic layering and giving it a more schistose appearance. A homogeneous dark gray mylonite with white quartz-feldspar clasts developed. The migmatized garnet mica gneiss is in places rich in hornblende, sometimes forming amphibolite layers in the gneiss. Locally, up to 1 m wide marble layers were observed within the migmatised schist of the Nordmannvik nappe.

3.3. Structural Geology

A variety of large-scale deformation structures was observed in the field. Along the nappe boundaries but also within the nappes intensive shearing occurs. Often wide zones of mylonites or alternating mylonitized and non-mylonitized rocks were observed making

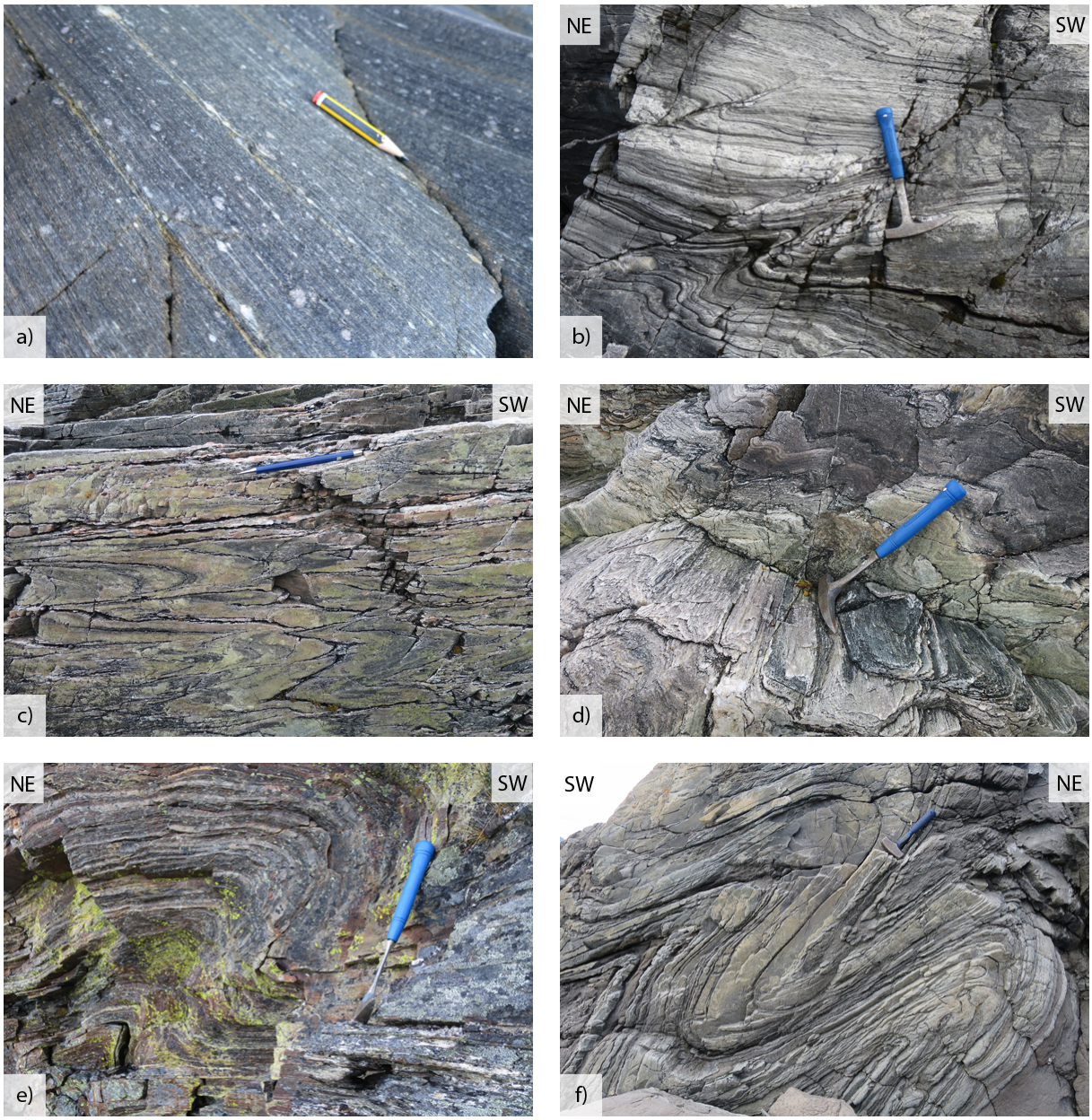

Fig. 3.8.: a) Shearing occurs within the nappes but especially along the nappe boundaries forming complex interfingering mylonitized contacts. Here the mylonitized migmatite from the boundary of the KNC and the Vaddas nappe in the northeast of the island is shown (UL458). b) Melt segregation along axial planes in orthogneisses of the KNC were observed along the northern coastline (UL325). c) Migmatitic isoclinal folds with the axial plane parallel to the foliation and the fold hinges parallel to the lineation are common in paragneisses of the KNC (UL320). d) Frequently isoclinal folds are associated with an intensive stretching lineation, here seen in gneisses at location UL321. e) Asymmetric close to open folds with moderately inclined axial planes and fold hinges sub-parallel to the stretching lineation were observed within meta-arkoses of the Vaddas nappe (UL340). f) Furthermore close symmetric folds in zoisite biotite schists with a similar geometry to the open folds are found in the Vaddas nappe (UL373).

it difficult to accurately place the nappe boundaries. An example for the variety of mylonites is shown in figure 3.8 a) (UL458; see also figs. 3.5 a), b), 3.6 a) and 3.13 c)). The mylonitized migmatite marks the boundary of the KNC with the Vaddas nappe northeast of the undefined fault in the north of the island.

In the KNC melt segregations along axial planes of tight folds (UL325; see fig. 3.8 b)), isoclinal folds and melt pockets around garnet in gneisses along the northern coastline were observed as evidence for migmatization. Isoclinal folds with axial planes parallel to the foliation and fold hinges parallel to the stretching lineation are generally common in the KNC (see also fig. 3.4 a)). In para- and orthogneisses isoclinal folds of compositional layering with the same orientation are developed often associated with a very strong lineation (UL320 and UL321; see fig. 3.8 c) and d)). Additionally open folds at a larger scale were observed in the KNC overprinting the isoclinal folds.

Within the Vaddas nappe similar fold structures are observed. In figure 3.5 d) a tight fold, developed in green-gray zoisite biotite schists, is refolded by an open fold indicating the presence of two fold generations (UL373). The tight fold forms a first generation fold and is oriented like the isoclinal folds in the KNC with the axial plane parallel to the foliation and the fold hinge parallel to the stretching lineation. The fold overprinting the tight fold belongs to the second fold generation and forms an asymmetrical, open fold with one short limb and two longer limbs that are almost parallel to the foliation, the axial plane is moderately inclined, slightly steeper than the planes of the isoclinal folds, and the fold hinge is sub-parallel to the stretching lineation. This type of open fold with the same geometry was also observed within meta-arkoses of the Vaddas nappe (UL340; see fig. 3.8 e)). Another example of folds in the Vaddas nappe is shown in 3.8 f) where symmetrical closed folds with moderately inclined axial planes and fold hinges sub-parallel to the stretching lineations are developed in green-gray zoisite biotite schists (UL373). However asymmetrical, open folds seem to be a lot more common than symmetrical, closed folds.

In the Kåfjord nappe again two types of folds were observed. A sheath fold as a special type of fold was seen in biotite schists, exposed in cross section as a flattened oval formed by an amphibolite layer (UL366; see fig. 3.9 a)). The axial plane is parallel to the foliation and the fold hinges are sub-parallel to the stretching lineation. An open asymmetrical fold with a similar orientation to the open folds in the Vaddas nappe overprinting isoclinal folds was seen in biotite gneisses along the western coast of Uløya (UL281; see fig. 3.9 b)). In the same outcrop very distinct shear sense indicators were observed formed by pegmatitic lenses showing a top to the SE sense of shear (UL281; see fig. 3.9 c)). Generally shear sense indicators observed in the field are ambiguous but the dominant sense of shear shows top to the SE movement.

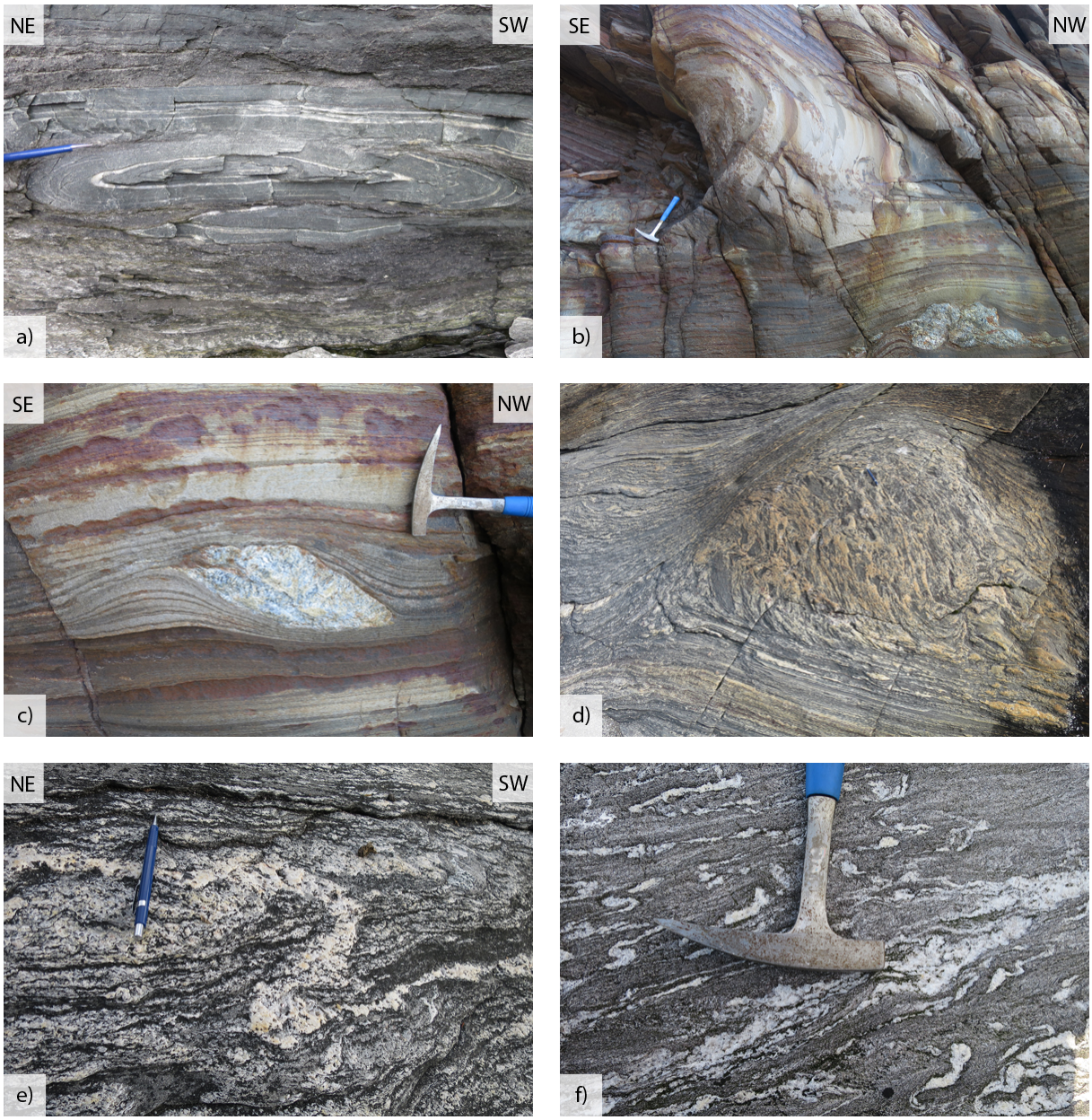

Fig. 3.9.: a) A sheath fold is exposed in the Kåfjord nappe with the axial plane parallel to the foliation and the fold hinge sub-parallel to the stretching lineation (UL366). b) In biotite gneisses of the Kåfjord nappe a sheared fold overprinting isoclinal folds was observed (UL281). c) Shear sense indicators are often ambiguous but the dominant sense of shear is top to the SE as observed in a pegmatitic lens within biotite gneisses of the Kåfjord nappe (UL281). d) Within the migmatites of the Nordmannvik nappe lenses with an older, preserved and less sheared fabric are observed. The foliation of the strongly sheared surrounding rock has a different orientation than the fabric in the lens and is deflected around the lens (UL278). e) In places leucosome layers within the migmatized garnet mica schists of the Nordmannvik nappe are isoclinally folded with the axial plane parallel to the foliation and the fold hinge parallel to the lineation (UL278). f) Isoclinal folds formed by leucosomes in the sheared Nordmannvik nappe show locally random orientations and undulate (UL286).

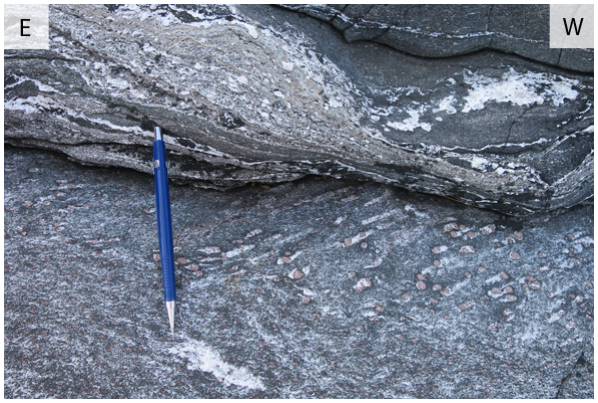

Fig. 3.10.: Melt pockets around garnet in migmatites of the Nordmannvik nappe are stretched in NE-SW direction parallel to the dominant stretching lineation proving syn-tectonic melting (UL280).

As in the other nappes strong shearing is observed within the Nordmannvik nappe. A shear zone with a strain gradient is shown in figure 3.7 (UL278). White quartz-feldspar-rich leucosome layers in the top of the picture are stretched but not disconnected while at the bottom of the picture the layers are stretched and disconnected into single clasts indicating higher shear strain. Furthermore a 1x1 m lens of less sheared migmatite was preserved within the strongly sheared migmatites of the Nordmannvik nappe (UL278; see fig. 3.8 b)). The older preserved fabric within the lens shows a different orientation than the strongly sheared foliation anastomosing around the lens. Additionally the Nordmannvik nappe shows also evidence of folding, often emphasized by the leucosome layers. An isoclinal fold formed by a leucosome layer with the axial plane parallel to the foliation and the fold hinge parallel to the stretching lineation is shown in figure 3.9 e). On the other hand undulating isoclinal folds with random orientations were also observed in the Nordmannvik nappe (see fig. 3.9 f)). Furthermore melt pockets around garnet grains are locally stretched into the NW-SE orientation of the regional stretching lineation (UL280; see fig. 3.10).

In summary isoclinal to tight folds as a first generation of folds were observed in all four nappes on Uløya, while close to open folds as a second generation were observed within the KNC, the Vaddas nappe and the Kåfjord nappe. Strong shearing affected all nappes and especially the nappe boundaries. Shear sense indicators are ambiguous but a dominant sense of shear with the top to the SE was determined. Evidence for migmatization was observed in the KNC and the Nordmannvik nappe.

3.3.1. Structural Data

The orientation of foliation, stretching lineation and folds was measured in the field. In general both foliation and lineation have a very consistent orientation across the whole

island as seen in the stereographic projections a) and c) in figure 3.11. The foliation shows a consistent orientation dipping shallowly to the SW. Especially the orientation of the Vaddas nappe, Kåfjord nappe and Nordmannvik nappe matches very well. Only the KNC shows a broader distribution of measurements dipping to the SW, SE and NE. For the poles of the foliation of the KNC a best fit great circle can be constructed (see fig. 3.11 b)). The pole of this great circle dips shallowly to the SE and coincides with the orientation of the stretching lineations plotted in figure 3.11 c). The lineations plunge consistently at a shallow angle to the NW and SE with the maximum in the SE. A distinct feature of the lineations from the Kåfjord nappe is that the measurements scatter along a great circle dipping shallowly to the SW (see fig. 3.11 d)). The lineations of the KNC and Vaddas nappe plunge both to the NW and the SE while the ones of the Nordmannvik nappe plunge mainly to the NW. Furthermore axial planes and fold hinges measured of isoclinal and open folds as two different fold generations are shown in figure 3.12 a). Both isoclinal and open folds show almost the same geometry. The poles to the axial planes correspond approximately with the poles of the foliation but the axial planes dip slightly more to the SE than the foliation. The fold hinges match the orientation of the stretching lineations very well with a maximum dipping at a shallow angle to the SE which is the same orientation as the pole to the great circle distribution of the KNC. Moreover the tectonic transport direction can be constructed from the intersection of the great circle distribution of the stretching lineations and the average great circle of the fold axial planes (see fig. 3.12 b)). The intersection point plunges at a low angle to the SSE showing approximately the same orientation as the stretching lineations and fold hinges. The constructed tectonic transport direction coincides approximately with the dominant sense of shear top to the SE observed in the field.

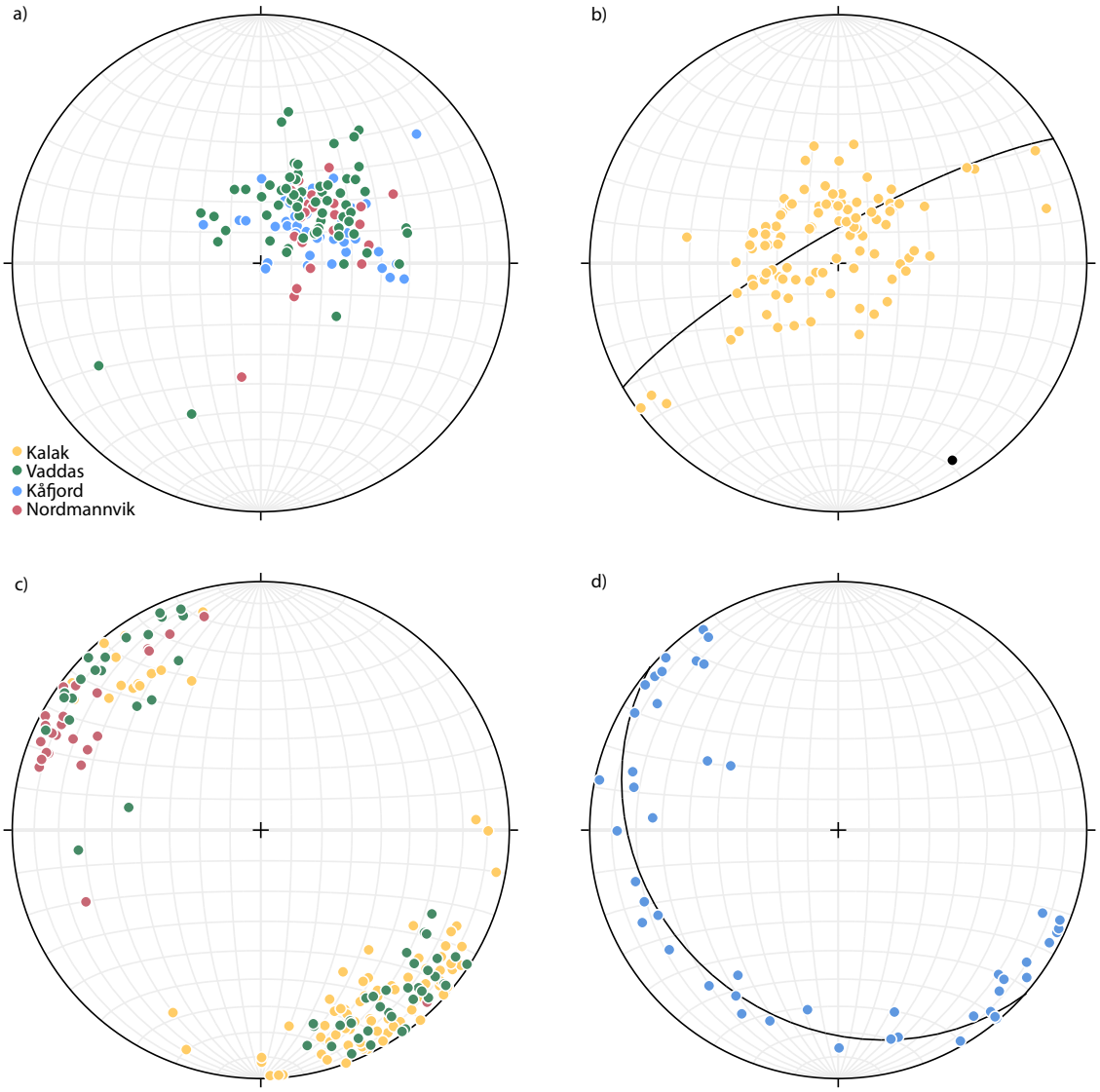

Fig. 3.11.: a) Poles to the foliation planes of the Vaddas nappe, Kåfjord nappe and Nordmannvik nappe plotted in a stereographic projection show that the foliation is consistent and dips shallowly to the SW (n=141). The different colors represent the different nappes according to the colors on the geological map (yellow for the KNC, green for Vaddas nappe, blue for Kåfjord nappe and red for Nordmannvik nappe). b) The poles to the foliation of the KNC vary in orientation for which a great circle can be plotted (n=101). The pole to this great circle plunges to the SE the same orientation as the stretching lineation. c) The lineations of the KNC, the Vaddas nappe and the Nordmannvik nappe plunge shallowly NE-SW with a maximum in the SE (n=182). d) Stretching lineations of the Kåfjord nappe scatter well distributed along a shallowly SW dipping great circle with two maxima in the NW and the SE (n=48).

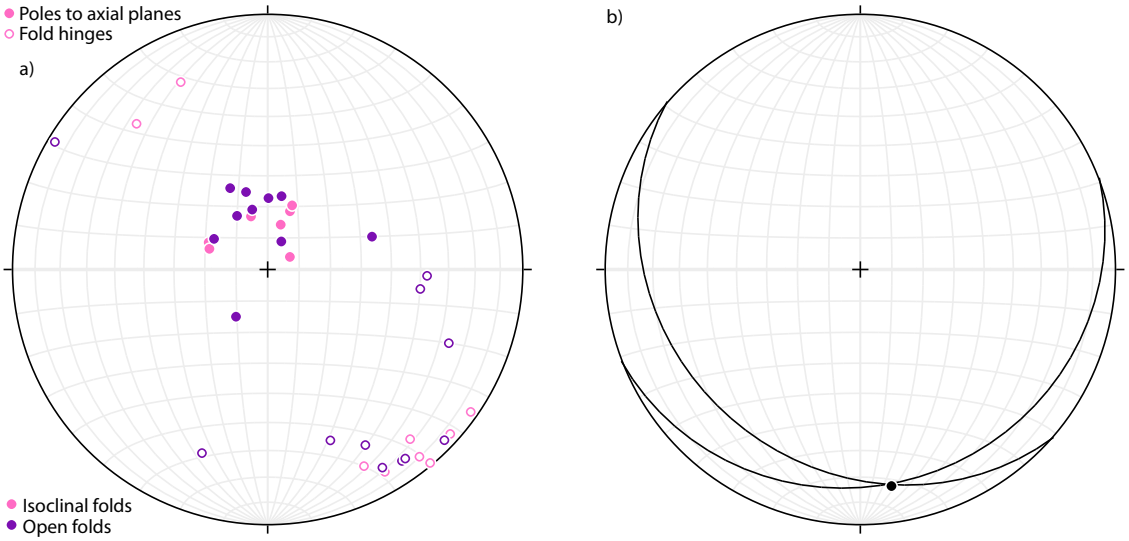

Fig. 3.12.: a) Poles to the axial surfaces (filled circles, n=19) and fold hinges (hollow circles, n=21) show a similar orientation for the different fold generations. The generations are distinguished by color. Isoclinal folds are pink and open folds purple. Furthermore the orientation of the axial planes coincides with the foliation orientation and the fold hinges with the lineation respectively. b) The intersection of the great circle along which the lineation plots and the average great circle of the fold axial planes shows the tectonic transport direction towards the SSE.

3.4. Petrography and Microstructures

3.4.1. Kalak Nappe Complex

Microscopically **meta-arkoses** have a coarse-grained (835/457 μm) matrix of elongate quartz (55 %) and alkali feldspar (30 %) grains forming a foliation (UL300; see fig. 3.13 a)). Single elongate flakes of muscovite (5-10 %) are distributed in the matrix oriented with the long axis parallel to the foliation. Small patches or thin layers of fine-grained (60/45 μm) quartz, alkali feldspar and muscovite are distributed within the coarse grained matrix. Furthermore short prismatic zoisite/clinozoisite (5 %) grains are scattered in the matrix parallel to the foliation. Opaque minerals are found as accessories.

As an example of the **garnet-mica schists** of the KNC thin section UL319 is described in detail. The rock shows layering of quartz-feldspar- and muscovite-biotite-rich layers of different thickness forming a foliation (see fig. 3.13 b)). Muscovite (10-15 %) and biotite (5-10 %) are aligned parallel to the foliation. Quartz (30-40 %) forms monomineralic thin recrystallized layers in the foliation. Remnants of mostly decomposed garnet grains (5 %) of various sizes (up to >4.5 mm) deflect the foliation as do plagioclase clasts. Plagioclase (25-30 %) is often sericitised and biotite locally chloritized. Accessories are zoisite/epidote (5 %), rutile, opaques, apatite and sphene.

Furthermore sample UL476 is presented as an example of a **gneiss** form the northern coast of Uløya. The coarse-grained rock (694/416 μm) is rich in feldspar (25-30 %), both alkali feldspar and plagiocalse, and quartz (30-40 %) forming a foliation due to elongate grain shape (see fig. 3.13 c)). Biotite (10-15 %) and minor amounts of muscovite (5 %) are distributed in the matrix parallel to the foliation. Elongate or idiomorphic garnet grains (5-10 %) are embedded in the matrix (783/494 μm). The centers of the garnets are rich in inclusions. Sphene, apatite, zircon and opaque minerals are found as accessory phases.

The macroscopically observed texture of the **amphibolites** is confirmed in thin section (UL297; see fig. 3.13 d)). Elongate green pleochroic hornblende crystals (70-75 %) with the typical amphibole cleavage are aligned parallel forming a coarse-grained matrix (1108/416 μm). Intergranular space is filled with plagioclase and quartz (together 10 %), both of which also form inclusions in the hornblende. Idiomorphic garnet grains (639/600 μm; 10-15 %) are distributed in the matrix sometimes forming small clusters. The garnet contains inclusions of quartz, sphene as well as opaques and is partly decomposed. Accessories are abundant diamond-shaped sphene (5 %) but also apatite, rutile and opaque minerals.

Sample UL250, a **quartzitic garnet-mica schist**, was chosen as a representative sample to perform P-T estimates on the KNC (see fig. 3.14 e)). The rock is coarse-grained (680/390 μm) and shows a foliation due to parallel alignment of elongate minerals.

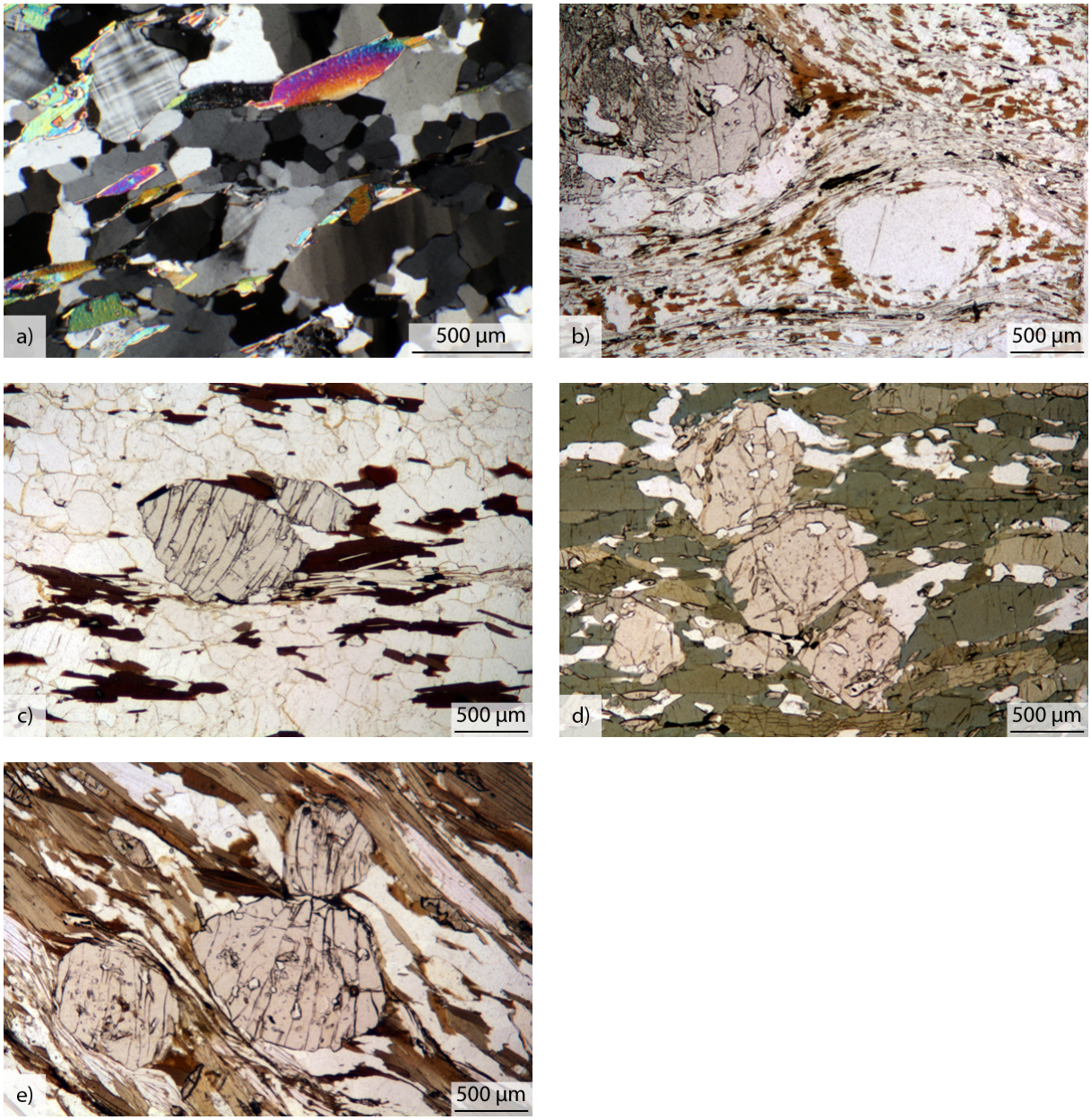

Fig. 3.13.: a) Coarse-grained meta-arkoses are rich in quartz and feldspar but also contain muscovite flakes forming a foliation (UL300). b) Quartzitic garnet mica schists show layering of mica- versus quartz-feldspar-rich layers containing garnet and feldspar clasts (UL319). c) Coarse-grained gneisses show a weak foliation due to alignment of biotite and muscovite. Garnet clasts are embedded in the quartz-feldspar-rich matrix (UL476). d) Amphibolites show a foliation due to parallel alignment of prismatic hornblende crystals and contain clusters of idiomorphic garnets (UL297). e) The coarse-grained quartzitic garnet mica schist UL250 was chosen for P-T estimates of the KNC.

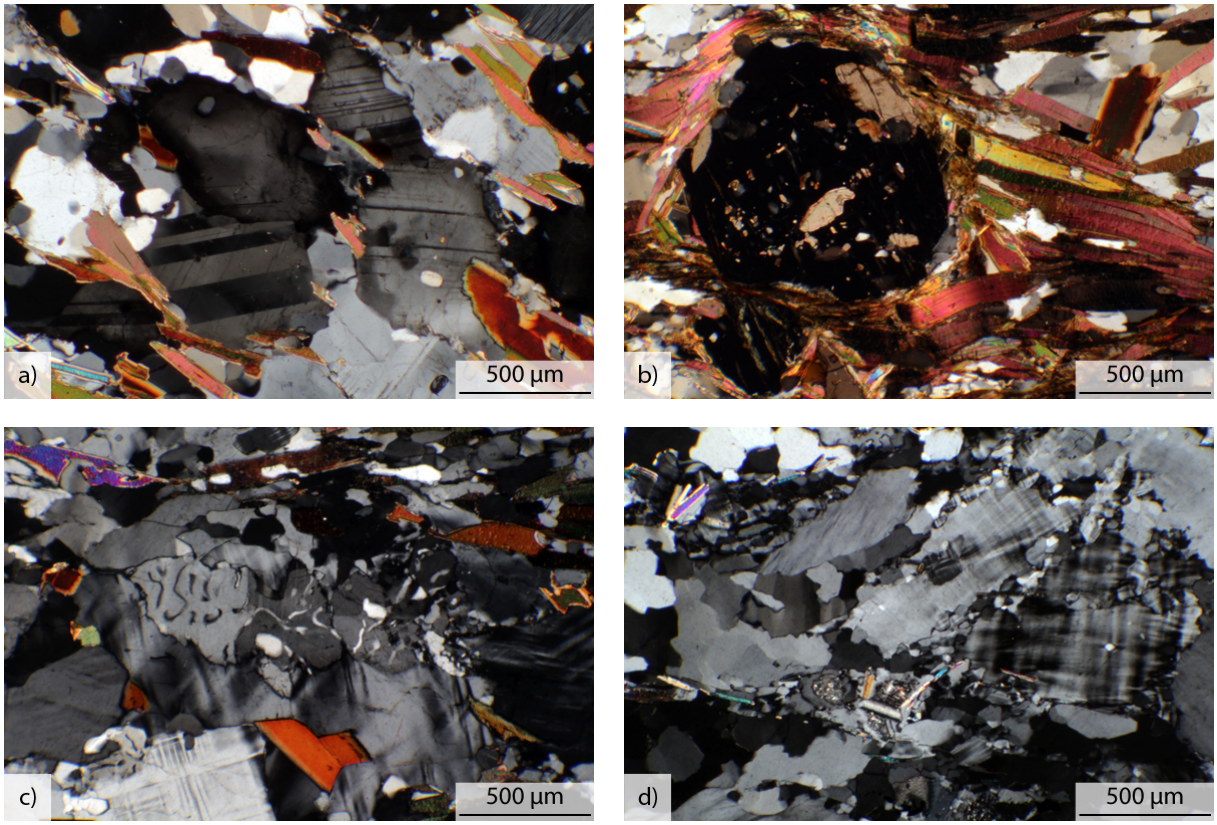

Fig. 3.14.: a) Plagioclase and alkali feldspar in the quartzitic garnet-mica schist UL250 show undulose extinction. Often the rim shows a different extinction orientation than the core of the grain. b) Biotite and muscovite are aligned parallel to the foliation. Some grains are bent around garnet porphyroclasts and some grow at an angle to the foliation (see biotite to the upper right). Idiomorphic garnet grains are inclusion-rich in the center (UL250). c) In the migmatitic gneiss UL476 myrmekitic intergrowth of plagioclase and quartz is observed adjacent to alkali feldspar grains. d) Rims of small recrystallized alkali feldspar grains and subgrains form around large alkali feldspar crystals in the meta-arkose UL300.

Large idiomorphic biotite grains (20-30 %) form layers together with large idiomorphic muscovite(5-10 %). Furthermore biotite and muscovite are distributed in the quartz- (10-15 %) and feldspar-rich (20 %) matrix. Both alkali feldspar and plagioclase are present in the matrix. Garnet grains (10 %) with inclusion-rich centers are distributed in the thin section. Sphene (5 %) forms an abundant accessory mineral and is also found as inclusions in garnet. Other accessories are rutile, zircon, opaque minerals, apatite and zoisite.

Microstructural descriptions of the KNC focus on the above described quartzitic garnet-mica schist UL250 which was selected for P-T estimates. Large elongate quartz grains ($640/295\,\mu m$) in the matrix show undulose extinction as well as smaller grains and subgrains that are elongate or polygonal. This is also observed in quartz in the meta-arkose UL300 as seen in the lower right corner of figure 3.13 a). Plagioclase and alkali feldspar exhibit undulose extinction, patches of polysynthetic twins, microfracturing and tapering

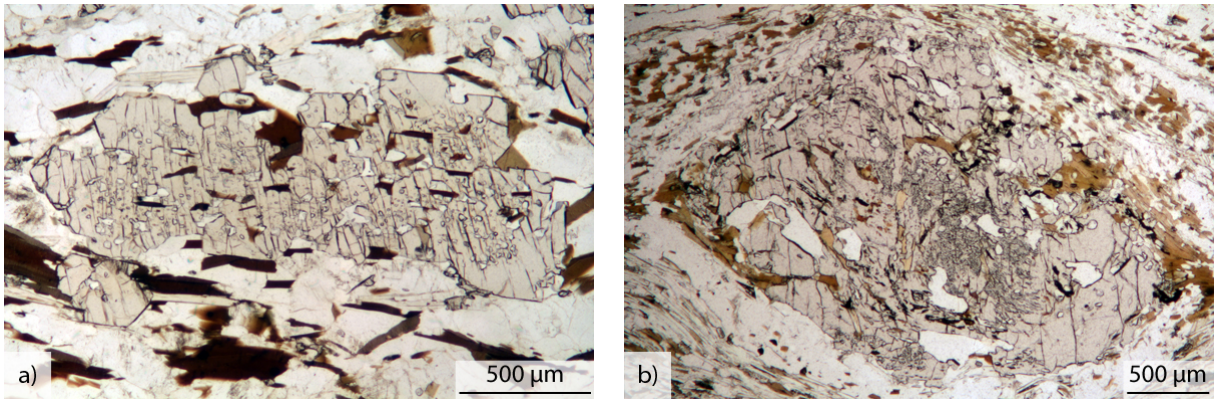

Fig. 3.15.: a) A garnet grain in the quartzitic garnet-mica schist UL250 is elongated parallel to the lineation and contains inclusions also parallel to the foliation. b) Large garnet porphyroclasts in the quartzitic garnet-mica schist UL319 are rich in inclusions forming twisted trails within the garnet indicating top to the SE shearing in the field.

deformation twins. Often the rims of the grains have a different extinction orientation than the core (see fig. 3.14 a)). Large idiomorphic biotite and muscovite crystals are aligned parallel to the foliation as are elongate quartz and feldspar grains. Both biotite and muscovite show undulose extinction and some grains are bent around garnet porphyroclasts (see fig. 3.14 b)). Individual biotite and muscovite grains grow across the foliation forming a later mica generation (see fig. 3.14 b)). Garnet porphyroclasts are idiomorphic and inclusion-rich in the center while the rims are inclusion-poor (see fig. 3.14 b)). Inclusions are formed by quartz, plagioclase, biotite and sphene. A few garnet grains are partly replaced by quartz or biotite. One distinct large garnet grain has an elongate shape parallel to the foliation and contains biotite inclusions which are also parallel to the foliation (see fig. 3.15 a)). Furthermore, sphene is very abundant in the whole thin section, oriented with the long axis parallel to the foliation. Small prismatic zoisite grains with a brown allanite core are also aligned parallel to the foliation. Similarly single rutile grains are distributed in the matrix. An overview over the mineral assemblage and the sequence of relative mineral growth for sample UL250 is shown in table 3.16.

In addition a few characteristic structures representative for the KNC in other samples were observed. Quartz veins in the quartzitic mica schist UL460 show very similar deformation as the quartz in the matrix of UL250. Very large grains ($980/605\,\mu m$) with slightly interlobate grain boundaries show undulose extinction and elongate subgrains. Myrmekitic intergrowth of plagioclase and quartz adjacent to alkali feldspar grains as well as subgrains and small alkali feldspar grains around larger alkali feldspar crystals are observed in the migmatitic gneiss UL476 (see fig. 3.14 c)). The meta-arkose UL300 contains large alkali feldspar crystals that are surrounded by rims of smaller alkali feldspar grains and subgrains (see fig. 3.14 d)). The grain boundaries of the large porphyroclasts

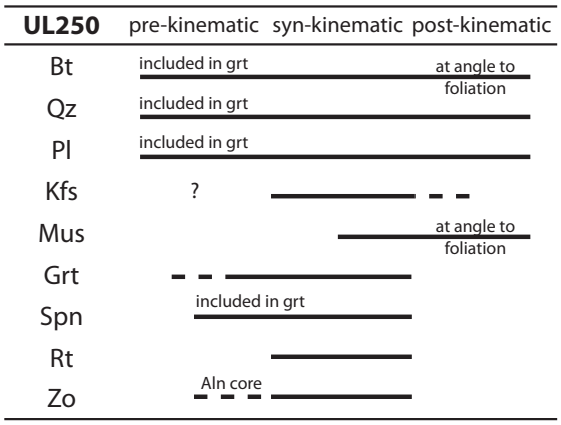

Fig. 3.16.: Overview over the mineral assemblage of sample UL250 and relative times of mineral growth.

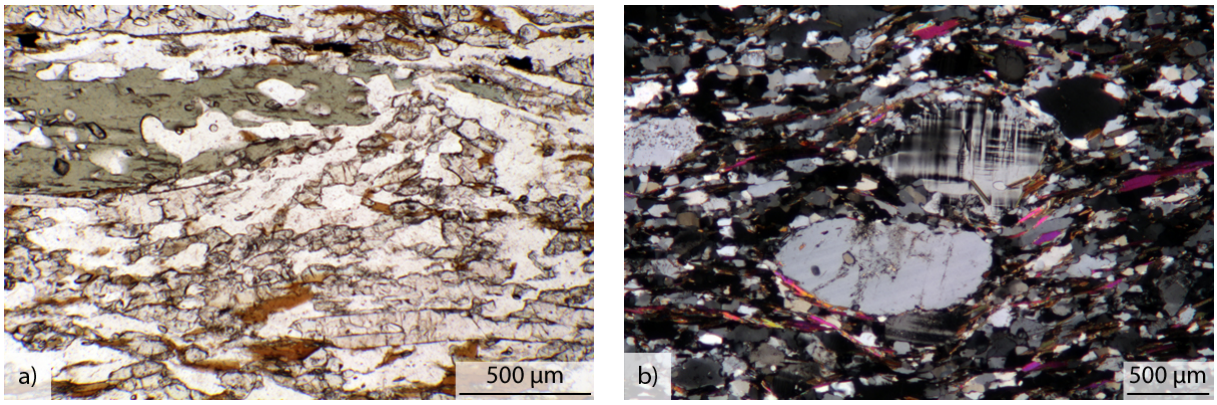

Fig. 3.17.: a) Zoisite-biotite schists show a clear foliation and have a medium- to fine-grained matrix. Transparent elongate zoisite with inclusions is abundant as well as elongate green hornblende (UL373). b) The garnet-mica gneiss UL248 was selected for P-T estimates. In the medium-grained matrix, crystals of plagioclase and alkali feldspar as well as a few garnet are embedded.

are slightly sutured. In the quartzitic garnet-mica schist UL319 large garnet grains are rich in inclusions which form twisted trails within the garnet corresponding to top to the SE shearing in the field (see fig. 3.15 b)). Moreover biotite in UL319 shows late chloritization.

3.4.2. Vaddas Nappe

Of the variety of rocks in the Vaddas nappe different kinds of schists are predominant. Therefore a zoisite-biotite schist is described as an example for the Vaddas nappe. The **zoisite-biotite schist** (sample UL373) has a medium- to fine-grained matrix ($133/80\,\mu m$) showing a strong foliation (see fig. 3.17 a)). This matrix is composed of recrystallized

quartz (35 %) aggregates, small zoisite and epidote grains, xenomorphic biotite grains (15 %) some calcite (10 %) and a low amount of plagioclase (10 %). Large elongate zoisite grains containing inclusions are abundant in the matrix (730/160 μm; together 25 %). Moreover elongate hornblende grains (665/175 μm; 5 %) also containing inclusions are distributed in the matrix. All elongate grains are oriented parallel forming a foliation and lineation. Opaque minerals and sphene are found as accessories.

Sample UL248, a **garnet-mica gneiss**, was selected for estimation of P-T conditions of the Vaddas nappe. The rock has a medium- to fine-grained (152/90 μm) matrix rich in quartz (40 %), but also alkali feldspar and plagioclase (together 30 %; see fig. 3.17 b)). Relatively small abundant biotite grains (15 %) are distributed in the matrix, as are bigger, less abundant idiomorphic grains of muscovite (10 %). Both micas are aligned parallel to the foliation. Embedded in the matrix are larger elongate feldspar crystals (780/520 μm), sometimes forming clusters of several grains. Few partially decomposed garnet grains (615/500 μm; 5 %) containing inclusions occur as porphyroclasts in the matrix. Thin irregular mono-mineralic quartz layers parallel to the foliation are sporadically present. Accessories are zircon, rutile, sphene, opaque minerals, apatite and zoisite.

In the Vaddas nappe microstructural descriptions focus on the garnet-mica gneiss UL248 which was selected for assessment of metamorphic P-T conditions of the nappe. The quartz in this sample has mostly a medium grain size (152/90 μm) and is distributed in the matrix. Sporadic undulating monomineralic quartz layers are observed formed by bigger grains (280/185 μm). Sometimes very elongate single crystals, that show undulose extinction and subgrains are observed in these layers (see fig. 3.18 a)). The subgrains are occasionally elongate just like in the samples from the KNC. Both plagioclase and alkali feldspar show clear undulose extinction, polysynthetic twinning, tapering deformation twins and microkinking. Myrmektitic intergrowth of quartz in plagioclase is observed along the rim of large alkali feldspar crystals (see fig. 3.18 b)). Both feldspars are partially sericitized. Biotite and muscovite are observed parallel to the foliation. Biotite has a small grain size and idiomorphic bigger muscovite grains are surrounded by a very thin biotite rim as a second later biotite generation (see fig. 3.18 c)). Large muscovite grains show usually undulose extinction and are occasionally bent. The sample contains only few medium-sized garnet crystals which are idiomorphic, contain few inclusions and start to be partially replaced by quartz along the rim. Inclusions are formed by quartz, plagioclase and biotite as well as sphene which is only found in the rim. Garnet grains are often cracked. Single small rutile and illmenite crystals distributed in the matrix oriented parallel to the foliation. The same applies for more abundant elongate sphene grains distributed in the matrix. Occasionally rutile grains are overgrown by a rim of sphene. An overview over the mineral assemblage and the sequence of relative mineral growth is

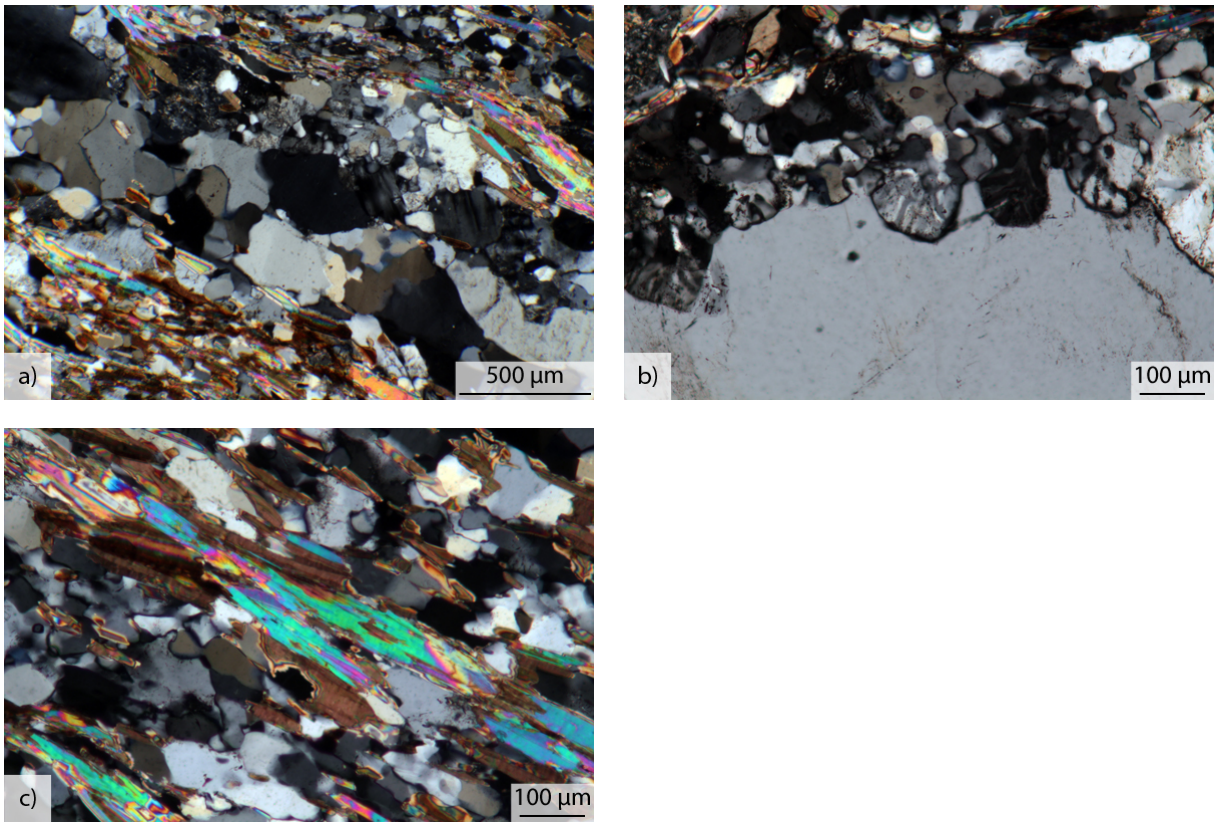

Fig. 3.18.: a) In the garnet-mica gneiss UL248 monomineralic quartz layers are formed by bigger grains showing undulose extinction and subgrains. b) Myrmekitic intergrowth of plagioclase in quartz is observed along the rim of big alkali feldspar crystals (UL248). c) Fine-grained biotite forms thin rims around large idiomorphic muscovite grains that are occasionally bent and show undulose extinction (UL248).

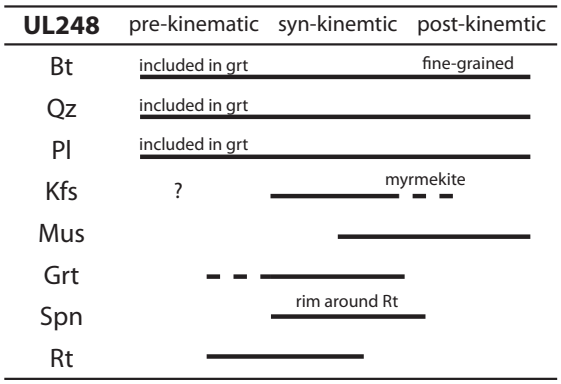

Fig. 3.19.: Overview over the mineral assemblage of sample UL248 and relative times of mineral growth.

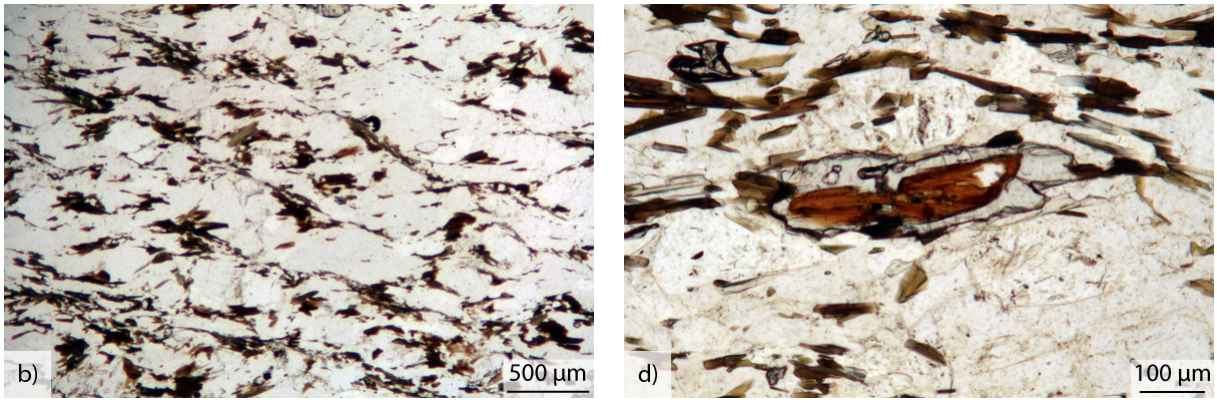

Fig. 3.20.: a) Shear bands formed by fine-grained biotite in the garnet-mica gneiss UL246 show a top to the NW sense of shear in the field. b) Zoisite is a common minerals in samples from the Vaddas nappe and often contains a brown allanite core (UL247).

shown in table 3.19.

Further samples from the Vaddas nappe show very similar microstructures. A distinct feature in the garnet-mica gneiss UL246 are C'-type shear bands formed by very fine-grained biotite indicating top to the NW shearing in the field (see fig. 3.20 a)). Garnet is in most samples meta-stable and largely replaced by quartz, chloritization occurs along cracks. A common mineral for samples from the Vaddas nappe is zoisite. It is found in different shapes, as small grains with a brown allanite core and a thin rim of zoisite with typical anomalous blue interference colors (UL247; see fig. 3.20 b)), as large elongate grains parallel to the foliation with anomalous gray-blue interference colors (UL373) or as large polygonal grains in a vein showing anomalous blue-yellow interference colors (UL463).

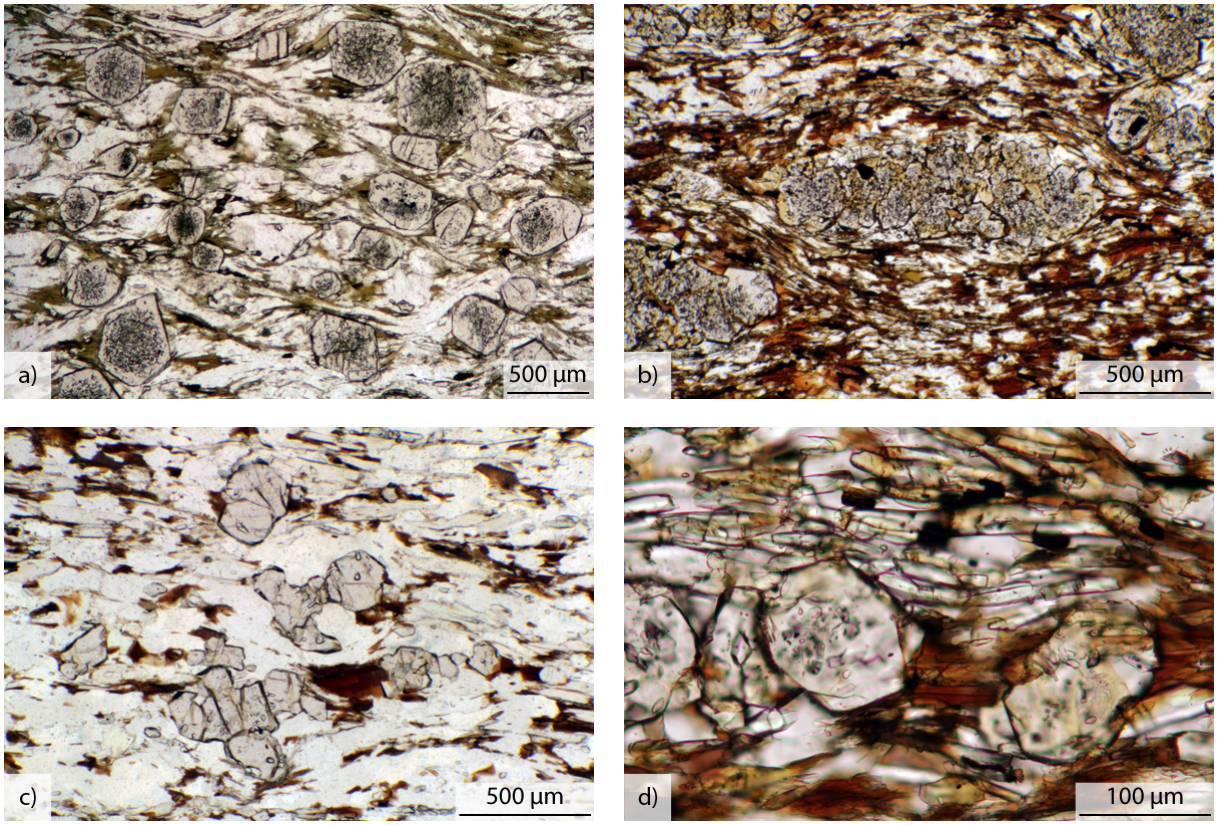

Fig. 3.21.: a) In some quartzitic garnet-mica schists of the Kåfjord nappe an SC'-type shear band cleavage is developed indicating a top to the SE regional sense of shear. Biotite is partially chloritized (UL366). b) The fine-grained kyanite-garnet-mica schists UL230 was chosen to assess P-T conditions of the Kåfjord nappe. Big garnet grains are embedded in the biotite-rich matrix. c) For estimation of P-T conditions of the boundary of the Kåfjord nappe with the Nordmannvik nappe UL234a as a quartzitic kyanite-garnet-mica schist was selected. d) Thin kyanite needles in UL230 are oriented parallel to the foliation and bend around garnet grains.

3.4.3. Kåfjord Nappe

Thin section UL366 is a typical **quartzitic garnet-mica schist** from the Kåfjord nappe (see fig. 3.21 a)). The rock exhibits a coarse- to medium grain-size ($223/121\,\mu m$) and due to strong shearing a C'-type shear band cleavage developed in the matrix indicating shearing top to the SE. The matrix is formed by elongate quartz (30-35 %) and plagioclase grains (20 %) as well as idiomorphic biotite (15-20 %) and muscovite (15 %) bent into the shear band cleavage. Quartz forms mono-mineralic aggregates which are interlayered with aggregates of biotite and/or muscovite. Minor amounts of prismatic tourmaline crystals (<3 %) are aligned parallel to the shear band cleavage. Idiomorphic garnet grains of different sizes ($429/377\,\mu m$; 10 %) are embedded in the matrix. The garnet has inclusion-rich centers surrounded by inclusion-poor rims. Relatively small elongate zoisite grains (<5 %) are distributed in the matrix. A wide ($4\,mm$) quartz vein crosscuts the thin section

parallel to the foliation. Accessories are rutile, sphene, tourmaline and zircon.

Kyanite-garnet-mica schist sample UL230 from the Kåfjord nappe was selected for estimation of P-T conditions during metamorphism (see fig. 3.21 b)). The fine-grained matrix (97/61 μm) is rich in biotite (35 %) and contains several slightly bigger muscovite grains (5-10 %). Quartz (25 %) fills intergranular space. Thin needles of kyanite (15 %) are abundant in the matrix aligned parallel to the foliation together with biotite and muscovite. Garnet grains (565/355 μm; 15 %) are embedded in the matrix deflecting the foliation. The garnet is rich in inclusions and the grains are often flattened parallel to the foliation. Tourmaline, monazite, opaques and apatite are found as accessory minerals.

The **quartzitic kyanite-garnet-mica schist** UL234a was chosen for assessment of the P-T conditions at the boundary of the Kåfjord nappe with the Nordmannvik nappe (see fig. 3.21 c)). The medium-grained (190/110 μm) schist has a relatively homogeneous matrix consisting of biotite (20 %) and muscovite (15 %) distributed between recrystallized quartz grains (30-40 %). Quartz grains are elongate and form a foliation together with the micas. A small amount of plagioclase and alkali feldspar (together 10 %) is also present. Clusters of relatively small idiomorphic garnet grains are distributed in the matrix (257/215 μm; 15 %). The garnet contains inclusions and is partially replaced by quartz or plagioclase. The clusters are stretched parallel to the foliation. Parts of the thin section contain abundant kyanite (5 %). The fine-grained short prisms and long needles are oriented parallel to the foliation. Accessories are zircon, rutile and opaque minerals .

The microstructural descriptions of the Kåfjord nappe focus on the kyanite-garnet-mica schist UL230 used for estimation of P-T conditions in the Kåfjord nappe itself and on the quartzitic kyanite-garnet-mica schist UL234a used for characterization of the P-T conditions at the boundary of the Kåfjord nappe with the Nordmannvik nappe. Sample UL230 is much more fine-grained than sample UL234a but the microstructures are very similar and because of the bigger grain size easier to recognize in UL234a. Relatively big quartz grains show even, undulose or stripy extinction as well as subgrains (see fig. 3.22 a)). Plagioclase and alkali feldspar show undulose extinction, tapering and bent twin lamellae as well as patches of polysynthetic twins. Furthermore small-scale myrmekite structures are observed in thin section UL234a (see fig. 3.22 b). Idiomorphic biotite and muscovite crystals are aligned parallel to the foliation (see fig. 3.22 a)). Both micas are surrounded by fine-grained biotite rims forming a later biotite generation. Muscovite grains are sometimes bent and show undulose extinction. Single muscovite grains grow across the foliation in thin section UL234a indicating post-kinematic growth. Medium-sized garnet crystals in UL230 are very rich in fine-grained inclusions with only a thin inclusion-poor rim. Inclusions are formed by biotite, quartz, plagioclase and opaques. The garnet grains are partially decomposed and sometimes elongate parallel to the foliation

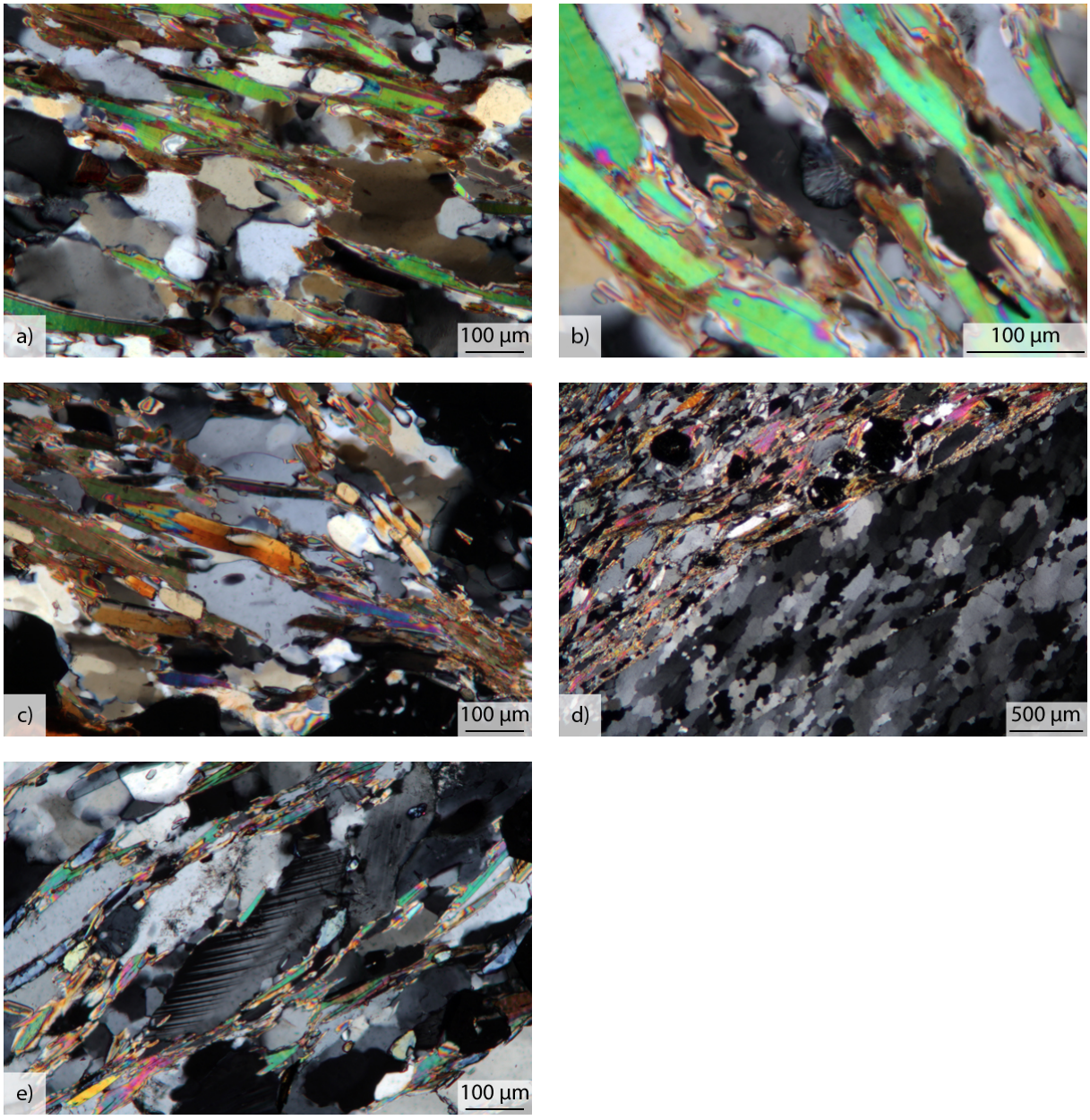

Fig. 3.22.: a) Quartz shows undulose extinction and subgrains in the quartzitic kyanite-garnet-mica schist UL234a. Biotite forms thin rims around muscovite grains. b) Small-scale myrmekite structures are observed in thin section UL234a. c) Abundant kyanite is aligned parallel to the foliation. Occasionally the crystals are bent showing undulose extinction or exhibit simple twinning (UL234a). d) Strongly elongate quartz grains in a vein in garnet-mica schist sample UL366 have a shape preferred orientation at an angle to the foliation indicating a top to the SE sense of shear in the field. e) Tapering twin lamellae in plagioclase are sometimes bent. Zoisite with the typical anomalous blue interference color is found as an accessory in some Kåfjord nappe samples (UL366).

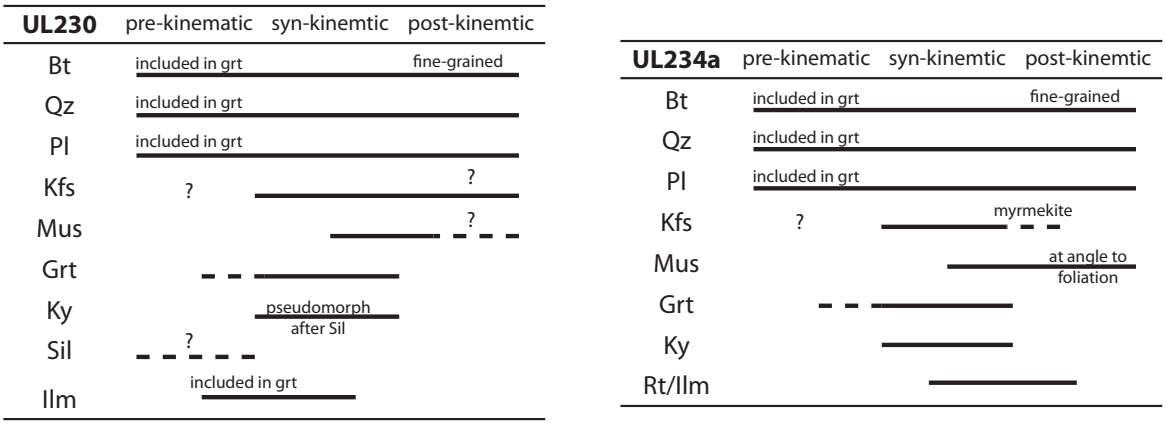

Fig. 3.23.: Overview over the mineral assemblage of sample UL230 and sample Ul234a showing relative times of mineral growth.

(see fig. 3.22 c)). In UL234a small idiomorphic garnet grains with few inclusions in the center form clusters parallel to the foliation (see fig. 3.22 d)). Inclusions are formed by biotite, quartz and plagioclase. Some garnet grains are partially replaced by quartz and have odd shapes. In UL230 thin kyanite needles are very abundant in the matrix parallel to the foliation (see fig. 3.21 d)). Kyanite grains exhibit a relatively low interference color and probably formed pseudomorph after sillimanite. Prismatic to short prismatic kyanite parallel to the foliation is also abundant in UL234a sometimes showing simple twinning. Occasionally kyanite is bent and shows distinct undulose extinction (see fig. 3.21 d) and 3.22 c)). Opaque minerals form an abundant accessory in thin section UL230 and the grains are aligned parallel to the foliation. In thin section UL234a both opaques and rutile are found as accessories parallel to the foliation but the opaques are more abundant. An overview over the mineral assemblage and the sequence of relative mineral growth for the samples UL230 and UL234a is shown in table 3.23.

A few other samples of the Kåfjord nappe show characteristic microstructures which are described below. A $0.4\,mm$ wide quartz vein in the garnet-mica schist UL366 runs parallel to the foliation (see fig. 3.22 b)). The large elongate quartz grains have interlobate boundaries, show undulose extinction and subgrains. The shape preferred orientation of the grains is at an angle to the foliation indicating top to the SE shearing in the field. C'-type shear bands in the matrix show the same sense of shear (see fig. 3.21 a)). The anastomosing and wavy shear bands are formed by very fine-grained biotite. In garnet-mica schist sample UL367 garnet sigma clasts and C'-type shear bands indicate a top to the ESE sense of shear. Furthermore grain boundaries of alkali feldspar and plagioclase crystals in UL366 are irregular, twin lamellae are bent and taper. Biotite in UL366 is partially chloritized.

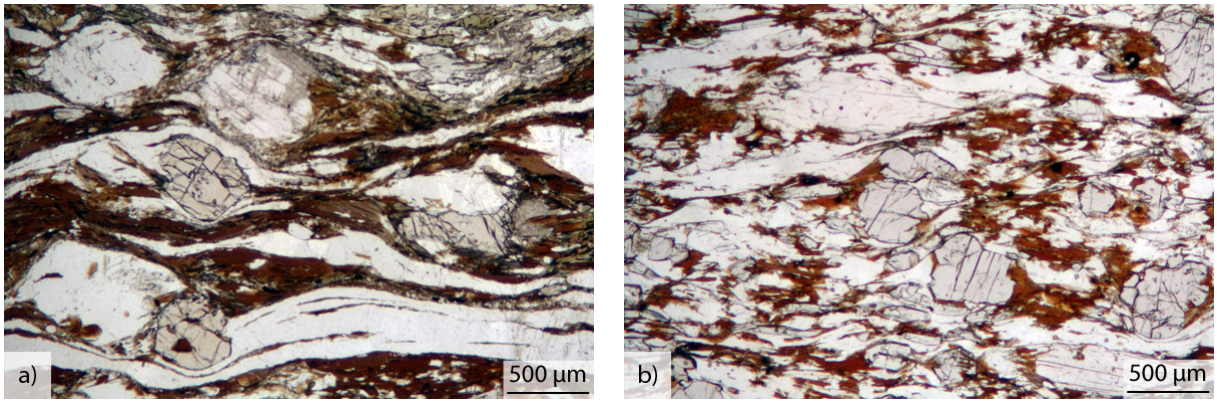

Fig. 3.24.: a) Migmatites of the Nordmannvik nappe show layering of quartz and biotite layers undulating around garnet and feldspar crystals. Biotite is partially chloritized and feldspar is sericitized (UL240). b) A sheared quartzitic kyanite garnet mica schist from the Nordmannvik nappe contains C'-type shear bands of fine-grained muscovite and biotite indicating a regional top to the SE sense of shear. Muscovite forms mica fish in the shear band cleavage and prismatic kyanite is bent around the garnet (UL237).

3.4.4. Nordmannvik Nappe

The microscopical structures of the **migmatised garnet-mica schist** UL240 are described representative for the less sheared Nordmannvik nappe (see fig. 3.24 a)). Recrystallized quartz (30-35 %) bands and bands of biotite (25-30 %) undulate around large crystals of often sericitized plagioclase (20 %) and hornblende (10 %; both up to >4.5 mm in diameter). The biotite layers contain fine-grained, recrystallized muscovite (<3 %). Only few garnet (671/521 μm; 5 %) grains are enclosed in the coarse-grained matrix. Biotite layers are sometimes fine-grained and partially chloritized. Elongate relatively small zoisite grains (330/150 μm, 3 %) that may contain a brown allanite core are distributed in the matrix. A relatively large leucosome in the thin section is formed by big recrystallized quartz grains and a very large sericitized plagioclase crystal. Zircon and apatite are found as accessories.

Sample UL237, a **kyanite-garnet-mica schist**, as a sheared sample form the Nordmannvik nappe was chosen to estimate P-T conditions (see fig. 3.24 b)). The medium-grained (420/195 μm) matrix shows shear band cleavage which is formed by idiomorphic biotite (35-40 %) and muscovite (10-15 %), elongate quartz grains (25-30 %) and prismatic kyanite (10-15 %). Furthermore, fine-grained biotite forms C'-type shear bands showing a top to the SE sense of shear. A few tourmaline crystals (<3 %) with clear zoning, observed as a change of color, are enclosed in the matrix. Relatively small idiomorphic garnet grains (468/359 μm; 5-10 %) are distributed in the matrix. Zircon, tourmaline, monazite, opaque minerals and apatite are found as accessory minerals.

Mircostructural descriptions of the Nordmannvik nappe concentrate mainly on the

sheared kyanite-garnet-mica schist UL237 chosen for P-T assessment. In monomineralic wavy quartz aggregates relatively big grains with bulging grain boundaries, undulose extinction and elongate subgrains are observed. This is seen very well in a leucosome of the less sheared migmatite sample UL242 (see fig. 3.25 a)). Here along the grain boundaries small ($46/37 \mu m$) recrystallized grains are observed and quartz grains are very large with more than $2.5\,mm$ in diameter. Feldspar in UL237 shows undulose extinction, tapering deformation lamellae and abundant flame perthite (see fig. 3.25 b)). Idiomorphic biotite is oriented parallel to the foliation. This idiomorphic biotite is overgrown by fine-grained biotite aggregates which also form C'-type shear bands in the matrix indicating a top to the SE sense of shear (see fig. 3.24 b)). This is in agreement with the C'-type shear bands in UL159. Bigger idiomorphic muscovite grains are aligned parallel to the foliation just like the biotite. The grains are often bent and form mica fish that show distinct undulose extinction. Small rounded garnet grains contain few inclusions of biotite, quartz, plagioclase and sometimes needles of sillimanite in the center (see 3.24 b)). Garnet is in general associated with quartz as well as biotite in the pressure shadow. Kyanite grains are distributed in the matrix parallel to the foliation and are occasionally bent (see fig. 3.25 c)). Opaque minerals are observed occasionally in thin section as well as relatively large tourmaline grains both aligned parallel to the foliation. An overview over the mineral assemblage and the sequence of relative mineral growth of sample UL237 is shown in table 3.26.

Other important microstructures for the Nordmannvik nappe are observed in the migmatitic samples UL240 and UL242. Large quartz grains in the leucosome of sample UL240 show rectangular subgrains as chessboard extinction (see fig. 3.25 d)). Furthermore large alkali feldspar crystals in the leucosome but also as porphyroclasts in the matrix show bent twin lamellae, tapering deformation twins, undulose extinction and microfractures. Parts of the large alkali feldspar porphyroclasts in UL242 show crystallographic misorientation along microfractures or twin lamellae (see fig. 3.25 e)). Moreover subgrains and smaller recrystallized grains are observed. In both thin sections some feldspar grains are almost completely sericitized, often sericitization occurs along twin lamellae or fractures. In the leucosome in migmatite sample UL242 very large muscovite crystals are folded, show distinct undulose extinction and occasionally kink bands (see fig. 3.25 f)). In the melanosome of thin section UL242 idiomorphic muscovite and brown green biotite grow at random orientations. Some crystals are bent and show undulose extinction. In UL240 biotite is strongly chloritized.

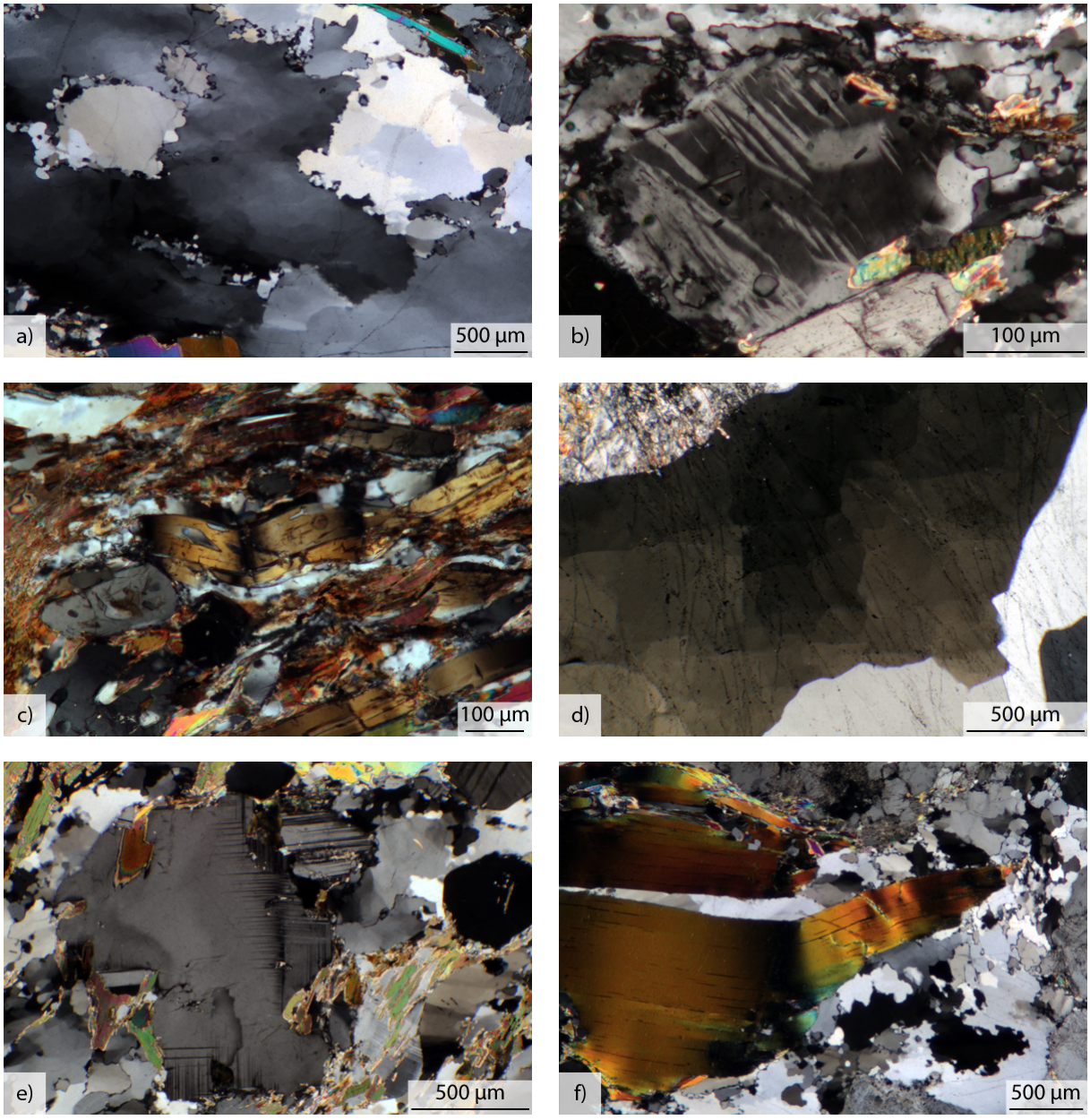

Fig. 3.25.: a) Leucosomes in the migmatite sample UL242 are formed by very large quartz grains with bulging boundaries. Small recrystallized grains along the boundaries are observed. Undulose extinction as well as subgrains are common. b) Flame perthite in alkali feldspar is abundant in thin section UL237. c) Abundant kyanite is oriented parallel to the foliation and occasionally bent showing undulose extinction (UL237). d) Large quartz grains in a leucosome in the migmatite UL240 show rectangular subgrains also known as chessboard extinction. e) Large subgrains are observed in alkali feldspar porphyorclasts as misorientation of part of the crystal along twin lamellae or microfractures (UL242). f) Very large muscovite grains in a leucosome in UL242 are folded and show distinct undulose extinction.

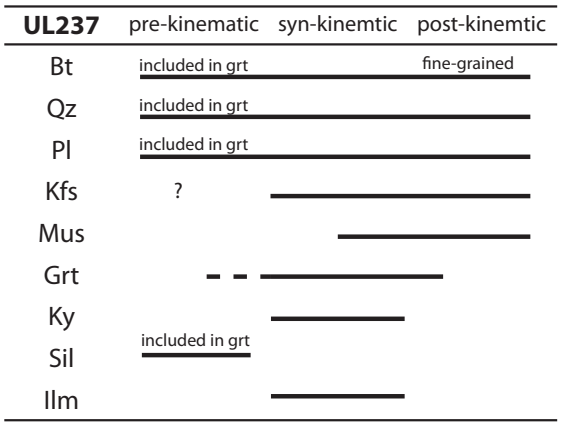

Fig. 3.26.: Overview over the mineral assemblage of sample UL237 and relative times of mineral growth.

3.5. Mineral Chemistry

Five samples from the different nappes exposed on Uløya and from the boundary of the Kåfjord with the Nordmannvik nappe were selected for phase equilibrium modeling. The microstructures of these samples were described above in detail. In the following the bulk rock chemical composition from XRF analysis and the chemical compositions of garnet, biotite, feldspar and muscovite from microprobe analysis are presented. Table 3.1 gives an overview of the mineral assemblages of the selected samples. The bulk rock chemical compositions are listed in table 3.2.

	Main minerals							Accessory minerals							
Sample	Bt	Pl	Qtz	Grt	Kfs	Ky/sil	Ms	Zrn	Tur	Mnz	Rt	Spn	Opq	Ap	Zoi/Aln/Ep
UL250	x	x	x	x	x		x	x			x	x	x	x	x
UL248	x	x	x	x	x		x	x			x	x	x	x	x
UL230	x	x	x	x	x	x/x	x		x	x			x	x	
UL234a	x	x	x	x	x	x	x	x			x		x		
UL237	x		x	x	x	x	x	x	x	x			x	x	

Table 3.1.: Paragenesis overview of the five samples selected for estimation of P-T conditions.

Sample	UL250	UL248	UL230	UL234a	UL237
Na_2O	3.36	2.61	1.10	1.15	0.70
MgO	1.76	0.98	2.46	2.14	2.55
Al_2O_3	14.69	13.41	20.25	15.43	18.66
SiO_2	66.43	72.31	58.59	66.21	60.21
P_2O_5	0.32	0.10	0.20	0.16	0.20
K_2O	2.26	3.78	4.46	4.50	5.00
CaO	3.10	1.75	1.07	1.15	0.29
TiO_2	1.23	0.68	0.95	0.87	0.90
MnO	0.15	0.09	0.10	0.08	0.09
Fe_2O_3	6.74	3.74	8.87	6.88	9.98
Cr_2O_3	0.01	b.d.	0.01	0.01	0.01
NiO	0.01	0.01	0.01	0.01	0.01
H_2O	0.05	0.06	0.06	0.04	0.06
LOI	0.61	0.52	1.01	0.73	0.52
Total Wt%	100.71	100.04	99.16	99.35	99.18

Table 3.2.: Bulk rock chemical composition of five samples from the different nappes and the Kåfjord-Nordmannvik boundary measured with XRF are given in wt%. (LOI - loss on ignition; b.d. - below detection)

3.5.1. Kalak Nappe Complex - Sample UL250

Sample UL250 was selected for phase equilibrium modeling representative for the KNC. The quartzitic garnet-mica schist composes of biotite, plagioclase, alkali feldspar, muscovite, garnet and quartz. Accessories are abundant sphene, as well as zircon, rutile, opaque minerals, apatite and zoisite. The bulk rock chemical composition of the sample is shown in table 3.2. Representative microprobe analyses of garnet, biotite, plagioclase and muscovite are shown in table 3.3.

Garnet contains a high proportion of the almandine component with an average mol fraction of 0.57. Mol fractions of grossular range from 0.23 to 0.32. With mol fractions of 0.01 to 0.15 the spessartine component is variable. X_{Mg} in garnet varies very little around the average value of 0.10. The variable mol fractions of the different endmembers indicate weak zoning of the garnet which is seen in garnet element maps and profiles (see fig. 3.27). Garnet cores are enriched in spessartine while the rims are enriched in almandine. Although the garnet zoning is weak, plotting the garnet measurements in a ternary diagram also shows a higher content of the almandine component in the garnet rims (see fig. 3.28).

Biotite shows chemical variation with X_{Mg}-values ranging from 0.35 to 0.45. The highest values were measured in biotite inclusions in garnet with values of 0.42 to 0.45 X_{Mg}. Atoms per formula unit (a.p.f.u) of Ti in biotite vary with values of 0.06 to 0.23 and an average of 0.15. Microprobe measurements of plagioclase show that the anorthite component in plagioclase ranges from 0.17 to 0.28 mol fractions (see fig. 3.29). Therefore plagioclase is classified as oligoclase. Muscovite shows X_{Mg}-values of 0.44 to 0.56 with an average of 0.53 X_{Mg}. A.p.f.u. of Si in muscovite show little variation with values of 3.04 to 3.22 and an average of 3.19.

UL250	Grt rim	Grt core	Bt	Bt inclusion	Pl	Mus
Wt%						
Analysis No.	658	679	730	719	767	732
SiO_2	37.74	37.57	36.21	36.60	62.20	46.84
TiO_2	0.00	0.06	1.88	2.21	0.00	0.87
Cr_2O_3	0.00	0.00	0.03	0.02	0.00	0.04
Al_2O_3	21.58	21.51	17.69	17.82	23.67	31.20
FeO	28.22	26.19	21.56	19.65	0.03	2.49
MnO	0.99	3.66	0.09	0.03	0.00	0.03
NiO	0.00	0.00	0.00	0.00	0.00	0.00
MgO	1.70	1.60	8.51	9.02	0.00	1.59
CaO	9.97	9.87	0.00	0.10	4.72	0.00
Na_2O	0.00	0.00	0.09	0.18	9.11	0.51
K_2O	0.00	0.00	9.14	9.41	0.15	10.64
Total	100.20	100.47	95.20	95.05	99.88	94.21
a.p.f.u.						
Oxygen No.	12	12	11	11	8	11
Si	2.99	2.98	2.86	2.88	2.75	3.17
Ti	0.00	0.00	0.11	0.13	0.00	0.04
Cr	0.00	0.00	0.00	0.00	0.00	0.00
Al	2.02	2.01	1.65	1.65	1.23	2.49
Fe^{3+}	0.00	0.03	0.00	0.00	0.00	0.06
Fe^{2+}	1.87	1.71	1.43	1.29	0.00	0.08
Mn	0.07	0.25	0.01	0.00	0.00	0.00
Ni	0.00	0.00	0.00	0.00	0.00	0.00
Mg	0.20	0.19	1.00	1.06	0.00	0.16
Ca	0.85	0.84	0.00	0.01	0.22	0.00
Na	0.00	0.00	0.01	0.03	0.78	0.07
K	0.00	0.00	0.92	0.94	0.01	0.92
H	-	-	2.00	2.00	-	2.00
F	-	-	0.00	0.00	-	0.00
Cl	-	-	0.00	0.00	-	0.00
Total	8.00	8.00	8.00	8.00	5.00	7.00
X_{Mg}	0.10	0.10	0.41	0.45		0.53
Prp	0.07	0.06				
Alm	0.62	0.56				
Grs	0.28	0.27				
Sps	0.02	0.08				
An					0.22	
Alb					0.77	
Or					0.01	

Table 3.3.: Representative microprobe analyses of garnet, biotite, plagioclase and muscovite of sample UL250 from the KNC. The measured weight percent of the oxides are shown as well as calculated a.p.f.u. and endmember concentrations of the different minerals in mol fractions.

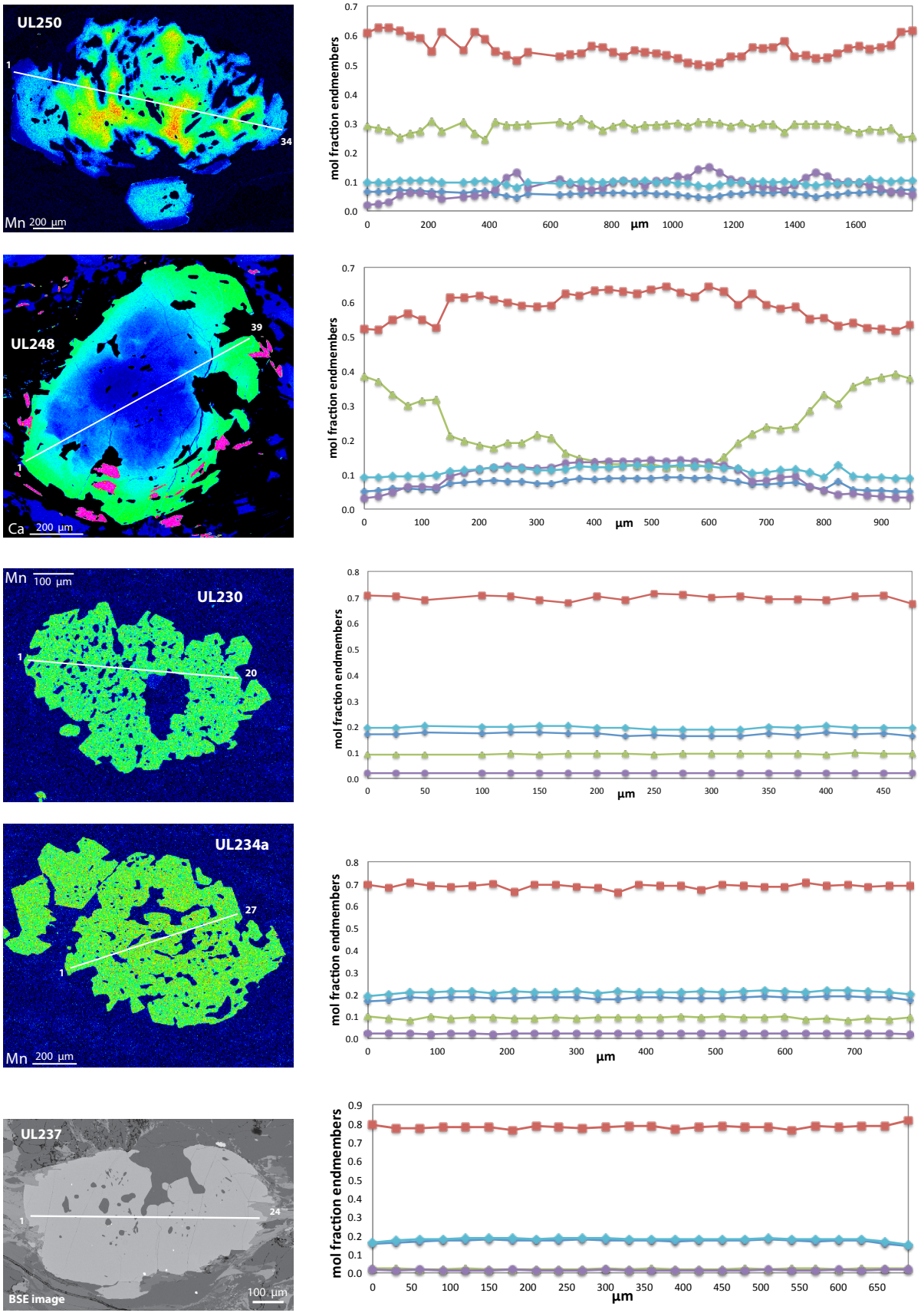

Fig. 3.27.: Garnet element maps or BSE pictures and corresponding profiles showing the end-member mol fractions of almandine (red), grossular (green), spessartine (purple) and pyrope (blue), as well as X_{Mg} (turquoise) for the samples UL250, UL248a, UL230, UL234a and UL237 from top to bottom.

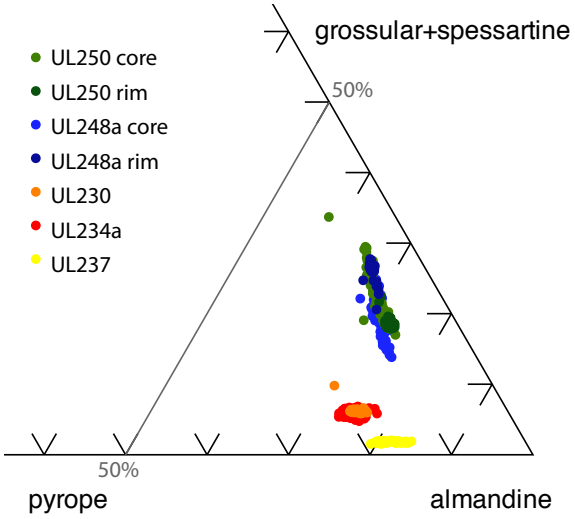

Fig. 3.28.: Compositions of garnet from all nappes plotted in a ternary diagram show that garnet contains a high amount of almandine component in all samples. In UL250 and UL248a, the garnet shows chemical zoning.

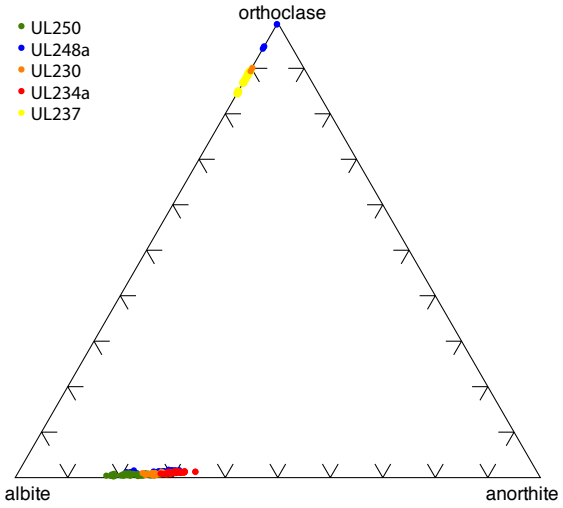

Fig. 3.29.: Feldspar compositions of all samples plotted in a ternary diagram show that both alkali feldspar and plagioclase are present in the samples. The plagioclase has a relatively high albite component and plots in the oligoclase and andesine field. Alkali feldspar has high orthoclase contents.

3.5.2. Vaddas Nappe - Sample UL248

Microprobe and whole rock analyses of sample UL248 were conducted to obtain the P-T conditions of metamorphism in the Vaddas nappe. The garnet-mica gneiss composes of biotite, plagioclase, alkali feldspar, muscovite, garnet and quartz. Accessory minerals are sphene, zircon, rutile, opaque minerals, apatite and zoisite. The bulk rock chemical composition is shown in table 3.2. Representative microprobe analyses of garnet, biotite, alkali feldspar, plagioclase and muscovite are listed in table 3.4.

With mol fractions of 0.51 to 0.66 almandine has the highest endmember concentration in garnet. Mol fractions of grossular range from 0.10 in the core to 0.40 in the rim of the garnet crystals. Spessartine mol fractions vary from 0.14 in the core to 0.03 in the rim. X_{Mg}-values in garnet show little variation between 0.08 and 0.13. The strong zoning of the garnet is seen in an element map and a garnet profile shown in figure 3.27. Opposite to garnet in the KNC the rims are slightly depleted in the almandine component which is also seen in the ternary diagram in which garnet compositions of all samples are shown 3.28. Furthermore garnet cores are enriched in spessartine whereas the rims are enriched in grossular.

X_{Mg} in biotite ranges from 0.35 to 0.46 similar to the values of X_{Mg} in biotite of the KNC. The cores and the rims of biotite grains show variable X_{Mg}-values as do inclusions of biotite in garnet. A.p.f.u of Ti in biotite show a range of values between 0.08 to 0.22. The anorthite component in plagioclase reaches mol fractions from 0.21 to 0.30 classifying the plagioclase as oligoclase. Alkali feldspar contains mol fractions of 0.94 to 0.99 orthoclase. Muscovite shows X_{Mg}-values of 0.42 to 0.58. The a.p.f.u. of Si in muscovite exhibit values from 3.08 to 3.27 with an average of 3.18.

3.5.3. Kåfjord Nappe - Sample UL230

The kyanite-garnet-mica schist UL230 was chemically analyzed for phase equilibrium modeling representative for the Kåfjord nappe. The rock is composed of biotite, plagioclase, alkali feldspar, muscovite, garnet, kyanite and quartz. Tourmaline, monazite, opaque minerals and apatite are found as accessory minerals. The bulk rock chemical composition is shown in table 3.2. Representative microprobe analyses of garnet, biotite, plagioclase, alkali feldspar and muscovite are listed in table 3.5.

Garnet contains high mol fractions of almandine which range from 0.66 to 0.72. Mol fractions of grossular vary little between 0.09 and 0.10. The spessartine component in garnet is low with mol fractions of 0.01 to 0.02. With a range of 0.18 to 0.21 the X_{Mg}-values in garnet vary also little. Therefore garnet profiles are flat and element maps do not show zoning (see fig. 3.27). The garnet is chemically different from the garnet of

UL248	Grt core	Grt rim	Bt	Bt inclusion	Pl	Kfs	Mus
Wt%							
Analysis No.	149	127	178	183	186	123	207
SiO_2	37.53	38.12	36.60	36.61	60.29	63.94	46.32
TiO_2	0.02	0.22	2.71	3.67	0.00	0.00	1.08
Cr_2O_3	0.00	0.00	0.00	0.00	0.00	0.00	0.03
Al_2O_3	21.60	21.42	17.20	18.46	24.75	18.59	33.27
FeO	29.03	24.11	22.16	18.16	0.07	0.22	2.41
MnO	6.33	1.42	0.17	0.20	0.00	0.00	0.02
NiO	0.00	0.00	0.00	0.00	0.00	0.00	0.00
MgO	2.33	1.34	7.44	8.52	0.00	0.00	1.09
CaO	4.40	13.84	0.01	0.00	6.18	0.00	0.00
Na_2O	0.00	0.00	0.05	0.20	8.17	0.62	0.36
K_2O	0.00	0.00	10.26	10.15	0.29	16.62	11.25
Total	101.24	100.47	96.61	95.97	99.75	99.99	95.81
a.p.f.u.							
Oxygen No.	12	12	11	11	8	8	11
Si	2.98	3.00	2.87	2.86	2.68	2.95	3.09
Ti	0.00	0.01	0.16	0.22	0.00	0.00	0.05
Cr	0.00	0.00	0.00	0.00	0.00	0.00	0.00
Al	2.02	1.99	1.59	1.70	1.30	1.01	2.61
Fe^{3+}	0.02	0.00	0.00	0.00	0.00	0.01	0.11
Fe^{2+}	1.90	1.59	1.46	1.18	0.00	0.00	0.03
Mn	0.43	0.09	0.01	0.01	0.00	0.00	0.00
Ni	0.00	0.00	0.00	0.00	0.00	0.00	0.00
Mg	0.28	0.16	0.87	0.99	0.00	0.00	0.11
Ca	0.37	1.17	0.00	0.00	0.29	0.00	0.00
Na	0.00	0.00	0.01	0.03	0.70	0.06	0.05
K	0.00	0.00	1.03	1.01	0.02	0.98	0.96
H	-	-	2.00	2.00	-	-	2.00
F	-	-	0.00	0.00	-	-	0.00
Cl	-	-	0.00	0.00	-	-	0.00
Total	8.00	8.00	8.00	8.00	5.00	5.00	7.00
X_{Mg}	0.12	0.09	0.37	0.46			0.45
Prp	0.09	0.05					
Alm	0.64	0.52					
Grs	0.12	0.38					
Sps	0.14	0.03					
An					0.29	0.00	
Alb					0.69	0.05	
Or					0.02	0.95	

Table 3.4.: Representative microprobe analyses of garnet, biotite, plagioclase, alkali feldspar and muscovite of sample UL248 from the Vaddas nappe. The measured weight percent of the oxides are shown as well as calculated a.p.f.u. and endmember concentrations of the different minerals in mol fractions.

UL230	Grt core	Grt rim	Bt	Bt inclusion	Pl	Kfs	Mus
Wt%							
Analysis No.	325	315	358	348	397	399	388
SiO_2	38.10	38.10	36.56	37.05	61.94	64.64	47.63
TiO_2	0.01	0.03	4.15	3.52	0.00	0.00	1.70
Cr_2O_3	0.00	0.00	0.03	0.06	0.00	0.00	0.03
Al_2O_3	21.85	21.79	18.81	18.55	24.23	18.55	33.78
FeO	32.61	32.62	15.96	15.24	0.14	0.29	1.00
MnO	0.89	0.99	0.05	0.05	0.00	0.00	0.03
NiO	0.00		0.00		0.00	0.00	0.00
MgO	4.25	4.41	9.37	11.06	0.00	0.00	1.19
CaO	3.30	3.29	0.00	0.00	5.35	0.03	0.00
Na_2O	0.00	0.00	0.10	0.10	9.03	1.20	0.38
K_2O	0.00	0.00	10.20	10.34	0.11	15.60	11.15
Total	101.01	101.23	95.22	95.97	100.80	100.31	96.90
a.p.f.u.							
Oxygen No.	12	12	11	11	8	8	11
Si	3.00	2.99	2.86	2.84	2.72	2.96	3.13
Ti	0.00	0.00	0.24	0.20	0.00	0.00	0.08
Cr	0.00	0.00	0.00	0.00	0.00	0.00	0.00
Al	2.03	2.01	1.73	1.68	1.25	1.00	2.62
Fe^{3+}	0.00	0.01	0.00	0.00	0.01	0.01	0.00
Fe^{2+}	2.14	2.13	1.04	0.98	0.00	0.00	0.05
Mn	0.06	0.07	0.00	0.00	0.00	0.00	0.00
Ni	0.00	0.00	0.00	0.00	0.00	0.00	0.00
Mg	0.50	0.52	1.09	1.26	0.00	0.00	0.12
Ca	0.28	0.28	0.00	0.00	0.25	0.00	0.00
Na	0.00	0.00	0.01	0.01	0.77	0.11	0.05
K	0.00	0.00	1.02	1.01	0.01	0.91	0.94
H	-	-	2.00	2.00	-	-	2.00
F	-	-	0.00	0.00	-	-	0.00
Cl	-	-	0.00	0.00	-	-	0.00
Total	8.00	8.00	8.00	8.00	5.00	5.00	7.00
X_{Mg}	0.19	0.19	0.51	0.56			0.68
Prp	0.17	0.17					
Alm	0.71	0.71					
Grs	0.09	0.09					
Sps	0.02	0.02					
An					0.25	0.00	
Alb					0.75	0.10	
Or					0.01	0.89	

Table 3.5.: Representative microprobe analyses of garnet, biotite, plagioclase, alkali feldspar and muscovite of sample UL230 from the Kåfjord nappe. The measured weight percent of the oxides are shown as well as calculated a.p.f.u. and the endmember concentrations of the different minerals in mol fractions.

the samples from the KNC and the Vaddas nappe containing a higher amount of the almandine component and a lower amount of the grossular and spessartine components (see fig. 3.28).

Biotite shows X_{Mg}-values of 0.51 to 0.57 with an average of 0.53. Inclusions of biotite in garnet show the highest values of 0.56 to 0.57. A.p.f.u. of Ti in biotite show a range of values from 0.13 to 0.25. Mol fractions of anorthite in plagioclase range from 0.24 to 0.29 similar to the KNC and the Vaddas nappe (see fig. 3.29). The plagioclase is therefore classified as oligoclase. With 0.89 to 0.90 the mol fractions of orthoclase in alkali feldspar are relatively high. Muscovite exhibits X_{Mg}-values of 0.59 to 0.69 with an average of 0.65. A.p.f.u. of Si in muscovite vary between 3.10 and 3.16.

3.5.4. Boundary Kåfjord with Nordmannvik Nappe - Sample UL234a

Sample UL234a was taken from the Kåfjord and Nordmannvik nappe boundary. The quartzitic kyanite-garnet-mica schist contains biotite, plagioclase, alkali feldspar, muscovite, garnet, kyanite and quartz. Accessory minerals are zircon, rutile and opaques. The bulk rock chemical composition is very similar to sample UL230 as shown in table 3.2. Representative microprobe analysis of garnet, biotite, plagioclase and muscovite are listed in table 3.6.

Mol fractions of almandine in garnet are high with values of 0.66 to 0.72. Grossular mol fractions range from 0.07 to 0.10. With values of 0.01 to 0.03, the mol fractions of spessartine are low. X_{Mg} in garnet varies between 0.17 and 0.22 with an average of 0.20. The chemical composition of the garnet is homogeneous confirmed by homogeneous element maps (see fig. 3.27). Only a thin rim with decreased X_{Mg}-values and increased mol fractions of grossular is seen in garnet profiles. In general garnet compositions are identical to the garnet in the Kåfjord nappe sample (see fig. 3.28).

X_{Mg} in biotite exhibits values of 0.50 to 0.63. High values between 0.57 and 0.63 were measured in biotite included in garnet. Furthermore biotite contains 0.11 to 0.25 a.p.f.u. Ti. Plagioclase contains mol fractions of anorthite between 0.27 and 0.34 with an average of 0.30. The plagioclase is classified as oligolcase (<0.30 An) and andesine (>0.30 An). Muscovite shows X_{Mg}-values of 0.62 to 0.71 with an average of 0.64. A.p.f.u. of Si in muscovite range from 3.11 to 3.15.

UL234a	Grt core	Grt rim	Bt	Bt inclusion	Pl	Mus
Wt%						
Analysis No.	50	38	106	90	114	181
SiO_2	38.38	37.84	36.38	37.06	59.51	46.93
TiO_2	0.05	0.03	3.41	3.44	0.00	1.69
Cr_2O_3	0.00	0.00	0.03	0.06	0.00	0.03
Al_2O_3	21.86	21.86	18.56	18.78	25.31	33.35
FeO	31.05	32.37	15.96	13.68	0.06	1.15
MnO	1.01	0.99	0.00	0.04	0.00	0.02
NiO	0.00	0.00		0.00	0.00	0.00
MgO	4.66	4.29	10.51	11.80	0.00	1.17
CaO	3.50	3.53	0.01	0.02	6.83	0.00
Na_2O	0.00	0.00	0.11	0.12	8.01	0.35
K_2O	0.00	0.00	10.02	9.99	0.23	11.09
Total	100.51	100.90	94.98	94.98	99.95	95.78
a.p.f.u.						
Oxygen No.	12	12	11	11	8	11
Si	3.02	2.98	2.83	2.85	2.64	3.13
Ti	0.00	0.00	0.20	0.20	0.00	0.09
Cr	0.00	0.00	0.00	0.00	0.00	0.00
Al	2.03	2.03	1.70	1.70	1.33	2.62
Fe^{3+}	0.00	0.02	0.00	0.00	0.00	0.00
Fe^{2+}	2.04	2.11	1.04	0.88	0.00	0.06
Mn	0.07	0.07	0.00	0.00	0.00	0.00
Ni	0.00	0.00	0.00	0.00	0.00	0.00
Mg	0.55	0.50	1.22	1.35	0.00	0.12
Ca	0.29	0.30	0.00	0.00	0.33	0.00
Na	0.00	0.00	0.02	0.02	0.69	0.05
K	0.00	0.00	0.99	0.98	0.01	0.94
H	-	-	2.00	2.00	-	2.00
F	-	-	0.00	0.00	-	0.00
Cl	-	-	0.00	0.00	-	0.00
Total	8.00	8.00	8.00	8.00	5.00	7.00
X_{Mg}	0.21	0.19	0.54	0.61		0.65
Prp	0.18	0.17				
Alm	0.66	0.70				
Grs	0.10	0.10				
Sps	0.02	0.02				
An					0.32	
Alb					0.67	
Or					0.01	

Table 3.6.: Representative microprobe analyses of garnet, biotite, plagioclase and muscovite of sample UL234a from the Kåfjord-Nordmannvik boundary. The measured weight percent of the oxides are shown as well as calculated a.p.f.u. and the endmember concentrations of the different minerals in mol fractions.

3.5.5. Nordmannvik Nappe - Sample UL237

The sheared kyanite-garnet-mica schist sample UL237 was chosen for phase equilibrium modeling of the Nordmannvik nappe. The rock is composed of biotite, plagioclase, alkali feldspar, muscovite, garnet, kyanite and quartz. Zircon, tourmaline, monazite, opaque minerals and apatite are found as accessories. The bulk rock chemical composition is shown in table 3.2. Representative microprobe analysis for garnet, biotite, alkali feldspar and muscovite are listed in table 3.7.

The garnet in UL237 exhibits the highest almandine components of all samples with mol fractions of 0.73 to 0.82. Mol fractions of grossular and spessartine are with values of 0.01 to 0.03 low. X_{Mg} in garnet varies between 0.14 and 0.19. Garnet profiles are flat

with only thin rims of increased mol fractions of almandine and decreased X_{Mg}-values (see fig. 3.27). The grossular and spessartine curves overlap in the profile as do the X_{Mg} and pyrope curves. Garnet element maps show a homogeneous garnet composition (see fig. 3.27). A depletion of the grossular and spessartine components in comparison to the other samples is seen in figure 3.28.

Biotite shows X_{Mg}-values of 0.45 to 0.59 again with the highest values of 0.54 and above observed in biotite included in garnet. Values of a.p.f.u. Ti in biotite show a range of 0.10 to 0.24. The orthoclase component in alkali feldspar reaches mol fractions of 0.85 to 0.89. Muscovite exhibits X_{Mg}-values of 0.55 to 0.61 with an average of 0.58. Furthermore a.p.f.u. Si in muscovite range from 3.09 to 3.13.

UL237	Grt core	Grt rim	Bt	Bt inclusion	Kfs	Mus
Wt%						
Analysis No.	328	319	354	412	470	355
SiO_2	38.02	37.82	35.91	36.64	64.53	46.59
TiO_2	0.00	0.04	3.23	3.46	0.00	1.06
Cr_2O_3	0.00	0.00	0.05	0.04	0.00	0.02
Al_2O_3	21.68	21.72	17.96	19.64	18.84	33.49
FeO	35.39	35.99	19.11	14.93	0.03	1.37
MnO	0.63	0.67	0.03	0.06	0.00	0.00
NiO	0.00	0.00	0.00	0.00	0.00	0.00
MgO	4.60	3.94	9.80	11.15	0.00	1.12
CaO	0.68	0.79	0.00	0.00	0.02	0.00
Na_2O	0.00	0.00	0.14	0.24	1.81	0.38
K_2O	0.00	0.00	10.04	10.26	15.06	11.38
Total	101.00	100.97	96.26	96.42	100.28	95.41
a.p.f.u.						
Oxygen No.	12	12	11	11	8	11
Si	3.00	3.00	2.78	2.79	2.95	3.11
Ti	0.00	0.00	0.19	0.20	0.00	0.05
Cr	0.00	0.00	0.00	0.00	0.00	0.00
Al	2.02	2.03	1.64	1.76	1.01	2.63
Fe^{3+}	0.00	0.00	0.00	0.00	0.00	0.06
Fe^{2+}	2.34	2.39	1.24	0.95	0.00	0.02
Mn	0.04	0.05	0.00	0.00	0.00	0.00
Ni	0.00	0.00	0.00	0.00	0.00	0.00
Mg	0.54	0.47	1.13	1.27	0.00	0.11
Ca	0.06	0.07	0.00	0.00	0.00	0.00
Na	0.00	0.00	0.02	0.04	0.16	0.05
K	0.00	0.00	0.99	1.00	0.88	0.97
H	-	-	2.00	2.00	-	2.00
F	-	-	0.00	0.00	-	0.00
Cl	-	-	0.00	0.00	-	0.00
Total	8.00	8.00	8.00	8.00	5.00	7.00
X_{Mg}	0.19	0.16	0.48	0.57		0.59
Prp	0.18	0.15				
Alm	0.78	0.79				
Grs	0.02	0.02				
Sps	0.01	0.01				
An					0.00	
Alb					0.15	
Or					0.84	

Table 3.7.: Representative microprobe analyses of garnet, biotite, alkali feldspar and muscovite of sample UL237 from the Nordmannvik nappe. The measured weight percent of the oxides are shown as well as calculated a.p.f.u. and the endmember concentrations of the different minerals in mol fractions.

3.6. Phase Equilibrium Modeling

Phase equilibrium modeling was conducted for five samples, one from each nappe and one from the boundary of the Kåfjord with the Nordmannvik nappe. Calculations were performed with PerpleX version 6.6.8 (Connolly 2005) in the MnNCKFMASHTi system using XRF whole rock compositions listed in table 3.2. For modeling, calcium in apatite was subtracted from the whole rock composition according to the measured amount of phosphor. Trivalent iron was recalculated into divalent iron. All pseudosections were calculated using weight percent of the oxides of the whole rock composition. Fluids in the calculations were regarded as a pure water phase. The phase mixing models used are listed in chapter 2 Methodology. Isopleths in the presented pseudosections are plotted to show the measured chemical compositions or volume percent of different minerals in the phase field of interest to better constrain the estimated P-T conditions.

3.6.1. Kalak Nappe Complex - Sample UL250

The quartzitic garnet-mica schist UL250 from the KNC was used for estimation of the P-T conditions of the KNC. The pseudosection was calculated with H_2O in excess (see fig. 3.30). The peak mineral assemblage is formed by biotite, plagioclase, alkali feldspar, muscovite, garnet, quartz, rutile and sphene. The results of the phase equilibrium modeling show a similar mineral assemblage but alkali feldspar and sphene are not stable in the phase field of peak metamorphic conditions. Alkali feldspar is absent in the pseudosection while sphene is stable towards lower temperatures. Metamorphic conditions are estimated to pressures of ∼9-12 kbar and temperatures of ∼610-690°C constrained by isopleths of 0.09-0.11 X_{Mg} in garnet and mol fractions of 0.23-0.31 of grossular in garnet. The actual estimate represents a P-T interval in which the isopleths of single garnet measurements cross corresponding to the garnet rim and core compositions. Isopleths of 0.04-0.07 mol fractions of spessartine in garnet rims plot also within the estimated P-T field. Furthermore isopleths of 0.38-0.43 X_{Mg} in biotite are in agreement with the P-T estimate. Very high X_{Mg}-values measured in biotite inclusions in garnet plot above the estimate at higher pressures. In addition the isopleths of 0.21-0.27 mol fractions of anorthite in plagioclase and 3.04-3.14 a.p.f.u. of Si in muscovite plot within the estimated P-T range.

3.6.2. Vaddas Nappe - Sample UL248

The garnet mica gneiss UL248 was used for assessment of P-T conditions in the Vaddas nappe. The pseudosection was calculated with H_2O in excess and is shown in figure 3.31. Biotite, plagioclase, alkali feldspar, muscovite, garnet, quartz, rutile and sphene form the peak mineral assemblage of the sample. Isopleths of 0.08-0.13 X_{Mg} in garnet and mol

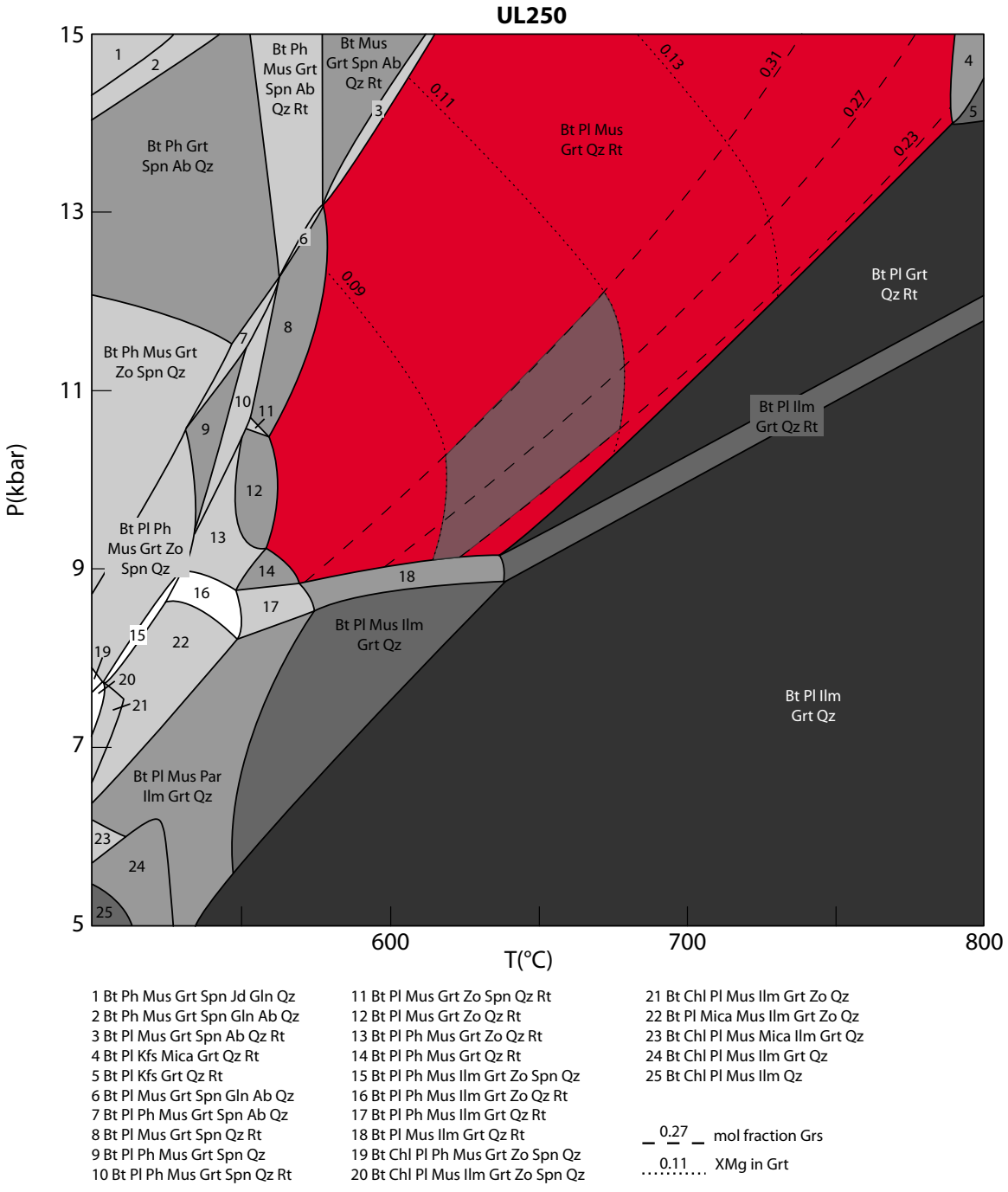

Fig. 3.30.: The pseudosection of sample UL250 from the KNC was calculated water-saturated. Isopleths showing the X_{Mg}-values in garnet and the mol fraction of grossular in garnet limit the P-T estimate to pressures of ∼9-12 kbar and temperatures of ∼610-690°C.

fractions of 0.10-0.40 of grossular in garnet were used to constrain the P-T estimate. Since the garnet is strongly zoned, as seen in element maps and garnet profiles described above (see fig. 3.27), the isopleths for single measurements cross over a range of P-T conditions. The endmembers of this P-T range are marked in the pseudosection. Garnet cores plot at pressures of ∼8.5-10 kbar and temperatures of ∼680-740°C while the garnet rims plot at ∼13-14 kbar and ∼670-710°C. Furthermore the garnet cores plot in a phase field where rutile is stable while the rims plot in a phase field where sphene is stable. Accordingly both minerals are found in thin section. Isopleths of 0.05-0.14 mol fractions of spessartine in garnet as well as isopleths of 0.35-0.39 X_{Mg} in biotite agree with the medium- to high-pressure estimate of the garnet rims while isopleths of 0.20-0.25 mol fractions of anorthite in plagioclase agree with the lower pressures of the garnet cores. The isopleths of 3.08-3.27 a.p.f.u. of Si in muscovite are in accordance with the whole range of pressures from the garnet cores to the rims.

3.6.3. Kåfjord Nappe - Sample UL230

The P-T estimate of the Kåfjord nappe was calculated for the kyanite-garnet-mica schist UL230. The peak assemblage is biotite, plagioclase, alkali feldspar, muscovite, garnet, kyanite and quartz (see fig. 3.32). The pseudosection was calculated with the LOI value from whole rock analysis as an estimate for the H_2O-content in the rock during metamorphism. Crossing isopleths of 0.18-0.21 X_{Mg} in garnet and mol fractions of 0.09-0.10 of grossular in garnet limit the P-T estimate to ∼11.5-13 kbar and ∼580-680°C. Isopleths of 0.01-0.02 mol fractions of spessartine agree with the P-T estimate. Furthermore isopleths of 0.51-0.57 X_{Mg}, the whole range of measured values, plot within the estimated P-T range. Isopleths of mol fractions of anorthite in plagioclase plot at lower pressures than the phase field of the peak mineral assemblage. Isopleths of 3.09-3.13 a.p.f.u. of Si in muscovite on the other hand confirm the P-T estimate. Higher values of Si in muscovite plot at higher pressures. The isopleths of the volume percent of kyanite, biotite and muscovite estimated in thin section are in accordance with the P-T estimate. However in contrast to the results of the modeling no rutile is present in thin section. Instead opaque minerals are abundant indicating the presence of ilmenite. Furthermore the phase field of the peak assemblage is bound towards higher temperatures by the melt-in curve. Since the pseudosection was calculated with the LOI value as an estimate of the amount of fluid the position of the melt-in curve is probably inaccurate. Depending on the amount of H_2O used in the calculation the position of the curve varies moving towards lower temperatures with increasing fluid content. To estimate the fluid content in the rock a T-X section for the estimated pressure with variable water content could be calculated. Since the rock did not show evidence of migmatization, using the LOI value as a fluid estimate seems to be appropriate.

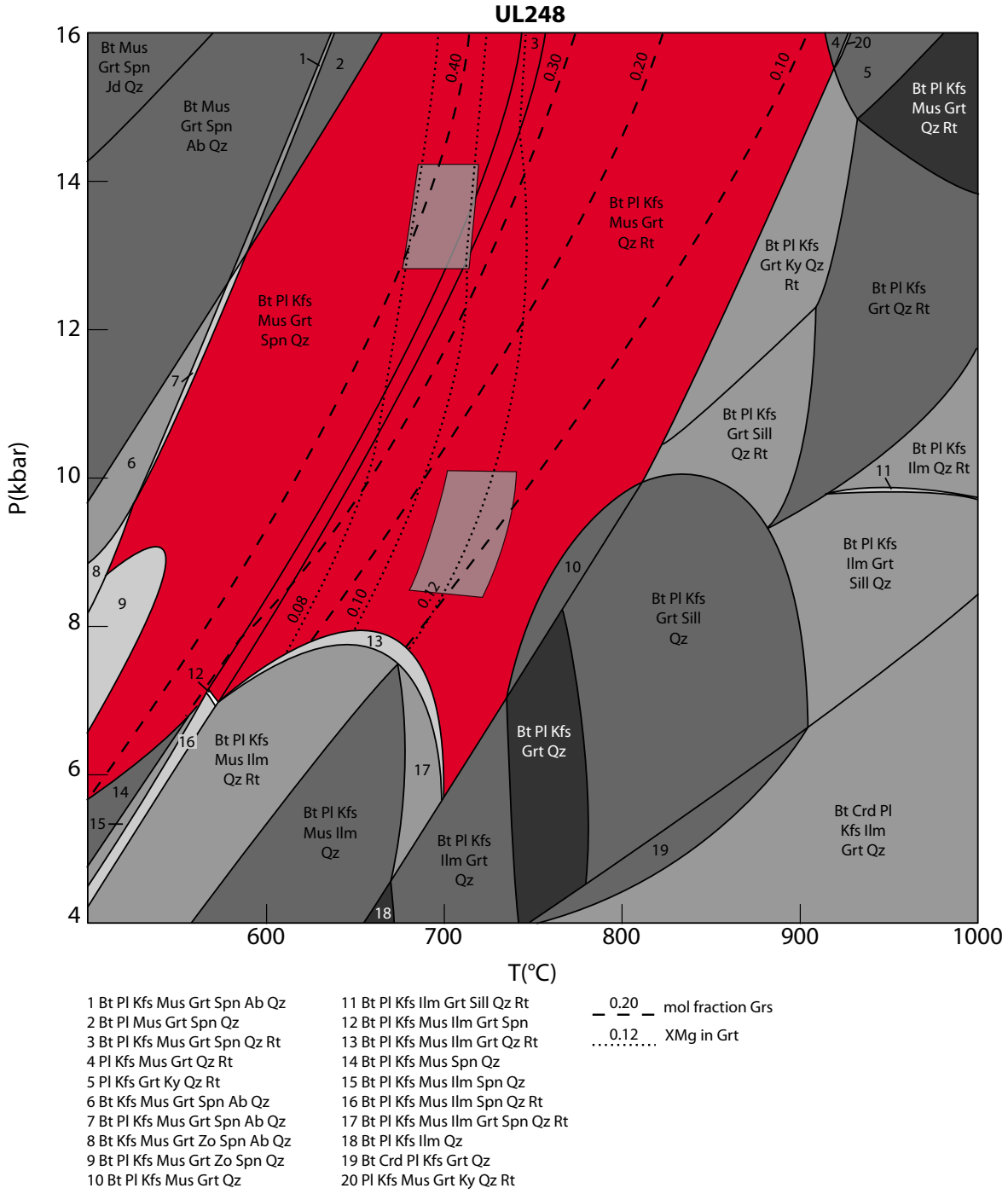

Fig. 3.31.: The pseudosection of sample UL248 from the Vaddas nappe was calculated water-saturated. Isopleths of X_{Mg} in garnet and mol fractions of grossular in garnet were used to constrain a P-T estimate. Garnet cores plot at pressures of ~8.5-10 kbar and temperatures of ~680-740°C while garnet rims plot at ~13-14 kbar and ~670-710°C.

3.6.4. Boundary Kåfjord with Nordmannvik Nappe - Sample UL234a

The kyanite-garnet-mica schist UL234a was used for P-T assessment of the boundary of the Kåfjord with the Nordmannvik nappe. The peak mineral assemblage is formed by biotite, plagioclase, alkali feldspar, muscovite, garnet, kyanite and quartz (see fig. 3.33). Since there is a possibility that the rock had undergone migmatization, the pseudosection was calculated with a water content of 0.7 wt% which was calculated from a T-X section at 10.5 kbar with a variable water content from 0 to 4 wt% (see appendix fig. A.2). The estimated water content of 0.7 wt% correlates to the lowest melting temperature of the peak mineral assemblage in the T-X section and approximates the H_2O-content at the water-saturated solidus of the sample. The T-X section was calculated at a pressure of 10.5 kbar. Isopleths of 0.17-0.22 X_{Mg} in garnet and 0.07-0.10 mol fractions of grossular in garnet constrain the P-T estimate for the Kåfjord-Nordmannvik nappe boundary to pressures of ∼9.5-12 kbar and temperatures of ∼720-800°C. Garnet cores plot in a phase field with the assemblage biotite, plagioclase, alkali feldspar, garnet, kyanite and quartz as well as melt indicating that the rock was partially migmatized at some point. Compositions of the thin garnet rims with slightly increased mol fractions of grossular and decreased X_{Mg}-values plot in the adjacent phase field with the assemblage biotite, plagioclase, alkali feldspar, muscovite, garnet, kyanite, quartz and the absence of melt. Partial migmatization with up to 2 % melt for the P-T estimate is indicated by isopleths of the volume percent of melt. The isopleths of 0.01-0.02 mol fractions of spessartine plot at higher pressures and temperatures than the estimate which is also the case for isopleths of 0.50-0.62 X_{Mg} in biotite. Isopleths of the anorthite component in plagioclase for mol fractions of 0.27-0.30 agree with the P-T estimate while higher mol fractions plot at lower pressures. The isopleths of 3.11-3.15 a.p.f.u. Si in muscovite plot at higher pressures above the P-T estimate in a phase field where rutile is stable, a mineral which is observed in thin section.

3.6.5. Nordmannvik Nappe - Sample UL237

For P-T assessment of the Nordmannvik nappe the kyanite-garnet-mica schist UL237 was modeled. Macroscopic fabrics as well as microstructures of the sample indicate that the rock was first migmatized and subsequently overprinted by shearing. Therefore two events for sample UL237 were modeled. First migmatization conditions were modeled using 1 wt% water calculated from a T-X section at 9 kbar with 0 to 4 wt% water content (see appendix fig. A.3). The water content of 1 wt% corresponds to the lowest melting temperature of the peak mineral assemblage in the T-X section and approximates the

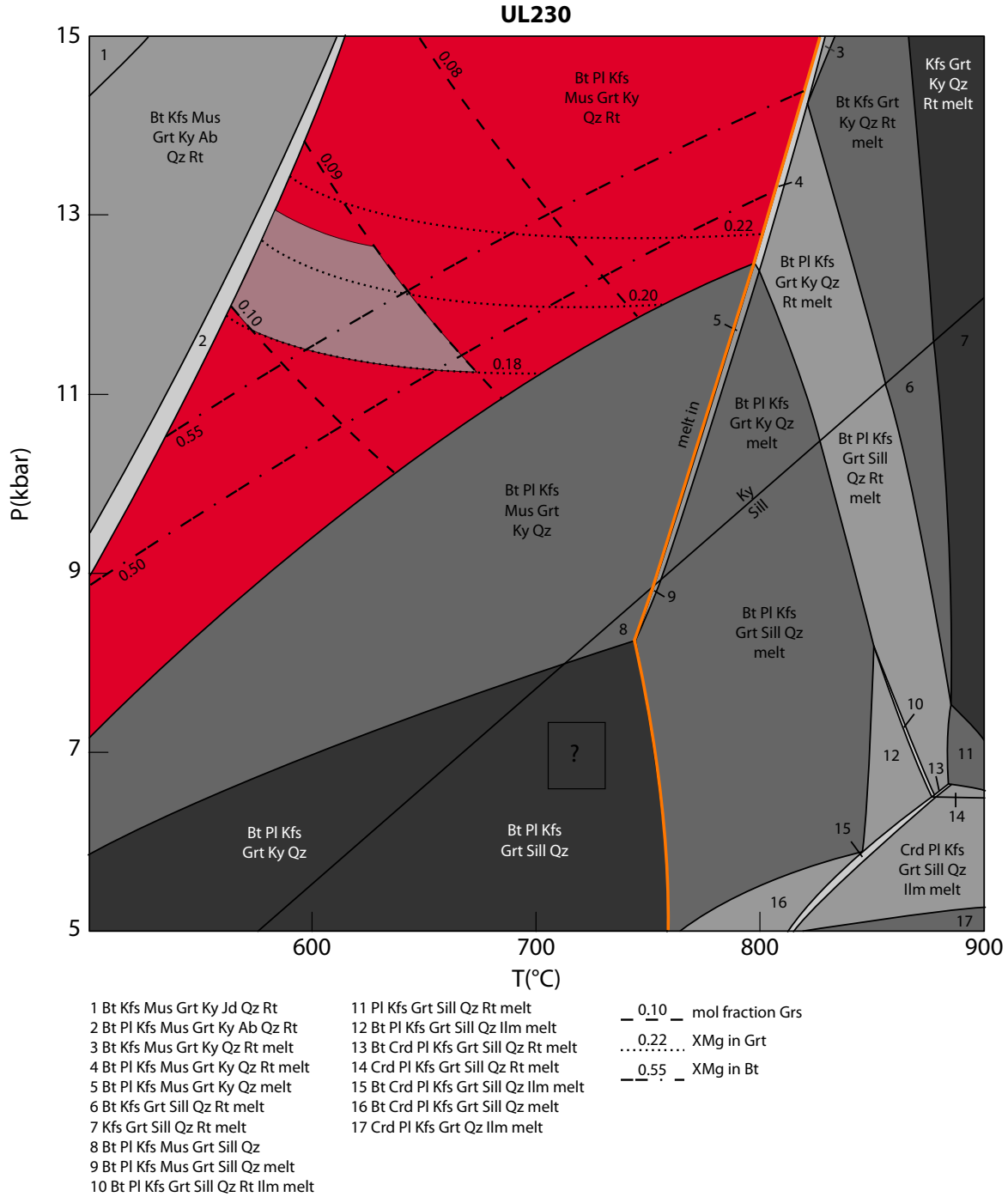

Fig. 3.32.: The pseudosection of sample UL230 fron the Kåfjord nappe was calculated using the LOI value as an estimate of the fluid content in the rock during metamorphosis. The P-T estimate of 11.5-13 kbar and 580-680°C is constrained by isopleths of X_{Mg} in garnet and mol fractions of grossular in garnet. Isoplathes of X_{Mg} in biotite agree with the estimate.

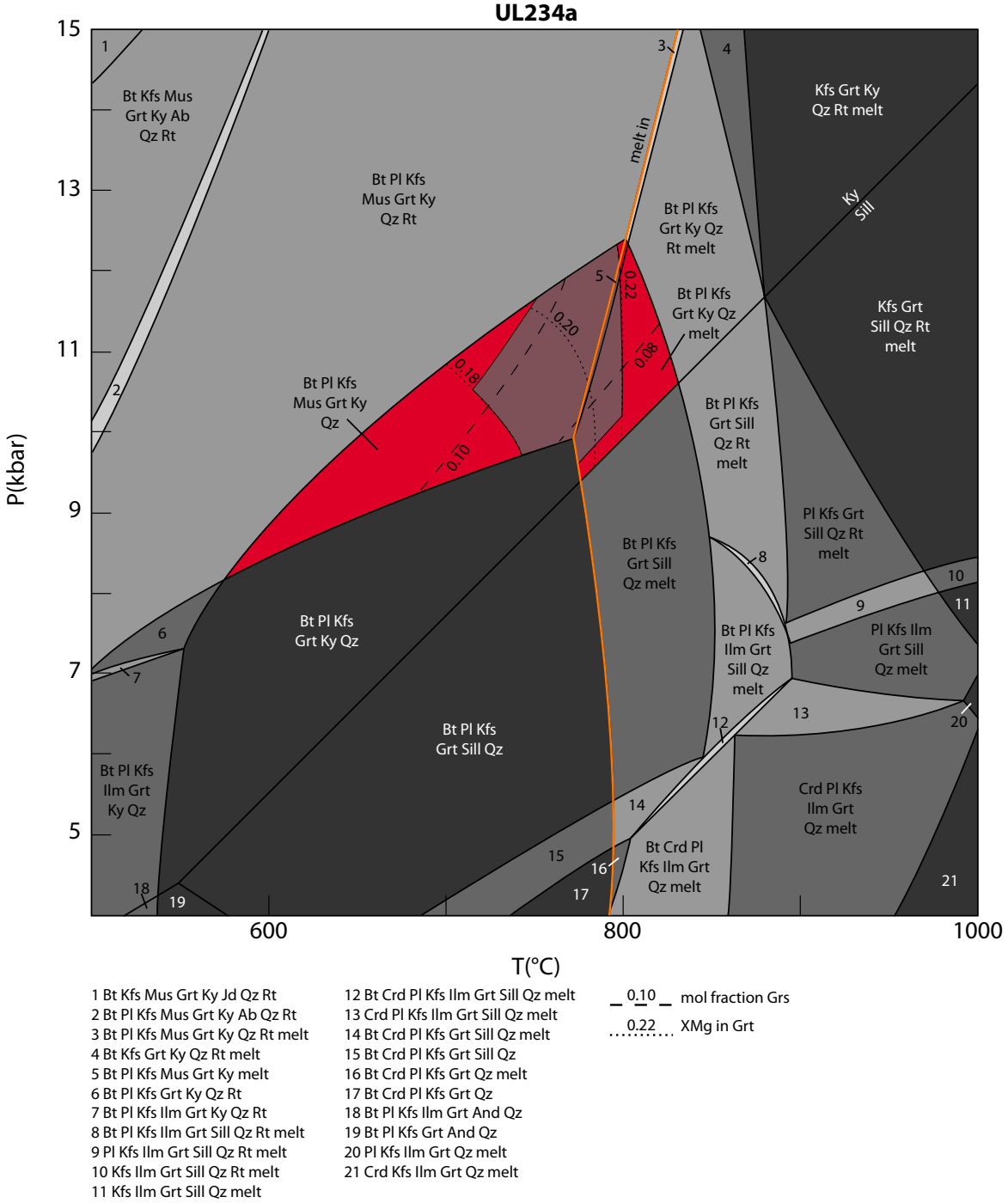

1 Bt Kfs Mus Grt Ky Jd Qz Rt
2 Bt Pl Kfs Mus Grt Ky Ab Qz Rt
3 Bt Pl Kfs Mus Grt Ky Qz Rt melt
4 Bt Kfs Grt Ky Qz Rt melt
5 Bt Pl Kfs Mus Grt Ky melt
6 Bt Pl Kfs Grt Ky Qz Rt
7 Bt Pl Kfs Ilm Grt Ky Qz Rt
8 Bt Pl Kfs Ilm Grt Sill Qz Rt melt
9 Pl Kfs Ilm Grt Sill Qz Rt melt
10 Kfs Ilm Grt Sill Qz Rt melt
11 Kfs Ilm Grt Sill Qz melt
12 Bt Crd Pl Kfs Ilm Grt Sill Qz melt
13 Crd Pl Kfs Ilm Grt Sill Qz melt
14 Bt Crd Pl Kfs Grt Sill Qz melt
15 Bt Crd Pl Kfs Grt Sill Qz
16 Bt Crd Pl Kfs Grt Qz melt
17 Bt Crd Pl Kfs Grt Qz
18 Bt Pl Kfs Ilm Grt And Qz
19 Bt Pl Kfs Grt And Qz
20 Pl Kfs Ilm Grt Qz melt
21 Crd Kfs Ilm Grt Qz melt

0.10 mol fraction Grs
0.22 XMg in Grt

Fig. 3.33.: Melting conditions of the kyanite-garnet-mica schist UL234a from the Kåfjord-Nordmannvik nappe boundary were calculated with a fluid estimate from a T-X section with variable water content at 10.5 kbar. The amount of water corresponds to the lowest melting temperature of the peak mineral assemblage. The P-T estimate of ~9.5-12 kbar and ~720-800°C is limited by isopleths of X_{Mg} in garnet and mol fractions of grossular in garnet.

H_2O-content at the water-saturated solidus of the sample. The T-X section was calculated at a pressure of 9 kbar. Biotite, alkali feldspar, garnet, kyanite and quartz form the peak mineral assemblage for migmatization as seen in the pseudosection (see fig. 3.34). Isopleths of 0.17-0.19 X_{Mg} in garnet according to the core composition and a volume percent of ∼10 % kyanite in thin section were used to constrain the pressures to ∼8.5-10 kbar and the temperatures to ∼750-780°C. Plagioclase and muscovite are stable towards lower temperatures below the melt-in curve. Most isopleths in the pseudosection are vertical which makes the estimate of the pressure difficult. Therefore the high percentage of kyanite in thin section was used to limit the pressure to the highest volume percent of kyanite in the pseudosection. Isopleths of 0.02-0.03 mol fractions of grossular and 0.01-0.02 mol fractions of spessartine in garnet overlap with the P-T estimate but show a wider temperature range towards higher and lower temperatures. Isopleths of 0.45-0.0.59 X_{Mg} in biotite plot at higher temperatures above 850°C. Sillimanite needles observed in garnet cores in thin section indicate that the rock went from sillimanite to kyanite stability conditions which are marked in the pseudosection with a box and a question mark since the conditions of sillimanite stability are unknown.

Solid-state shearing as the second event overprinting the migmatization event was modeled with H_2O in excess because shearing is assumed to be assisted by the presence of water. The peak mineral assemblage is biotite, plagioclase/albite, muscovite, garnet and quartz (see fig. 3.35). Estimated pressures of ∼11.5-13.5 kbar and temperatures of ∼660-720°C are limited by isopleths of 0.16-0.19 X_{Mg} in garnet corresponding to the rim composition and 3.09-3.13 a.p.f.u. Si in muscovite. Kyanite is present in the adjacent phase field towards lower pressures and higher temperatures. Isopleths of 0.01-0.02 mol fractions of grossular plot at lower temperatures than the estimate while mol fractions of 0.01-0.02 of spessartine span over a range of temperatures including the P-T estimate. X_{Mg}-isopleths of 0.45-0.48 overlap with the P-T estimate. Higher X_{Mg}-values measured in biotite inclusions in garnet plot at higher pressures.

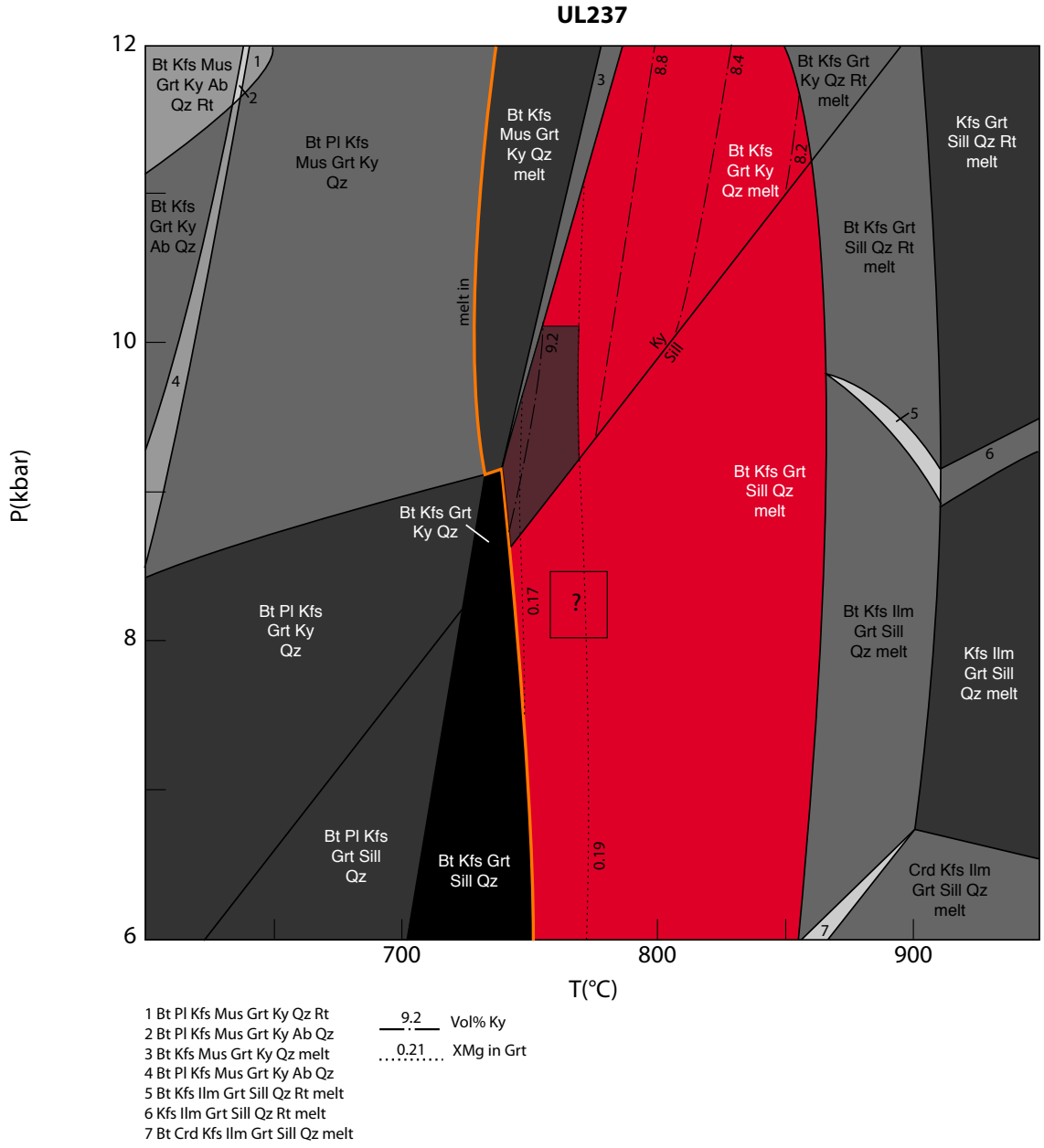

Fig. 3.34.: Melting conditions of the sheared kyanite-garnet-mica schist UL237 from the Nordmannvik nappe were calculated with a fluid estimate from a T-X section with variable water content at 9 kbar. The amount of water corresponds to the lowest melting temperature of the peak mineral assemblage. The P-T estimate of ∼8.5-10 kbar and ∼750-780°C is limited by isopleths of X_{Mg} in garnet and the high volume percent of kyanite present in the sample. Sillimanite observed in garnet cores indicates that the sample went from sillimanite to kyanite present conditions marked in the pseudosection with a question mark.

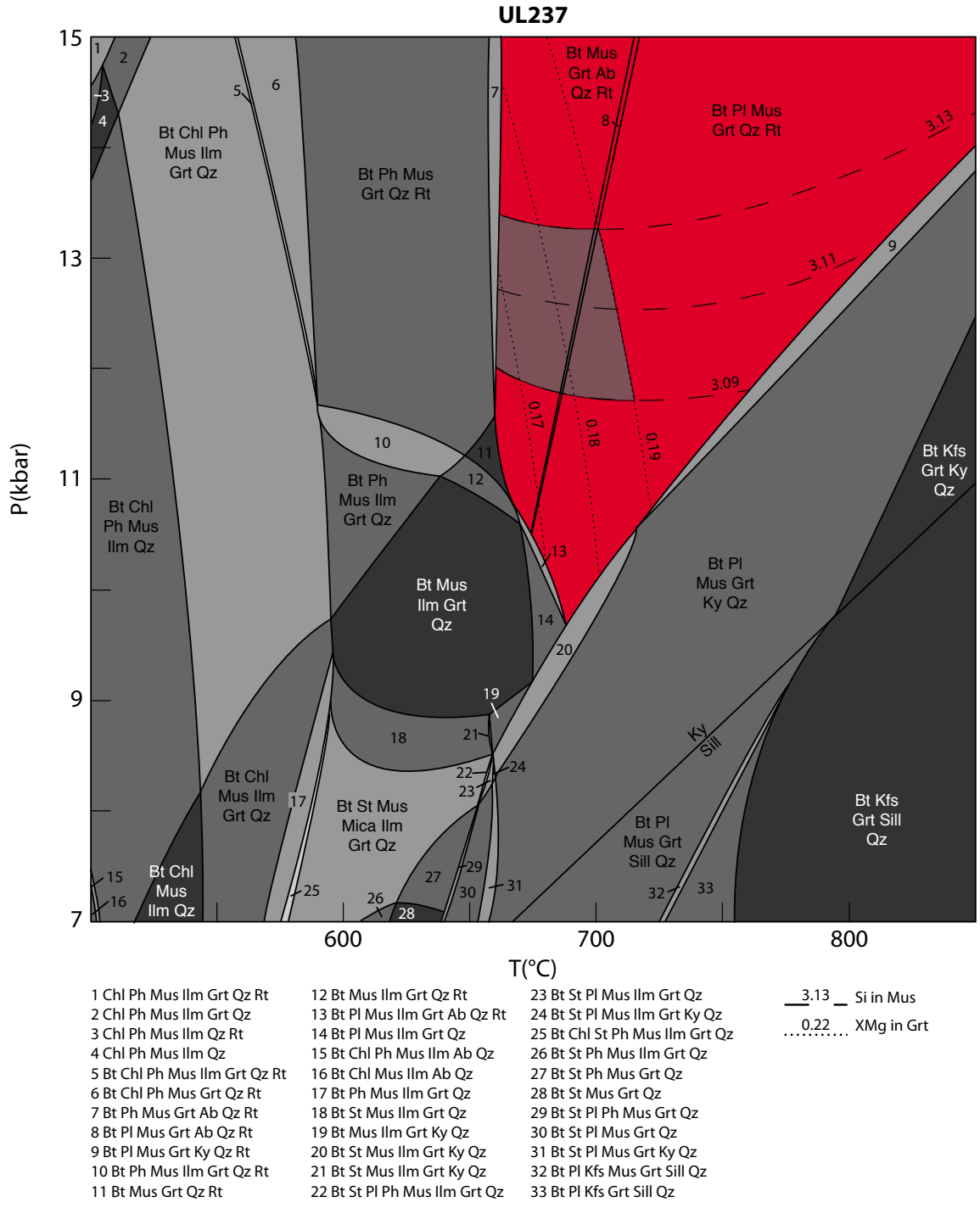

Fig. 3.35.: Solid state shearing overprinting the migmatization event in the Nordmannvik nappe was modeled for the same sample UL237 under water-saturated conditions. The P-T estimate of ∼11.5-13.5 kbar and ∼660-720°C is restricted by isopleths of a.p.f.u. Si in muscovite in agreement with isopleths of X_{Mg} in garnet and X_{Mg} in biotite.

4. Discussion

In the following chapter the above described results are discussed. First the large-scale structures observed in the field and stereographic projections are interpreted. Then microstructures from thin section analysis are discussed to infer mechanisms and temperatures of deformation of the four Caledonian nappes exposed on Uløya. Subsequently the metamorphic conditions of all four nappes estimated by phase equilibrium modeling are interpreted integrating the microstructures to finally reconstruct the tectonometamorphic history of Caledonian nappe emplacement on Uløya.

4.1. Caledonian Deformation

A penetrative SW dipping foliation and NW-SE-trending stretching lineation in all four nappes is well developed throughout Uløya. The foliation is axial-planar to tight to isoclinal folds and the lineation is parallel to the fold hinges. This penetrative axial-planar foliation is termed S_1. Comparison of the foliation orientation of the different nappes shows that the foliation planes in the KNC scatter more than in the other nappes. This is probably caused by previous deformation of the KNC and pre-existing structures could have been partially or completely reoriented during the Caledonian deformation. The averaged great circle for the pole distribution of the KNC has a pole dipping at a relatively shallow angle to the SE, the same orientation as the Caledonian stretching lineation and fold hinges (see fig. 3.11). This supports a Caledonian reorientation of pre-existing structures in the KNC. The polpoint distributions of the foliation of the Vaddas, Kåfjord and Nordmannvik nappes scatter only little with few outliers but a clear maximum indicating a consistent foliation dipping shallowly to the SW.

The Caledonian stretching lineation L_1 pluges shallowly to the NW and SE with a maximum to the SE. This indicates, together with the microscopic and macroscopic dominant top to the SE sense of shear, a tectonic transport direction to SE during Caledonian deformation. The distribution of the stretching lineation in the KNC and the Vaddas nappe is almost identical and shows the orientation described above. The lineations in the Kåfjord nappe on the other hand scatter along a great circle dipping shallowly to the SW with two distribution maxima in the NW and the SE. This scatter of the Caledonian stretching

lineation can have different origins. One explanation is that pre-existing structures in the Kåfjord nappe were reoriented during Caledonian deformation leading to a consistent scatter of the stretching lineation along a great circle with two maxima in the NW and the SE. This great circle shows the same orientation as the penetrative S_2 foliation arguing for Caledonian reorientation of pre-existing structures. However pre-existing structures were not observed in the field probably due to the strong Caledonian overprint.

In contrast to the underlying nappes all stretching lineations in the Nordmannvik nappe plunge shallowly to the NW. This could be explained by the fact that all measurements of the Nordmannvik nappe were taken along the western coast of the island leading to limited statistic representation of the measurements. Besides, the Nordmannvik nappe shows signs of syn-kinematic Caledonian melting which might have influenced the orientation of the stretching lineation.

At least two distinct Caledonian fold generations are identified on Uløya. The generation of folds are isoclinal to tight F_1 folds that formed at the same time as the main S_1 foliation which is axial-planar to these folds. Moreover the fold hinges are parallel to the stretching lineation. These first generation folds are found in the KNC, the Vaddas, the Kåfjord and the Nordmannvik nappes. The presence of sheath folds indicates high layer-parallel shear strain deformation during folding (Skjernaa, 1989). The second fold generation F_2 is formed by closed to open folds that fold the S_1 foliation and refold the first generation folds. These folds are observed in the KNC, the Vaddas and the Kåfjord nappe. As described in chapter 3.3 Structural Geology both fold generations have a very similar geometry which is confirmed by the stereographic projection of the two generations (see fig. 3.12). The axial planes of the second fold generation dip slightly steeper than the ones of the first generation and scatter a little more in orientation dipping to the NE, SE and SW. However, the similar geometry of the two fold generations suggests that both developed under in the same strain regime only that the isoclinal folds formed early in the process while the open folds were formed later, overprinting the first generation of folds. Thus both generations are assigned to the main deformation phase D_1 which is verified by the parallelism of the fold hinges to the Caledonian stretching lineation.

In the Nordmannvik nappe folds are formed by folded leucosome layers. A few tight to isoclinal folds with the axial plane parallel to the foliation and the fold hinge parallel to the stretching lineation are observed belonging to the first generation folds. Nevertheless most folds, even though they are isoclinal, show more random orientations (see fig. 3.9 f)). Hence both solid state deformation and syn-tectonic migmatization occur creating first generation folds and randomly oriented folds. Folds of the second generation were not observed in the Nordmannvik nappe which might again be due to the fact that the Nordmannvik shows high-grade deformation or that only part of the Nordmannvik nappe

was accessed within the framework of this project.

Signs of migmatization were observed in both the KNC and the Nordmannvik nappe. In orthogneisses from the KNC along the northern coastline of the island melt segregation along axial planes of tight folds was observed indicating partial melting during deformation (Vernon and Paterson, 2001). Migmatization within the KNC is known from the Fagervik Complex and the Eidvågeid Paragneiss during the Proterozoic (Kirkland et al., 2008b, 2006b). The orthogneisses on Uløya could be related to orthogneisses of the Fagervik Complex in which melting events occurred at 1765±9 and 1730±11 Ma (Kirkland et al., 2008b) long before Caledonian deformation. On the other hand fold structures on Uløya associated with migmatization show Caledonian orientation. Without dating it is not possible to say whether pre-existing folds associated with migmatization on Uløya were reoriented during Caledonian deformation or whether migmatization is Caledonian. In the Nordmannvik nappe there are indicators that migmatization is syn-kinematic to Caledonian deformation. The above described isoclinal folds with Caledonian orientation are one example. Another example are observed melt pockets around garnet grains which in one location were stretched in the same orientation as the Caledonian NW-SE oriented stretching lineation (see fig. 3.9).

The intersection of the great circle of the Caledonian reoriented stretching lineations from the Kåfjord nappe with the averaged great circle of the F_1 and F_2 fold axial planes shows tectonic transport during the Caledonian towards the SSE (see fig. 3.12 b)). This constructed direction agrees approximately with the tectonic transport indicated by the stretching lineation and the dominant top to the SE sense of shear.

Overall the Caledonian nappe emplacement on Uløya was accompanied by very high shear strains leading to the formation of a penetrative foliation and stretching lineation as well as high-grade mylonites along the nappe boundaries. Nappe emplacement and thrusting took place towards the SE. The KNC, the Vaddas and the Kåfjord nappe were affected by two fold phases during Caledonian deformation, an early phase forming isoclinal to tight folds which were later overprinted by close to open folds. The folds of both events show similar orientation indicating formation in the same strain regime. Syn-tectonic migmatization and folding of the first phase is observed in the Nordmannvik nappe. It is unclear if migmatization in the KNC is pre-Caledonian or Caledonian.

The above described structures of the D_1 deformation event are in agreement with D_2 structures described by Zwaan and Roberts (1978). In the article a first low-grade deformation phase is described which is not well preserved in large parts of northern Norway due to subsequent higher-grade overprint. This is probably also the case on Uløya where no evidence of an earlier deformation phase was found. A second deformation event D_2 described by Zwaan and Roberts (1978) comprises of tight to isoclinal folds a

NW-SE stretching lineation and a regional S_2 schistosity axial-planar to the folds in the Nordreisa area agreeing with the D_1 deformation structures characterized in the present work. However, the fold hinges probably developed parallel to the stretching lineation and were not rotated as suggested by Zwaan and Roberts (1978). The D_3 folds described by Zwaan and Roberts (1978) have a similar orientation to the above specified F_2 folds which are here interpreted as late Caledonian folds.

4.1.1. Caledonian Microstructures

In the following, microstructures of quartz and feldspar are discussed to estimate temperatures of deformation in the four Caledonian nappes exposed on Uløya. The presence of a pervasive foliation and stretching lineation as well as the frequent mylonite zones indicate that ductile shear and crystal-plastic deformation were the dominant deformation mechanisms.

Kalak Nappe Complex

The microstructures in the KNC focus on the quartzitic garnet-mica schist sample UL250 and a few other samples showing distinct microstructures.

In thin section UL250 relatively large quartz grains with general undulose extinction, sometimes sweeping, sometimes forming stripes as well as smaller subgrains are observed as evidence for intracrystalline deformation and the presence of dislocations in the crystal lattice. Often the quartz grains are elongate parallel to the foliation. These quartz structures are probably formed by combined subgrain rotation (SGR) and grain boundary migration (GBM) recrystallization (corresponding to dislocation creep regimes 2 and 3 of Hirth and Tullis (1992)). Large grains are formed by GBM recrystallization, a high temperature process where grain boundaries become highly mobile and can sweep through an entire crystal (e.g. Guillope and Poirier, 1979). Smaller grains and subgrains are formed by SGR recrystallization where the crystal lattice of subgrains is progressively rotated until a new grain boundary is formed (Urai et al., 1986). Recrystallization by combined SGR and GBM at a given strain rate of 10-12 s^{-1} indicates recrystallization temperatures around ~500°C according to Stipp et al. (2002). For quartz to recrystallize it is assumed that at least trace amounts of water were present in the crystal lattice (Hobbs, 1968).

Big alkali feldspar and plagioclase crystals in the matrix show undulose extinction, irregular patterns of polysynthetic twins, microfracturing as well as tapering deformation twins. Furthermore, often the rims of plagioclase grains have a different extinction orientation than the cores indicating zoning of the feldspar (see fig. 3.14 a)). This zoning is probably the result of late diffusion and not growth zoning since the rims are often

thin and follow the irregular shapes of the grains. Diffusion in feldspar becomes faster at temperatures above 650°C (Kruse and Stünitz, 1999). In sample UL300 small grains and subgrains form mantle structures around large alkali feldspar porphyroclasts (see fig. 3.14 d)). This is indicative for SGR recrystallization, a dynamic recrystallization mechanism indicating temperatures above ~600-650°C where dislocation climb and recovery in feldspar become relatively easy and subgrain structures form (Vidal et al., 1980; Pryer, 1993; Kruse and Stünitz, 1999). Myrmekite, undulose extinction, subgrains and new grains as well as fractures are observed in alkali feldspar in UL476 (see fig. 3.13 c)). Generally myrmekite becomes important towards higher temperatures and is abundant at high-grade conditions above ~600°C (Passchier and Trouw, 2005). This agrees with the high temperatures necessary for dynamic recrystallization of feldspar by SGR.

Together recrystallization of quartz and feldspar indicate deformation temperatures above ~600-650°C in the KNC. The high grade deformation is in agreement with partial melting observed in gneisses of the KNC.

Vaddas Nappe

Microstructures of the Vaddas nappe focus on the garnet-mica gneiss UL248 and are generally similar to the structures observed in the KNC.

Thin undulating quartz layers parallel to the matrix are formed by relatively large often elongate quartz grains that show undulose extinction sweeping across the grain or forming diffuse deformation bands (see fig. 3.18 a)). Smaller grains and subgrains are observed in the matrix but also in the quartz layers. Sometimes the layers contain very large elongate single crystals indicating recrystallization by GBM. The presence of subgrains and small recrystallized grains indicates that also SGR recrystallization was active. Therefore like in the KNC probably both SGR and GBM recrystallization formed the quartz microstructures indicating temperatures around ~500°C for a given strain rate of 10-12 s^{-1} (Stipp et al., 2002).

Alkali feldspar and plagioclase form part of the matrix but also larger porphyroclasts embedded in the matrix. Undulose extinction is common as well as patchy polysynthetic twinning, sometimes with tapering twin lamellae (see fig. 3.17 b)) and microkinking which probably developed due to pinning of dislocations at microperthitic lamellae (Pryer, 1993). Along the rims of alkali feldspar porphyroclasts myrmekite structures are often observed on crystal faces parallel to the foliation (see fig. 3.18 b)). This could indicate deformation induced replacement of alkali feldspar according to Simpson and Wintsch (1989). No clear core-and-mantle structures as evidence of dynamic recrystallization are observed. Nevertheless, the presence of myrmekite indicates temperatures around ~600°C. Furthermore partial sericitization of both alkali feldspar and plagioclase is common as a retrograde

overprint.

In summary the presence of myrmekite as well as recrystallization of quartz by SGR and GBM indicates relatively high deformation temperatures above ~600°C.

Kåfjord Nappe

The microstructures in the Kåfjord nappe focus mainly on thin sections UL230 and UL234a but also a few other samples from the Kåfjord nappe with characteristic microstructures.

Quartz in thin section UL234a forms relatively big grains showing even extinction but also undulose extinction, stripy extinction and subgrains (see fig. 3.22 a)). Similar structures are observed in a quartz vein in the quartzitic garnet-mica schist UL366. Large strongly elongate quartz grains show undulose extinction and form together with small subgrains and recrystallized grains an oblique foliation within the vein (see fig. 3.21 c)). According to Passchier and Trouw (2005) oblique foliations are formed by combined SGR and GBM recrystallization which agrees with the observed structures. Therefore like in the KNC and Vaddas nappe metamorphic temperatures around ~500°C for a strain rate of 10-12 s^{-1} are indicated (Stipp et al., 2002).

Alkali feldspar and plagioclase porphyroclasts as well as matrix grains show undulose extinction, tapering and/or bent deformation twins and patches of polysynthetic twins (see fig. 3.22 d)). Irregular feldspar grain boundaries in thin section UL366 are indicative for recrystallization (Pryer, 1993) but often the grains are surrounded by fine-grained biotite inhibiting recrystallization by pinning. In thin section UL234a small-scale myrmekite structures are observed (see fig. 3.22 b)). These microstructures are similar to the ones in sample UL248 described above indicating high-grade temperatures around ~600°C. Moreover retrograde sericitization of feldspar along twin lamellae or as patches is observed in UL366.

In summary metamorphic conditions in the Kåfjord nappe lie above ~600°C indicated by SGR and GBM recrystallization of quartz and myrmekite structures in feldspar similar to the samples described above.

Nordmannvik Nappe

Microstructures form the Nordmannvik nappe concentrate on the sheared kyanite-garnet-mica schist UL237 as well as on the migmatite samples UL240 and UL242.

Within the leucosome in migmatite sample UL242 very large quartz grains with irregular, amoeboid shapes, bulging grain boundaries and elongate subgrains are observed (see fig. 3.25 a)). These large grains are probably formed by GBM recrystallization (corresponding to dislocation creep regime 3 of Hirth and Tullis (1992)), a high temperature

mechanism active at temperatures above ~500°C (for a strain rate of 10-12 s^{-1}; Stipp et al., 2002). The presence of elongate subgrains indicates that the large recrystallized grains are not strain free. Recovery leads to arrangement of internal dislocations in crystal planes forming equant or elongate subgrains (Passchier and Trouw, 2005). The grain boundaries of the large grains are serrated on a small scale and small recrystallized grains along the boundaries are observed. These probably formed as the result of bulging (BLG) recrystallization (corresponding to dislocation creep regime 1 of Hirth and Tullis (1992)). Localized grain boundary migration leads to bulging of the grain boundaries and new small recrystallized grains can form when the bulges are separated from the old grain (Bailey and Hirsch, 1962). This is a low temperature mechanism occurring in quartz at temperatures of ~280-400°C for a strain rate of 10-12 s^{-1} (Stipp et al., 2002). Here BLG occurs as a retrograde process overprinting the high grade microstructures in quartz. Similar quartz structures are also observed in the sheared migmatite sample UL237 where layers of quartz are stretched parallel to the foliation.

Large quartz grains with straight boundaries in the leucosome of migmatite sample UL240 show rectangular subgrains, a pattern also known as chessboard extinction (see fig. 3.25 d)). Chessboard extinction forms due to combined basal <a> and prism [c] slip of dislocations within the crystal lattice (Mainprice et al., 1986; Blumenfeld et al., 1986). This is observed above the α-β transition in quartz at temperatures above ~600-700°C when prism [c] slip becomes active (Kruhl, 1996). Chessboard extinction can be used as a geothermometer because subgrain boundaries are generally stable during post-tectonic annealing (Kruhl, 1996) indicating here that part of the Nordmannvik nappe reached metamorphic temperatures above ~700°C.

In thin section UL237 alkali feldspar crystals distributed in the matrix show undulose extinction and abundant flame perthite structures (see fig. 3.25 b)). According to Pryer (1993), flame perthite is a replacement texture which results from the breakdown of plagioclase during deformation under retrograde metamorphic conditions. This correlates with the change from lower amphibolite to upper greenschist facies conditions at temperatures between 450-500°C (Pryer, 1993). Alkali feldspar in UL240 and UL242 exhibits undulose extinction, tempering twins and patches of polysynthetic twins. In plagioclase porphyroclasts chemical zoning is visible due to a different extinction orientation of the rim compared to the core. Recrystallization of alkali feldspar is indicated by grain misorientation along microfractures or twin lamellae (see fig. 3.25 e)). Very large subgrains are rotated along the microfractures or twin lamellae leading to the formation of a new grain as described by Hanmer (1982). Further indications for dynamic recrystallization are small recrystallized grains and subgrains indicating temperatures above ~600-650°C (Vidal et al., 1980; Pryer, 1993; Passchier and Trouw, 2005). In addition retrograde seric-

itization of feldspar crystals in UL240 and UL242 is very dominant leading to almost complete replacement of some grains.

The samples from the Nordmannvik nappe show different microstructures than the samples from the nappes below. High grade deformation above ∼500°C is indicated by GBM recrystallization of quartz. Dynamic recrystallization of feldspar suggests deformation temperatures of ∼600-650°C. Chessboard extinction proves the highest temperatures of deformation above ∼600-700°C. Abundant flame perthite in alkali feldspar indicates retrograde conditions at temperatures between 450-500°C. Furthermore BLG recrystallization at temperatures of ∼280-400°C overprinted the high-grade quartz structures.

4.2. Metamorphic Conditions

In the following chapter the results of the phase equilibrium modeling are discussed in relation to the microstructures. When possible metamorphic reactions from both the microsturctures and the pseudosections are inferred. An overview over the P-T conditions in the different nappes as well as the origin of the samples used for phase equilibrium modeling is shown in figure 4.1.

4.2.1. Kalak Nappe Complex

During prograde conditions biotite, plagioclase quartz and sphene were stable in the quartzitic garnet-mica schist from the KNC. Biotite, plagioclase, quartz and sphene are found included in garnet indicating prograde growth of these minerals.

The peak mineral assemblage is formed by the assemblage of biotite, plagioclase, alkali feldspar, muscovite, garnet, quartz, rutile and sphene. This is confirmed by the alignment of elongate quartz and feldspar grains as well as biotite and muscovite parallel to the foliation. Undulose extinction and bending of muscovite and biotite crystals is also evidence for peak metamorphic presence of these minerals. Syn-kinematic garnet growth is confirmed by twisted inclusion trails, elongate grains parallel to the foliation and a deflection of the foliation around the garnet porphyroclasts. Moreover diamond-shaped sphene oriented parallel to the foliation is part of the peak assemblage.

According to phase equilibrium modeling metamorphic peak conditions in the KNC reached pressures of ∼9-12 kbar and temperatures of ∼610-690°C. However alkali feldspar and sphene are not predicted in the peak mineral assemblage of modeling. It is possible that alkali feldspar formed during peak metamorhpic conditions due to breakdown of muscovite even though this reaction is not indicated by phase equilibrium modeling. If this was the case muscovite would form part of the post-kinematic assemblage. Sphene is stable towards lower temperatures and therefore it is possible that calcium was underestimated

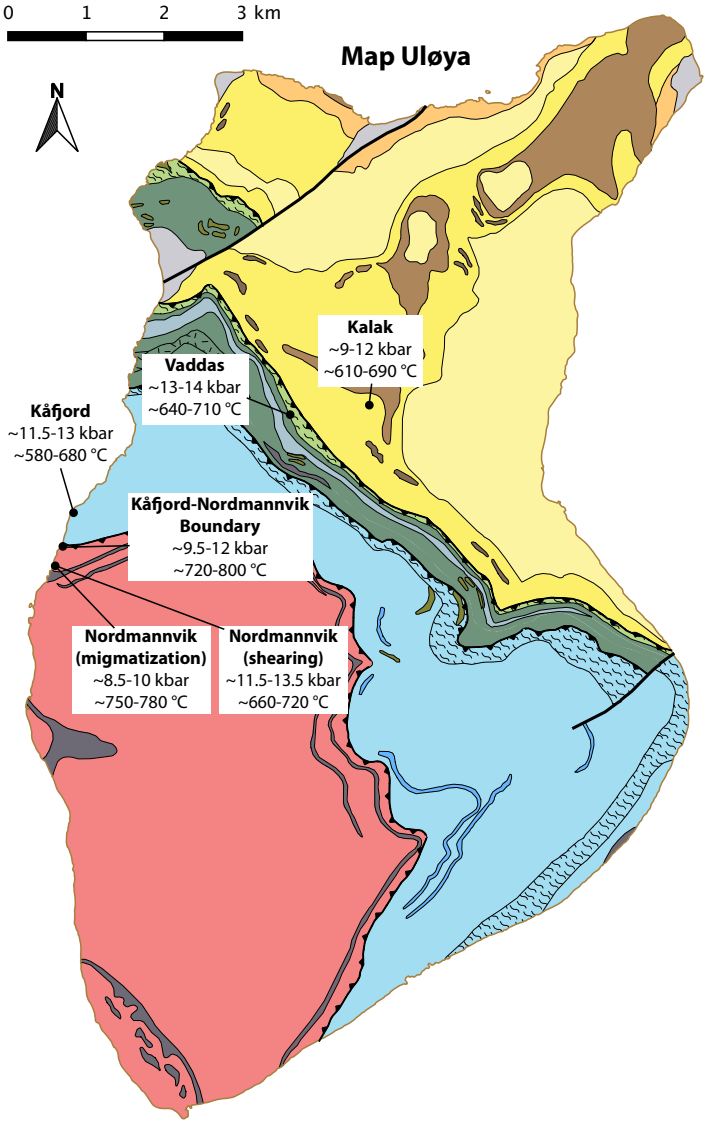

Fig. 4.1.: Estimated P-T conditions of all nappes exposed on Uløya are shown in relation to the geological map. The black circles indicate the location of the samples for phase equilibrium modeling.

in the XRF whole rock analysis. On the other hand it is possible that shpene formed during nappe thrusting (i.e. emplacement to lower P-T conditions). The present calcium was probably incorporated in other minerals e.g. garnet or plagioclase. This would explain why sphene is not included in the peak assemblage of modeling.

The P-T estimate is constrained by isopleths of X_{Mg} in garnet and mol fractions of grossular in garnet corresponding to core and rim composition. Weak zoning of the garnet is observed mostly in the almandine and spessartine component of the garnet. Isopleths of the low mol fractions of spessartine in garnet rims correspond to the P-T estimate. Isopleths of X_{Mg} in biotite, mol fractions of anorthite in plagioclase and a.p.f.u. Si in muscovite partly agree with the P-T estimate confirming that the minerals of the peak matrix assemblage were in chemical equilibrium with the garnet rims. Isopleths of higher mol fractions of spessartine corresponding to the garnet cores plot at lower temperatures and pressures confirming prograde garnet growth. The higher values of a.p.f.u. Si in muscovite plot above the P-T estimate. This might indicate that the rock reached higher pressures than suggested by the chemical compositions of the other minerals. Late muscovite growth is inferred in thin section from muscovite grains oriented at an angle to the foliation. Higher X_{Mg}-values measured in biotite inclusions in garnet also plot above the P-T estimate. The inclusions were sealed in the garnet and therefore not at equilibrium with matrix minerals.

Biotite and muscovite grains growing at an angle to the foliation are part of the post-kinematic assemblage. Furthermore the breakdown of alkali feldspar into quartz and plagioclase with oligoclase composition (see fig. 3.29) forming myrmekite structures according to the reaction below (see equation (1) after Becke, 1908) is presumably a retrograde reaction. Necessary cations were possibly transported by fluids which also provided H_2O for the formation of biotite and muscovite. Decomposition of garnet is seen in thin section as partial replacement of the garnet by biotite, quartz and plagioclase (see fig. 3.15). Retrograde metamorphic conditions are moreover documented by chloritization of biotite and sericitization of feldspar in other thin sections from the KNC than the one used for phase equilibrium modeling.

$$(1)\ \mathrm{Or} + \mathrm{Na^+} + \mathrm{Ca^{2+}} \rightarrow \mathrm{Ab} + \mathrm{An} + \mathrm{Qz} + \mathrm{K^+}$$

In summary the mineral assemblage and P-T conditions show amphibolite facies metamorphism for the sample from the KNC (see fig. 4.2).

4.2.2. Vaddas Nappe

The minerals biotite, plagioclase and quartz formed during prograde metamorphism in the garnet-mica gneiss from the Vaddas nappe. All of these minerals are observed as

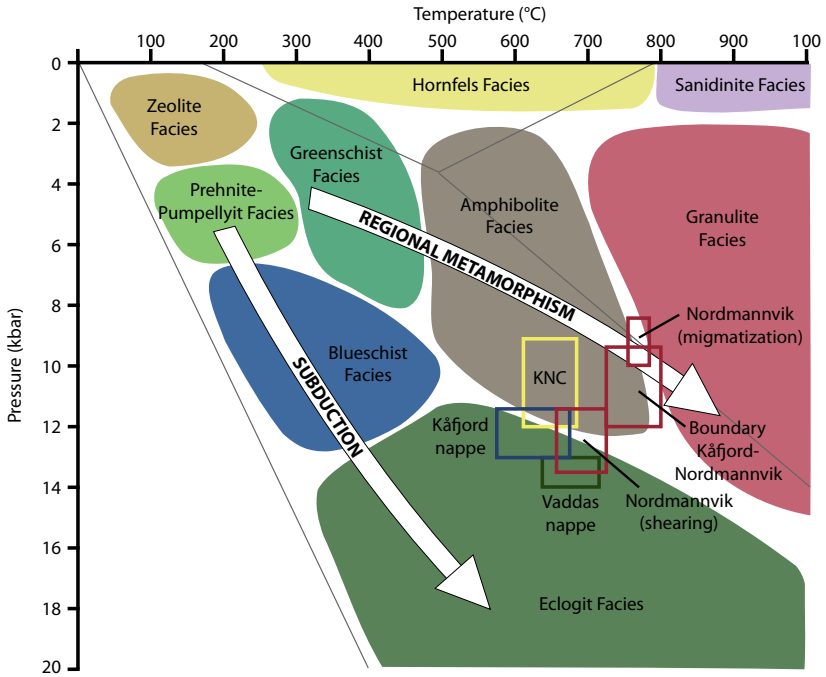

Fig. 4.2.: In a facies diagram the P-T estimates of all samples are plotted to identify the metamorphic facies and the tectonic regime.

inclusions in garnet.

At the peak of metamorphism the mineral assemblage included biotite, plagioclase, alkali feldspar, muscovite, garnet, quartz as well as rutile and sphene. In thin section elongate feldspar and quartz grains as well as biotite and muscovite are oriented parallel to the foliation confirming syn-kinematic presence. Garnet porphyroclasts deflect the foliation again as evidence for syn-kinematic presence.

Phase equilibrium modeling shows an anticlockwise pressure increase with slightly decreasing temperatures from ~8.5-10 kbar and ~680-740°C to 13-14 kbar and ~670-710°C for peak metamorphism in the Vaddas nappe. This increase in pressure and decrease in temperature is indicated by continuously zoned garnet. The garnet cores plot in a phase field in which rutile is stable while the garnet rims plot in a phase field where sphene is stable. In thin section both minerals are found and it is occasionally observed that sphene grows as a rim around rutile grains. Furthermore sphene is more abundant in the matrix than rutile. These observations are in agreement with the results of phase equilibrium modeling and a change from rutile to sphene stability.

The isopleths of X_{Mg} in garnet and mol fractions of grossular in garnet are used to confine the P-T estimate. Strong zoning of the garnet results in different P-T estimates for garnet cores and rims. Isopleths of mol fractions of spessartine in garnet agree showing higher mol fractions of spessatine for the core estimate and lower mol fractions for the

rim estimate. X_{Mg}-isopleths of biotite are very similar to the isopleths of mol fractions of spessartine and agree with the P-T estimate. Only high X_{Mg}-values from biotite included in garnet plot above the estimate. The inclusions were sealed in the garnet and therefore not at equilibrium with the matrix minerals and garnet rims. The high X_{Mg}-values in biotite suggest that the pressure might have been higher than the estimate. Mol fractions of anorthite in plagioclase are in accordance with the P-T conditions of the garnet cores, higher values plot at lower pressures. This could be explained by an underestimate of calcium in XRF analysis or inaccuracy of the solution model. Isopleths of a.p.f.u. of Si in muscovite range over the whole P-T estimate. The overall match of the chemistry of different minerals indicates that the matrix and the garnet rims reached phase equilibrium.

Fine-grained biotite rims around muscovite formed retrograde after peak metamorphism. Furthermore the breakdown of alkali feldspar into quartz and plagioclase with oligoclase composition (see fig. 3.29) forming myrmekite structures occurred retrograde (see equation (1) above) which is also the case for partial replacement of garnet by quartz and plagioclase along the rim. In addition chloritization along cracks in garnet as well as partial sericitization of feldspar indicate retrograde conditions. In most of these reactions fluids were involved.

Overall the P-T estimate indicates eclogite facies metamorphism for the Vaddas nappe (see fig. 4.2). However further indications for eclogite facies metamorphism are not found in the mineral assemblage and microstructural deformation.

4.2.3. Kåfjord Nappe

Minerals that were stable during prograde conditions in the kyanite-garnet-mica schist from the Kåfjord nappe are biotite, plagioclase, quartz and possibly sillimanite. Like in the samples described above this is indicated by inclusions of the minerals in garnet but also the pseudomorph growth of kyanite after sillimanite.

The peak metamorphic assemblage is formed by biotite, plagioclase, alkali feldspar, muscovite, garnet, kyanite and quartz. Elongate mineral grains like biotite, muscovite and kyanite but also elongate quartz and feldspar grains are aligned parallel to the foliation indicating syn-kinematic growth. Often garnet grains have elongate grain shapes and are oriented parallel to the foliation which is deflect around the garnet indicating syn-kinematic presence of garnet.

Peak metamorphic conditions of ∼11.5-13 kbar and ∼580-680°C are estimated by phase equilibrium modeling. The peak mineral assemblage from modeling predicts besides biotite, plagioclase, alkali feldspar, muscovite, garnet, kyanite and quartz also rutile which is not observed in thin section. Instead abundant opaque minerals are found in thin section indicating the presence of ilmenite. This could indicate a retrograde reaction since

ilmenite often overgrows rutile during retrogression. Alternatively this discrepancy could be due to a high Fe content in the XRF bulk rock analysis.

Isopleths of X_{Mg} in garnet and mol fractions of grossular in garnet are used to confine the P-T estimate. Mol fractions of spessartine in garnet are very low but the P-T estimate lies in between the isopleths for mol fractions of spessartine. Measured X_{Mg} in biotite, including values of biotite inclusions in garnet, agree with the estimated P-T conditions. The mol fractions of anorthite in plagioclase plot at lower pressures than the P-T estimate. A possible explanation is that calcium was underestimated in XRF analysis. The isopleths of a.p.f.u. Si in muscovite are in accordance with the estimated P-T range, but higher values plot towards higher pressures. This could indicate that higher pressures were reached which is not recorded by other minerals. Furthermore the isopleths of the volume percent of biotite, muscovite and kyanite estimated in thin section agree with the results of modeling. Even though rutile instead of ilmenite was predicted for the peak assemblage of phase equilibrium modeling the overall agreement of the isopleths prove a well constrained P-T estimate with chemical equilibrium of biotite, garnet and muscovite.

Retrograde conditions are documented by the growth of fine-grained biotite indicating the presence of fluids. In other samples from the Kåfjord nappe retrograde chloritization and sericitization is observed. Furthermore a shear band cleavage formed by the retrograde fine-grained biotite is observed which developed during the same mylonitic event as the foliation but later overprinting the older foliation. This indicates that shearing was active over a relatively long period of time during retrograde conditions.

In summary the P-T estimate predicts amphibolite to eclogite facies metamorphism for the Kåfjord nappe (see fig. 4.2). Like in the sample from the Vaddas nappe no further evidence for eclogite facies metamorphism is found neither in the mineral assemblage nor the microstructures.

Boundary Kåfjord with Nordmannvik Nappe

During prograde conditions biotite, plagioclase and quartz were stable in the quartzitic kyanite-garnet-mica schist from the Kåfjord-Nordmannvik nappe boundary. These minerals are found as inclusions in garnet cores.

At the peak of metamorphism a mineral assemblage of biotite, plagioclase, alkali feldspar, muscovite, garnet, kyanite and quartz formed. This is indicated by the alignment of biotite, muscovite and kyanite parallel to the foliation. Furthermore recrystallization of quartz and deformation of plagioclase and alkali feldspar and the deflection of the foliation around garnet porphyroclasts indicate syn-kinematic presence of these minerals.

Phase equilibrium modeling estimates pressures of ~9.5-12 kbar and temperatures of ~720-800°C for the peak of metamorphism. The composition of garnet cores plot in a

phase field with the assemblage biotite, plagioclase, alkali feldspar, garnet, kyanite, quartz and melt while the garnet rims plot in a phase field with the assemblage biotite, plagioclase, alkali feldspar, muscovite, garnet, kyanite and quartz. Assuming that the H_2O content for modeling was calculated correctly, this indicates that the sample was partially molten at the peak of metamorphism. Furthermore deformation and metamorphism continued as the rock crossed the solidus to lower temperatures evidenced by the solid-state mylonitic fabric. A low percentage of 2 % melt for the P-T estimate is predicted by phase equilibrium modeling. At conditions of partial melting muscovite was not stable indicating that the melt formed by a dehydration reaction of muscovite. A possible reaction is shown below in the equation (2) according to Le Breton and Thompson (1988); Kohn et al. (1997); Indares and Dunning (2001). Another possible melting reaction occurring at higher temperatures than muscovite dehydration melting is a dehydration reaction of biotite forming garnet, alkali feldspar and melt at the expense of biotite as well as kyanite, plagioclase and quartz (e.g. Indares and Dunning, 2001, see equation (3)). This reaction is active towards higher temperatures than the P-T estimate which is indicated by the sudden decrease of the volume percentage of biotite above 850°C shown by isopleths of the volume percentage of biotite in the pseudosection. At temperatures above 900°C biotite is no longer stable. A two stage process of first muscovite and then biotite breakdown melting is indicated as described by Le Breton and Thompson (1988).

(2) Ms ± Pl + Qz –> Kfs + Ky + melt

(3) Bt + Ky ± Pl + Qz –> Grt + Kfs + melt

The estimated T-P conditions are constrained by isopleths of X_{Mg} in garnet and mol fractions of grossular in garnet. The isopleths of mol fractions of spessartine and the isopleths of $_{Mg}$ in biotite plot in the phase fields adjacent to the P-T estimate at higher pressures and temperatures. Mol fractions of spessartine are with values of 0.01-0.2 low and plot therefore possibly not as accurate. Furthermore the solution models might not be as accurate for conditions of partial melting. The isopleths of mol fractions of anorthite in plagioclase partially overlap with the P-T estimate, but higher values plot at lower pressures. Like in the Vaddas and Kåfjord nappe this could be due to an underestimate of calcium in XRF whole rock analysis. Furthermore the isopleths of a.p.f.u. of Si in muscovite plot at higher pressures in the phase field adjacent to the melt-absent mineral assemblage. In the same phase field rutile is stable. No inclusions of rutile in garnet are observed in thin section. Instead rutile is distributed in the matrix and some of the grains are aligned parallel to the foliation indicating that rutile grew at a late stage of deformation. The partial discrepancy of chemical compositions of different minerals indicates that the sample did not reach complete chemical equilibrium. Other explanations are

that the H_2O-estimate is not accurate enough or that solution models for partial melting conditions are not as accurate.

Isopleths of a.p.f.u. Si in muscovite as well as microstructures indicate that muscovite formed after the peak of metamorphism during subsequent shearing at fluid present conditions. Some muscovite grains grew at an angle to the foliation forming later than the shearing event. Fine-grained biotite rims around muscovite and biotite formed even later during retrograde conditions. Moreover the decomposition of alkali feldspar into quartz and plagioclase with oligoclase composition (see fig. 3.29) forming myrmekite structures (see equation (1)) documents retrograde conditions.

All in all according to phase equilibrium modeling, the sample from the Kåfjord-Nordmannvik nappe boundary indicates metamorphic conditions of upper amphibolite to granulite facies and migmatization.

4.2.4. Nordmannvik Nappe

As indicated by macroscopic as well as microscopic structures, the kyanite-garnet-mica schist sample from the Nordmannvik nappe first underwent migmatization and was subsequently sheared similar to the sample from the Kåfjord-Nordmannvik boundary. For both of these events phase equilibrium modeling was conducted. Minerals that were stable during prograde metamorphic conditions are biotite, plagioclase, quartz and sillimanite. All of these minerals are found as inclusions in garnet cores.

The peak mineral assemblage of the migmatization event is formed by biotite, alkali feldspar, garnet, kyanite and quartz. Phase equilibrium modeling estimates pressures of ∼8.5-10 kbar and temperatures of ∼750-800°C for migmatization of the sample. Muscovite as well as plagioclase are not stable during conditions of partial melting indicating the formation of melt by a dehydration reaction of muscovite producing alkali feldspar similar to the sample from the Kåfjord-Nordmannvik nappe boundary (see equation (2)). A rapid decrease of the volume percentage of biotite above 850°C is indicated by isopleths of the volume percentage of biotite in the pseudosection. Hence the temperatures of the P-T estimate were not high enough to produce melt by dehydration of biotite as described in equation (3).

The P-T estimate for partial melting is constrained by X_{Mg} in garnet isopleths corresponding to the core composition as well as isopleths of the volume percent of kyanite. Mol fractions of grossular and spessartine in garnet are low and overlap with the P-T estimate but plot towards lower and higher temperatures. The isopleths of X_{Mg} in biotite plot at higher pressures and temperatures than the P-T estimate possibly due to inaccuracy of the solution model for partial melting similar to sample UL234a. Isopleths of the volume percent of melt indicate up to 4 % melt which is in accordance with field observations.

In summary the P-T estimate for the migmatization event is not as well constrained. This can be explained by overprinting during subsequent shearing. Another possibility is that the estimate for the H_2O-content is not accurate enough. Other samples which show distinct evidence for migmatization in the form of leucosomes and melanosomes applicable for constraining P-T conditions of migmatization did not contain a suitable mineral assemblage for phase equilibrium modeling. Sillimanite in garnet cores indicate that the sample went from sillimanite present conditions to kyanite present conditions but with the data at hand it is not possible to constrain pressures and temperatures for the sillimanite-bearing assemblage.

The mineral assemblage for the shearing event includes biotite, plagioclase, muscovite, garnet and quartz. The estimated metamorphic conditions are pressures of ∼11.5-13.5 kbar and temperatures of ∼660-720°C. Kyanite is not stable during shearing. Instead muscovite is stable indicating that the back-reaction of equation (2) was active producing muscovite, plagioclase and quartz at the expense of alkali feldspar, kyanite and melt according to Kohn et al. (1997) assuming that the melt was not mobile (see equation (4)). However it is more likely that the muscovite formed from a reaction with water. Besides the named minerals, phase equilibrium modeling predicts rutile for the shearing event which was not observed in thin section. Instead opaque minerals are observed in thin section indicating the presence of ilmenite. Often ilmenite overgrows rutile as a retrograde reaction.

(4) Kfs + Ky + melt (H_2O) –> Mus + Pl + Qz

The P-T estimate is constrained by isopleths of X_{Mg} in garnet according to the core composition and isopleths of a.p.f.u. Si in muscovite. Garnet compositions in the thin rims show slightly lower X_{Mg}-values and plot in the adjacent phase field at lower pressures. Isopleths of the low mol fraction of spessartine in garnet plot at temperatures around 500°C while the isopleths of the low mol fractions of spessartine in garnet span over a range of temperatures including the P-T estimate. The isopleths of X_{Mg} in biotite overlap with the estimate only higher values of inclusions in garnet plot at higher pressures. These were sealed in the garnet and possibly indicate that the rock reached higher pressures than suggested by the other minerals. The mismatch of chemical compositions indicates that either no chemical equilibrium was reached during shearing, that the solution models are not suitable for the mineral compositions in the sample or that the mineral compositions are due to overprinting complex.

In summary the analyzed sample form the Nordmannvik nappe shows amphibolite to granulite facies metamorphism for the migmatization event and amphibolite to eclogite facies for the shearing event. However the modeled sample probably shows a chemical

composition for a deformation stage in between the two modeled events. Therefore no phase equilibrium for either of the events is reached.

4.3. Tectonometamorphic History

The shallow pervasive SW dipping foliation as well as the dominant NW and SE plunging stretching lineations are according to previous studies associated with Caledonian deformation (e.g. Gasser et al., 2015). Furthermore the top to the SE sense of shear which was observed macroscopically and microscopically indicates Caledonian thrusting to the SE also described by previous studies (e.g. Townsend, 1987). The foliation is axial-planar to isoclinal and tight folds forming the first fold generation. A second later fold generation with a similar orientation is formed by close to open folds refolding the first generation folds. Both fold generations show Caledonian orientation with fold axes parallel to the stretching lineation which is in agreement with observations of Zwaan and Roberts (1978) in the Nordreisa area. Strong shearing during Caledonian nappe emplacement is recorded by the penetrative foliation, frequent mylonite zones, shear band cleavages and sheath folds.

The KNC on Uløya is formed by mainly clastic meta-sedimentary rocks and unidentified gneisses in accordance with Gayer et al. (1985) and Ramsay et al. (1985). Evidence of migmatization was observed in gneisses along the northern coast of Uløya. Caledonian metamorphic peak conditions of ∼9-12 kbar and ∼610-690°C are constrained by phase equilibrium modeling. This is in agreement with deformation temperatures above ∼600-650°C estimated from quartz and feldspar microstructures.

Gasser et al. (2015) modeled two metamorphic events for meta-sedimentary rocks from the KNC using two different samples with different fabrics from the same location. One sample from an older fabric preserved as a lens within a younger Caledonian deformed fabric from which the second sample was taken. The older event is characterized by P-T conditions of 8.8-9.8 kbar and 760-775°C in the kyanite stability field above the solidus indicating migmatization (Gasser et al., 2015). The younger Caledonian event is constrained to 10-12 kbar and 600-660°C (Gasser et al., 2015) which is in accordance with the P-T conditions determined for the KNC in the present work. Furthermore gneisses along the northern coast of Uløya show migmatization which could be related to the older event described by Gasser et al. (2015) or en even older event described for the Fagervik Complex (Kirkland et al., 2008b).

The Vaddas nappe sandwiched between the KNC and the Kåfjord nappe is composed of meta-sediments and meta-volcanics in accordance with Lindahl et al. (2005). The peak of metamorphism in the Vaddas nappe is constrained to ∼13-14 kbar and ∼670-710°C.

These estimates are the highest pressure estimates on Uløya. Te estimate is slightly higher in temperatures than the underlying KNC. Quartz and feldspar microstructures indicated deformation temperatures above ∼600°C in agreement with the results of modeling. The P-T conditions imply eclogite facies metamorphism in the Vaddas nappe which is higher grade metamorphism than the amphibolite facies deformation described by Andersen (1988).

The Kåfjord nappe is formed by mainly mica schists as described by Zwaan (1988). These schists often contain zoisite, possibly indicating the formation from calcium-rich source material, for example marl. Phase equilibrium modeling for the Kåfjord nappe estimates the peak of metamorphism to ∼11.5-13 kbar and 580-680°C which is lower both in pressure and temperature than the underlying Vaddas nappe. However the pressure is higher than in the KNC and the temperatures are similar to the KNC. Metamorphic conditions in the Kåfjord nappe correspond to amphibolite/eclogite facies metamorphism. Microstructures of quartz and feldspar indicate deformation temperatures above ∼600°C which is, considering the accuracy of modeling and of temperature estimates from microstructures, in accordance with the results of modeling. Andersen (1988) described amphibolite facies metamorphism for the Kåfjord nappe.

The metamorphic conditions of the Kåfjord-Nordmannvik nappe boundary are constrained to ∼9.5-12 kbar and ∼720-800°C indicating partial melting by muscovite and possibly biotite dehydration. A temperature increase within the Kåfjord nappe towards the boundary is inferred which is in agreement with observations by Zwaan (1988) describing increased migmatization towards the boundary with the Nordmannvik nappe. However migmatization was strongly overprinted by subsequent solid-state shearing which is probably the reason why migmatization was observed neither macroscopically nor microscopically. Therefore microstructures of quartz and feldspar indicate much lower temperatures above ∼600°C. Estimated P-T conditions correlate to amphibolite/granulite facies metamorphism.

As described by Zwaan (1988) the Nordmannvik nappe is composed of migmatized garnet-mica gneisses. Similar to the sample from the Kåfjord-Nordmannvik nappe boundary, the rocks from the Nordmannvik nappe were first affected by migmatization which was followed by solid-state shearing. P-T conditions of migmatization by muscovite and possibly biotite dehydration are estimated to ∼8.5-10 kbar and ∼750-780°C correlating to amphibolite/granulite facies metamorphism as described by Andersen (1988). These high grade conditions are confirmed by high temperature microstructures in quartz and feldspar above ∼600-700°C. Subsequent shearing was constrained to conditions of ∼11.5-13.5 kbar and ∼660-720°C indicating amphibolite to eclogite facies metamorphism. Retrograde deformation temperatures of ∼500°C and below are documented by abundant flame perthite

and BLG recrystallization of quartz. Furthermore P-T conditions of partial melting for the sample from the Kåfjord-Nordmannvik nappe boundary fall in the P-T range between the conditions of migmatization and shearing in the Nordmannvik nappe (see fig. 4.2). A polymetamorphic history of the Nordmannvik nappe as previously described is confirmed (e.g. Andresen and Bergh, 1985; Bergh and Andresen, 1985).

The conditions of migmatization in the Nordmannvik nappe are very similar to P-T conditions of Neoproterozoic migmatization in the KNC described by Gasser et al. (2015) (8.8-9.8 kbar and 760-775°C). Moreover Caledonian shearing in the Nordmannvik nappe is similar to shearing of the KNC described by Gasser et al. (2015) (10-12 kbar and 600-660°C) occuring at slightly higher pressures and temperatures in the Nordmannvik nappe as expected higher up in the nappe stack. Considering the observations from Gasser et al. (2015) as well as the observed deformation structures and the modeled P-T conditions for the KNC and the Nordmannvik nappe in the present study, the nappes show some similarities. Both nappes were at least partly migmatized and subsequently sheared and both nappes show almost the same P-T conditions for the two events suggesting that the Nordmannvik nappe could be reworked Baltica basemen similar to the KNC.

Two interpretations can explain the similarities: (1) the KNC and the Nordmannvik nappe form part of the same continental margin and share the same tectonometamorphic history of Neoproterozoic migmatization and Caledonian shearing, or, (2) both, migmatization and shearing in the Nordmannvik nappe are Caledonian. In the first case the Vaddas and Kåfjord nappe would have been deposited as sedimentary basins on the continental margin and would have been thrust on top of the KNC together with the Nordmannvik nappe during Caledonian thrusting. However this first hypothesis is in contrast to the high pressure estimates for the Vaddas nappe. In the second case the Nordmannvik nappe would have been migmatized and sheared during Caledonian deformation while the KNC was migmatized in the Neoproterozoic. Evidence for Caledonian migmatization in the Nordmannvik nappe are leucosomes that show Caledonian orientation e.g. melt pockets around garnet stretched in NE-SW orientation parallel to the stretching lineation or isoclinal folds with fold axes parallel to the Caledonian stretching lineation. On the other hand these structures could have been reoriented during Caledonian deformation. Furthermore migmatization in the Nordmannvik nappe is much more pervasive than in the KNC where migmatization occurs mostly in gneisses or in lenses preserving an older fabric. However this is probably a result of higher P-T conditions reached in the Nordmannvik nappe which is to be expected higher up in the nappe stack. Age dates of the Nordmannvik nappe would be necessary to draw a clear conclusion.

In general the P-T conditions of the four nappes are typical for regional metamorphism in a collisional mountain belt partially reaching eclogite facies metamorphism indicating

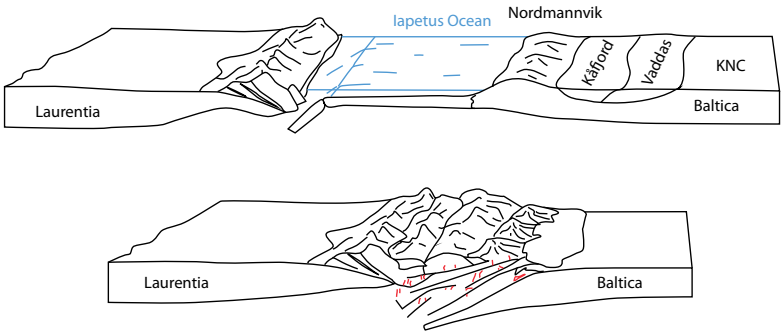

Fig. 4.3.: The schematic figure shows subduction of the Iapetus Ocean and collision of Baltica and Laurentia modified after Ramberg et al. (2006). The interpreted position of the KNC, the Vaddas, the Kåfjord and the Nordmannvik nappe before collision is indicated for hypothesis (1) where the KNC and the Nordmannvik nappe form part of the same continental margin.

subduction (see fig. 4.2). This is in accordance with the plate tectonic context where the closure of the Iapetus Ocean led to the subduction of parts of Baltica beneath Laurentia followed by continent-continent collision of Baltica and Laurentia. Tectonic units involved in this process were subducted, exhumed and thrust on top of each other forming a nappe stack. It is typical for nappe stacks that the metamorphic grade increases from bottom to top (in-sequence-thrusting). The P-T conditions estimated for Caledonian shearing of the KNC, the Vaddas nappe, the Kåfjord and the Nordmannvik nappe exposed on Uløya are similar indicating a common deformation history according to described subduction, exhumation and thrusting processes (see fig. 4.2). Figure 4.3 shows schematically subduction of the Iapetus Ocean and the collision of Baltica with Laurentia modified after Ramberg et al. (2006). The interpreted position of the nappes before collision is indicated for hypothesis (1). The KNC represents meta-sediments from the Baltic shelf, the Vaddas nappe formed by meta-sedimentary and meta-volcanic rocks and the Kåfjord nappe forming meta-pelites with high calcium content were deposited as sedimentary basins on the Baltican shelf while the Nordmannvik nappe together with the KNC forms part of the shelf itself.

The KNC experienced the lowest pressures, the Kåfjord nappe experienced higher pressures and similar temperatures to the KNC and the shearing of the Nordmannvik nappe took place at higher temperatures but similar pressures to the Kåfjord nappe. The Vaddas nappe however, sandwiched between the KNC and the Kåfjord nappe, experienced the highest pressures at similar temperatures to the Nordmannvik nappe indicating that the Vaddas nappe was subducted to greater depth. It is possible that the Vaddas nappe formed a flake/sliver that was subducted to greather depth by an unknown mechanism or out-of-sequence-thrusting and was subsequently exhumed together with the surrounding

nappes. To better understand this anomaly it would be helpful to perform phase equilibrium modeling of rocks from the Vaddas nappe from another location to examine if the result is reproducible. Furthermore, from the described evidence it cannot be ruled out that the KNC and the Nordmannvik underwent the same polymetamorphic history indicating the same continental margin origin for both nappes.

In northern Norway the Caledonian deformation is with ca. 500 Ma the oldest in the Gaissa and the Laksefjord Nappe Complexes as the lowest nappes of the nappe stack and becomes younger upwards in the nappe stack (Sundvoll and Roberts, 2003; Kirkland et al., 2005; Corfu et al., 2006, 2011). U-Pb sphene ages from meta-sedimentary rocks of the KNC constrain Caledonian thrusting at temperatures below ~550°C to ca. 440-420 Ma (Gasser et al., 2015). Other Caledonian ages in the KNC span from ca. 450-425 Ma derived from granitic, pegmatitic and metamorphic fabrics (Kirkland et al., 2006a, 2007a,b; Corfu et al., 2006). On Margerøy, which is considered part of the Vaddas nappe, Caledonian deformation is dated to ca. 430-425 Ma years (Corfu et al., 2011). For the Kåfjord and Nordmannvik nappe no age dates have been obtained.

Furthermore on the basis of the present work the base of the Vaddas should not be associated with the KNC as proposed by Lindahl et al. (2005). Phase equilibrium modeling shows very different P-T conditions for the KNC and the base of the Vaddas nappe. This is already indicated by distinct garnet zoning in the two samples analyzed in the present work. Similarities of the top of the Vaddas nappe with the Kåfjord nappe cannot be addressed with the presented data because the analyzed sample from the Vaddas nappe originated from the base of the nappe.

5. Conclusions

The four Caledonian nappes exposed on Uløya, the KNC, the Vaddas, the Kåfjord and the Nordmannvik nappe, exhibit a penetrative foliation dipping shallowly SW as well as a pervasive stretching lineation plunging shallowly to the NW or the SE. Reconstruction of the tectonic transport direction as well as shear sense indicators determined Caledonian thrusting to the SE. Nappe emplacement was accompanied by strong shearing indicated by the pervasive foliation and various mylonite zones. Two fold generations were identified. Isoclinal to tight folds which are axialplanar to the foliation and overprinting close to open folds, forming the second fold generation. Both fold generations have fold axes parallel to the Caledonian stretching lineation trending NW-SE, indicating a typical Caledonian orientation.

Metamorphism of meta-sediments from the KNC is estimated to ∼9-12 kbar and ∼610-690°C in agreement with Gasser et al. (2015). Signs of migmatization observed in orthogneisses in the north of Uløya are probably pre-Caledonian which is in accordance with migmatization in the KNC described by other authors (e.g. Kirkland et al., 2006a; Gasser et al., 2015).

The peak metamorphism in meta-sedimentary and meta-volcanic rocks of the Vaddas nappe reached 13-14 kbar and ∼670-710°C. Increasing pressures and slightly decreasing temperatures are indicated by garnet zoning. With this estimate the Vaddas nappe reached the highest estimated pressures on Uløya and may have been subducted by a different mechanism or out-of-sequence-thrusting to greater depth than the overlying nappes.

The mica schists of the Kåfjord nappe reached the peak of metamorphism at ∼11.5-13 kbar and ∼580-680°C. Increasing metamorphic temperatures within the nappe towards the boundary with the Nordmannvik nappe are indicated by a P-T estimate of ∼9.5-12 kbar and ∼720-800°C for the boundary. Phase equilibrium modeling indicates muscovite and possibly biotite dehydration melting at these P-T conditions.

For the migmatized garnet-mica schists of the Nordmannvik nappe two tectonometamorphic events were modeled according to field observations where partial melting was observed in the form of quartz- and feldspar-rich leucosomes that were overprinted by solid-state shearing. The first event with conditions of ∼8.5-10 kbar and ∼750-800°C proves partial melting in the Nordmannvik nappe by muscovite and possibly biotite de-

hydration reactions. Melt pockets around garnet porphyroclasts are stretched parallel to the NE-SW Caledonian stretching lineation and isoclinal folds are partially oriented with the fold axis also parallel to the stretching lineation. The second tectonometamorphic event at ∼11.5-13.5 kbar and ∼660-720°C estimates conditions of Caledonian thrusting and nappe emplacement of the Nordmannvik nappe.

Gasser et al. (2015) estimated P-T conditions of migmatization in meta-sedimentary rocks from the KNC during Neoproterozoic to almost the same P-T conditions as migmatization in the Nordmannvik nappe. This might indicate a similar tectonometamorphic history for the KNC and the Nordmannvik nappe where previous migmatization structures in the Nordmannvik nappe were reoriented during Caledonian shearing.

The estimated metamorphic conditions are in agreement with the large-scale plate tectonic setting of subduction of parts of Baltica beneath Laurentia followed by collision of the two continents. Subduction is suggested by prograde pressure and temperature increase while retrograde reactions indicate subsequent exhumation and nappe stacking with pressure and temperature decrease. As expected for a nappe stack the metamorphic conditions in the nappes exposed on Uløya increase from bottom to top with the exception of the Vaddas nappe showing the highest pressures up to eclogite facies. Therefore a different mechanism for subduction and exhumation of the Vaddas nappe might have been active.

Further research is necessary to fully understand the Caledonian emplacement of the KNC, the Vaddas, the Kåfjord and the Nordmannvik nappe. Especially dating is needed to understand the relationship of the KNC and the Nordmannvik nappe as well as to better understand the origin and emplacement of the Vaddas and Kåfjord nappe.

Acknowledgments

I would like to thank my supervisors Professor Holger Stünitz and Professor Jiří Konopásek for making this project, combining structural geology and petrology, possible. Thank you very much for always answering my questions and being open for discussions, sometimes even via Skype.

A special thanks goes furthermore to Carly Farber who has helped me throughout my whole thesis from field work and cutting rocks to taking samples for RXF analysis to South Africa and explaining PerpleX to me. Thank you very much for always having time for me even though you had your own work to do.

Furthermore I would like to thank the University of Tromsø more precisely Trine Dahl and Karina Monsen for the preparation of thin sections. I thank the University of Kiel for a lot of time at the microprobe. Babara Mader and Peter Appel deserve a thank you for friendly and patient instructions on how to use the microprobe. Another thank you goes to the University of Cape Town for XRF bulk rock chemical analysis.

In addition I would like to thank my friends in Tromsø for a fun and adventurous time in Norway. And thank you Marie for being a first-class office mate even though it was just a short time.

Moreover I thank my family and friends in Germany, Italy, Wales or traveling around the world. Long distance friendships are not always easy but I am very happy to know you guys. My mum deserves a special thank you for always being there for me during the past two years, especially during the frustrating but also the happy moments of my masters project.

Bibliography

Andersen, A. (1988). Caledonian terranes of Northern Norway and their characteristics. Trabajos de Geologia, 17:103–117.

Andréasson, P. G., Gee, D. G., Whitehouse, M. J., and Schöberg, H. (2003). Subduction-flip during lapetus Ocean closure and Baltica-Laurentia collision, Scandinavian Caledonides. Terra Nova, 15(6):362–369.

Andresen, A. and Bergh, S. G. (1985). Stratigraphy and tectonometamorphic evolution of the Ordovician-Silurian Balsfjord Group, Lyngen Nappe, north Norwegian Caledonides. The Caledanide Orogen-Scandinavia and related areas, John Wiley and Sons, London, pages 579–591.

Andresen, A. and Steltenpohl, M. G. (1994). Evidence for ophiolite obduction, terrane accretion and polyorogenic evolution of the north Scandinavian Caledonides. Tectonophysics, 231(1-3):59–70.

Augland, L. E., Andresen, a., Gasser, D., and Steltenpohl, M. G. (2013). Early Ordovician to Silurian evolution of exotic terranes in the Scandinavian Caledonides of the Ofoten-Troms area - terrane characterization and correlation based on new U-Pb zircon ages and Lu-Hf isotopic data. Geological Society, London, Special Publications, 390(1):655–678.

Bailey, J. E. and Hirsch, P. B. (1962). The recrystallization process in some polycrystalline metals. In Proceedings of the Royal Society of London A: Mathematical, Physical and Engineering Sciences, volume 267, pages 11–30. The Royal Society.

Becke, F. (1908). Ueber Myrmekite. Schweizerische und Petrographische Mitteilungen, 27:377–390.

Bergh, S. G. and Andresen, A. (1985). Tectonometamorphic evolution of the allochthonous Caledonian rocks between Malangen and Balsfjord, Troms, North Norway. Norges Geologiske Undersøkelse Bulletin, 401:1–34.

Bergström, S. M. (1979). Whiterockian (Ordovician) conodonts from the Hølonda Limestone of the Trondheim Region, Norwegian Caledonides. Norsk Geologisk Tidsskrift, 59:295–307.

Binns, R. E. and Matthews, D. W. (1981). Stratigraphy and structure of the Ordovician-Silurian Balsfjord Supergroup, Troms, North Norway. Norges Geologiske Undersøkelse Bulletin, 365:59–90.

Blumenfeld, P., Mainprice, D., and Bouchez, J. L. (1986). C-slip in quartz from subsolidus deformed granite. Tectonophysics, 127(1-2):97–115.

Coggon, R. and Holland, T. J. B. (2002). Mixing properties of phengitic micas and revised garnet-phengite thermobarometers. Journal of Metamorphic Geology, 20(7):683–696.

Coker-Dewey, J., Steltenpohl, M. G., and Andresen, A. (2000). Geology of western Ullsfjord, North Norway, with emphasis on the development of an inverted metamorphic gradient at the top of the Lyngen Nappe Complex. Norsk Geologisk Tidsskrift, 80(2):111–118.

Corfu, F., Andersen, T. B., and Gasser, D. (2014a). The Scandinavian Caledonides: main features, conceptual advances and critical questions. Geological Society, London, Special Publications, 390(1):9–43.

Corfu, F., Gasser, D., and Chew, D. M. (2014b). New perspectives on the Caledonides of Scandinavia and related areas: introduction. Geological Society, London, Special Publications, 390(1):1–8.

Corfu, F., Gerber, M., Andersen, T. B., Torsvik, T. H., and Ashwal, L. D. (2011). Age and significance of Grenvillian and Silurian orogenic events in the Finnmarkian Caledonides, northern Norway. Canadian Journal of Earth Sciences, 48(2):419–440.

Corfu, F., Roberts, R. J., Torsvik, T. H., Ashwal, L. D., and Ramsay, D. M. (2007). Peri-Gondwanan elements in the Caledonian Nappes of Finnmark, Northern Norway: Implications for the paleogeographic framework of the Scandinavian Caledonides. American Journal of Science, 307(2):434–458.

Corfu, F., Torsvik, T. H., Andersen, T. B., Ashwal, L. D., Ramsay, D. M., and Roberts, R. J. (2006). Early Silurian mafic ,Äì ultramafic and granitic plutonism in contemporaneous flysch , Magerøy , northern Norway : U ,Äì Pb ages and regional significance. Journal of the Geological Society, 163:291–301.

Fuhrman, M. L. and Lindsley, D. H. (1988). Ternary-feldspar modeling and thermometry. American Mineralogist, 73(3-4):201–215.

Gasser, D. (2013). The Caledonides of Greenland, Svalbard and other Arctic areas: status of research and open questions. Geological Society, London, Special Publications, 390(1):93–129.

Gasser, D., Jerabek, P., Faber, C., Stunitz, H., Menegon, L., Corfu, F., Erambert, M., and Whitehouse, M. J. (2015). Behaviour of geochronometers and timing of metamorphic reactions during deformation at lower crustal conditions: Phase equilibrium modelling and U-Pb dating of zircon, monazite, rutile and titanite from the Kalak Nappe Complex, northern Norway. Journal of Metamorphic Geology, pages 513–534.

Gayer, R. A., Hayes, S. J., and Rice, A. H. N. (1985). The structural development of the Kalak Nappe Complex of eastern and central Porsangerhalvøya, Finnmark, Norway. Norges Geologiske Undersøkelse Bulletin, 400:67–68.

Gayer, R. A. and Roberts, J. D. (1973). Stratigraphic review of the Finnmark Caledonides, with possible tectonic implications. Proceedings of the Geologists' Association, 84, Part 4(0):405–IN3.

Gee, D. G. (1975). A tectonic model for the central part of the Scandinavian Caledonides. American Journal of Science, 275:468–515.

Gee, D. G. (1978). Nappe displacement in the Scandinavian Caledonides. Tectonophysics, 47(3-4).

Gee, D. G. and Sturt, B. A. (1985). The Caledonide orogen: Scandinavia and related areas. 2.

Guillope, M. and Poirier, J. P. (1979). Dynamic recrystallization during creep of single-crystalline halite: An experimental study. Journal of Geophysical Research, 84(2):5557–5567.

Hanmer, S. K. (1982). Microstructure and geochemistry of plagioclase and microcline in naturally deformed granite. Journal of Structural Geology, 4(1):197–213.

Hirth, G. and Tullis, J. (1992). Dislocation creep regimes in quartz aggregates. Journal of Structural Geology, 14(2):145–159.

Hobbs, B. (1968). Recrystallization of single crystals of quartz. Tectonophysics, 6(5):353–401.

Holland, T. I. M. and Powell, R. (2001). Calculation of phase relations involving haplogranitic melts using an internally consistent thermodynamic dataset. Journal of Petrology, 42(4):673–683.

Holland, T. J. B. and Powell, R. (1998). An internally consistent thermodynamic data set for phases of petrological interest. Journal of metamorphic Geology, 16(3):309–343.

Indares, A. and Dunning, G. (2001). Partial melting of high-P,ÄìT metapelites from the Tshenukutish Terrane (Grenville Province): petrography and U,ÄìPb geochronology. Journal of Petrology, 42(8):1547–1565.

Kirkland, C., Stephen Daly, J., and Whitehouse, M. (2007a). Provenance and Terrane Evolution of the Kalak Nappe Complex, Norwegian Caledonides: Implications for Neoproterozoic Paleogeography and Tectonics. The Journal of Geology, 115(1):21–41.

Kirkland, C. L., Daly, J. S., Chew, D. M., and Page, L. M. (2008a). The Finnmarkian Orogeny revisited: An isotopic investigation in eastern Finnmark, Arctic Norway. Tectonophysics, 460(1-4):158–177.

Kirkland, C. L., Daly, J. S., Eide, E. A., and Whitehouse, M. J. (2006a). The structure and timing of lateral escape during the Scandian Orogeny: A combined strain and geochronological investigation in Finnmark, Arctic Norwegian Caledonides. Tectonophysics, 425(1-4):159–189.

Kirkland, C. L., Daly, J. S., Eide, E. A., and Whitehouse, M. J. (2007b). Tectonic evolution of the Arctic Norwegian Caledonides from a texturally- and structurally-constrained multi-isotopic (Ar-Ar, Rb-Sr, Sm-Nd, U-Pb) study. American Journal of Science, 307(2):459–526.

Kirkland, C. L., Daly, J. S., and Whitehouse, M. J. (2005). Early Silurian magmatism and the Scandian evolution of the Kalak Nappe Complex, Finnmark, Arctic Norway. Journal of the Geological Society, 162(6):985–1003.

Kirkland, C. L., Daly, J. S., and Whitehouse, M. J. (2006b). Granitic magmatism of grenvillian and late neoproterozoic age in Finnmark, Arctic Norway - Constraining pre-Scandian deformation in the Kalak Nappe Complex. Precambrian Research, 145(1-2):24–52.

Kirkland, C. L., Daly, J. S., and Whitehouse, M. J. (2008b). Basement-cover relationships of the Kalak Nappe Complex, Arctic Norwegian Caledonides and constraints on Neoproterozoic terrane assembly in the North Atlantic region. Precambrian Research, 160(3-4):245–276.

Kohn, M. J., Spear, F. S., and Valley, J. W. (1997). Dehydration-Melting and Fluid Recycling during Metamorphism: Rangeley Formation, New Hampshire, USA. Journal of Petrology, 38(9):1255–1277.

Krogh, E. J., Andresen, A., Bryhni, I., Broks, T. M., and Kristensen, S. E. (1990). Eclogites and polyphase P-T cycling in the Caledonian Uppermost Allochthon in Troms, northern Norway. Journal of Metamorphic Geology, 8(3):289–309.

Kruhl, J. (1996). Prism- and basal-plane parallel subgrain boundaries in quartz: a microstructural geothermobaromether. Journal of Metamorphic Geology, 14:581–589.

Kruse, R. and Stünitz, H. (1999). Deformation mechanisms and phase distribution in mafic high-temperature mylonites from the Jotun Nappe, southern Norway. Tectonophysics, 303(1-4):223–249.

Le Breton, N. and Thompson, A. B. (1988). Fluid-absent (dehydration) melting of biotite in metapelites in the early stages of crustal anatexis. Contributions to Mineralogy and Petrology, 99(2):226–237.

Lindahl, I., Stevens, B. P. J., and Zwaan, K. B. (2005). The geology of the Váddás area, Troms: a key to our understanding of the Upper Allochthon in the Caledonides of northern Norway. Norges Geologiske Undersøkelse Bulletin, 445:5–43.

Mainprice, D., Bouchez, J. L., Blumenfeld, P., and Tubia, J. M. (1986). Dominant-C Slip in Naturally Deformed Quartz - Implications for Dramatic Plastic Softening at High-Temperature. Geology, 14(10):819–822.

Minsaas, O. and Sturt, B. A. (1985). The Ordovician-Silurian clastics sequence overlying the Lyngen Gabbro Complex, and its environmental significance. The Caledonide Orogen:-Scandinavia and related areas, 1:569–577.

Nystuen, J. P., Andresen, A., Kumpulainen, R. A., and Siedlecka, A. (2008). Neoproterozoic basin evolution in Fennoscandia, East Greenland and Svalbard. Episodes, 31(1):35–43.

Passchier, C. W. and Trouw, R. a. J. (2005). Microtectonics. Springer, second edi edition.

Pedersen, R. B., Dunning, G. R., and Robins, B. (1989). U-Pb ages of nepheline syenite pegmatites from the Seiland Magmatic Province, N. Norway. The Caledonide Geology of Scandinavia. Graham and Trotman, London, pages 3–8.

Pryer, L. L. (1993). Microstructures in feldspars from a major crustal thrust zone: The Grenville Front, Ontario, Canada. Journal of Structural Geology, 15(1):21–36.

Ramberg, I. B., Bryhni, I., and Nøttvedt, A. (2006). Landet blir til - Norges geologi. Norsk Geologisk Forening (NGF), first edit edition.

Ramsay, D. M., Sturt, B. A., Zwaan, K. B., and Roberts, D. (1985). Caledonides of northern Norway. The Caledonian Orogen: Scandinavia and related areas. Edited by DG Gee and BA Sturt. Wiley, Chichester, UK, pages 163–184.

Rice, a. H. N. (2014). Restoration of the External Caledonides, Finnmark, North Norway. Geological Society, London, Special Publications, 390(1):271–299.

Roberts, D. (2003). The Scandinavian Caledonides: Event chronology, palaeogeographic settings and likely modern analogues. Tectonophysics, 365(1-4):283–299.

Roberts, D. and Gee, D. G. (1985). An introduction to the structure of the Scandinavian Caledonides. The Caledonian Orogen: Scandinavia and related areas. Edited by DG Gee and BA Sturt. Wiley, Chichester, UK, pages 55–68.

Roberts, D. and Gromet, L. P. (2009). AU,ÄìPb zircon Archaean age for granitoid rocks in the Kunes Nappe, Laksefjord Nappe Complex, Finnmark, North Norway. Norges geologiske undersøkelse Bulletin, 449:1–8.

Roberts, D., Nordgulen, Ø., and Melezhik, V. (2007). The Uppermost Allochthon in the Scandinavian Caledonides: From a Laurentian ancestry through Taconian orogeny to Scandian crustal growth on Baltica. Geological Society of America Memoirs, 200:357–377.

Siedlecka, A., Roberts, D., Nystuen, J. P., and Olovyanishnikov, V. G. (2004). North-eastern and northwestern margins of Baltica in Neoproterozoic time: evidence from the Timanian and Caledonian Orogens. Geological Society, London, Memoirs, 30(1):169–190.

Simpson, C. and Wintsch, R. P. (1989). Evidence for deformation-induced K-feldspar replacement by myrmekite. Journal of Metamorphic Geology, 7:261–275.

Skjernaa, L. (1989). Tubular folds and sheath folds: definitions and conceptual models for their development, with examples from the Grapesvare area, northern Sweden. Journal of Structural Geology, 11(6):689–703.

Slagstad, T., Melezhik, V. A., Kirkland, C. L., Zwaan, K. B., Roberts, D., Gorokhov, I. M., and Fallick, A. E. (2006). Carbonate isotope chemostratigraphy suggests revisions to the geological history of the West Finnmark Caledonides, northern Norway. Journal of the Geological Society, 163(2):277–289.

Stephens, M. B. and Gee, D. G. (1985). A tectonic model for the evolution of the eugeoclinal terranes in the central Scandinavian Caledonides. The Caledonide Orogen: Scandinavia and Related Areas. Wiley, Chichester, pages 953–978.

Stephens, M. B. and Gee, D. G. (1989). Terranes and polyphase accretionary history in the Scandinavian Caledonides. Geological Society of America Special Papers, 230:17–30.

Stipp, M., Stünitz, H., Heilbronner, R., and Schmid, S. M. (2002). The eastern Tonale fault zone: A 'natural laboratory' for crystal plastic deformation of quartz over a temperature range from 250 to 700 C. Journal of Structural Geology, 24(12):1861–1884.

Sundvoll, B. and Roberts, D. (2003). A likely Early Ordovician age for the regional, penetrative cleavage in the Gaissa Nappe Complex, northern Norway. Norges geologiske undersøkelse Bulletin, 441:51–59.

Tajčmanová, L., Connolly, J. A. D., and Cesare, B. (2009). A thermodynamic model for titanium and ferric iron solution in biotite. Journal of Metamorphic Geology, 27(2):153–165.

Terry, M. P., Robinson, P., Hamilton, M. A., and Jercinovic, M. J. (2000). Monazite geochronology of UHP and HP metamorphism, deformation, and exhumation Nordøyane, Western Gneiss Region, Norway. American Mineralogist, 85(11-12):1651–1664.

Townsend, C. (1987). Thrust transport directions and thrust sheet restoration in the Caledonides of Finnmark, North Norway. Journal of Structural Geology, 9(3):245–352.

Urai, J. L., Means, W. D., and Lister, G. S. (1986). Dynamic recrystallization of minerals. Mineral and Rock Deformation: Laboratory Studies: The Paterson Volume, pages 161–199.

Vernon, R. H. and Paterson, S. R. (2001). Axial-surface leucosomes in anatectic migmatites. Tectonophysics, 335(1-2):183–192.

Vidal, J.-L., Kubin, L., Debat, P., and Soula, J.-C. (1980). Deformation and dynamic recrystallization of K feldspar augen in orthogneiss from Montagne Noire, Occitania, Southern France. Lithos, 13(3):247–255.

Whitney, D. L. and Evans, B. W. (2010). Abbreviations for names of rock-forming minerals. American Mineralogist, 95(1):185–187.

Zwaan, K. B. (1988). Nordreisa, berggrunnsgeologisk kart-M 1: 250 000. Norges geologiske undersøkelse.

Zwaan, K. B. and Roberts, D. (1978). Tectonostratigraphic Succession and Development of the Finnmarkian Nappe Sequence , North Norway. Norges geologiske undersokelse,, 343:55–71.

A. Appendix

A.1. Geological map with all locations

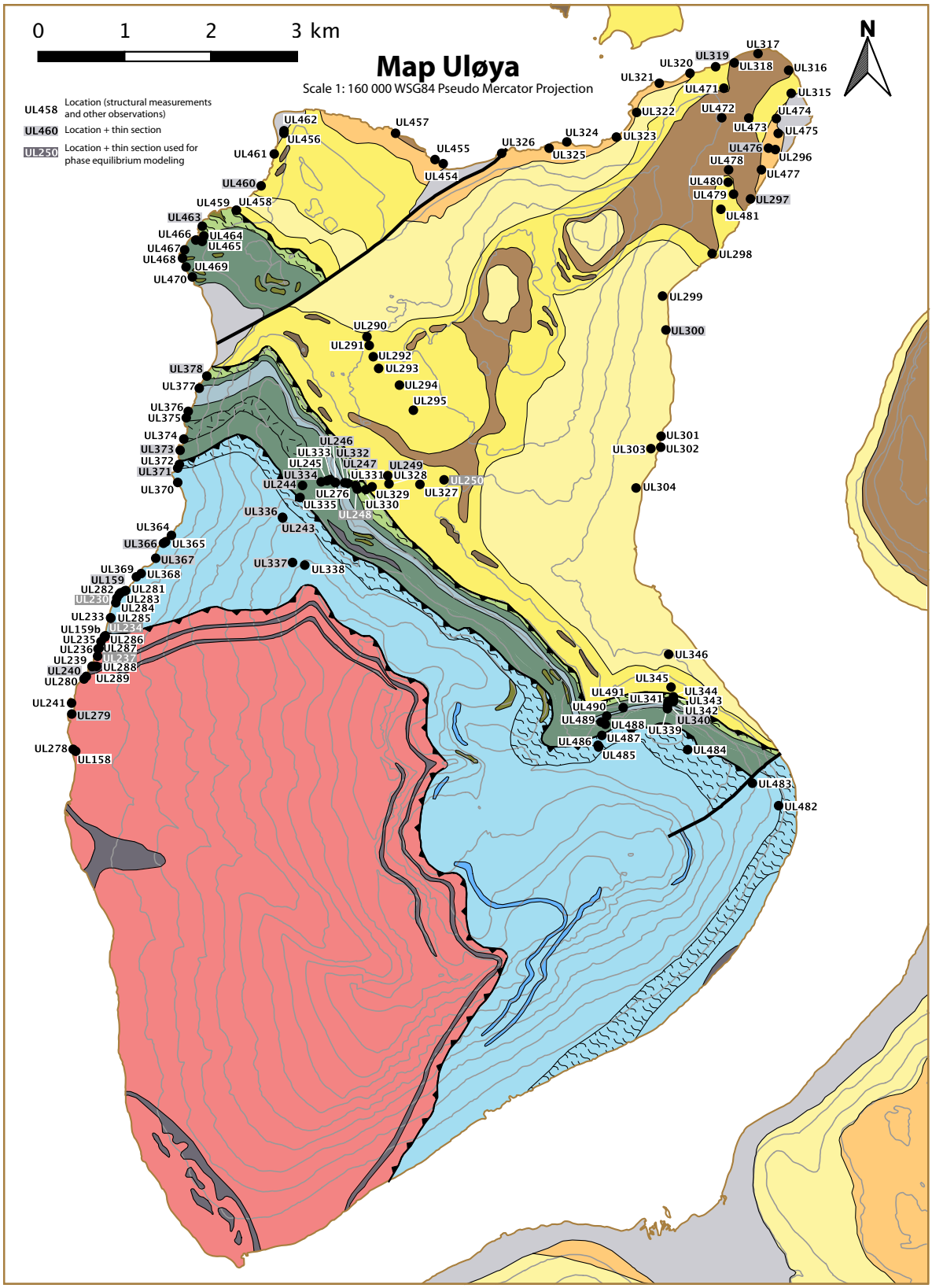
0 1 2 3 km
Map Uløya
Scale 1: 160 000 WSG84 Pseudo Mercator Projection
N
UL458 Location (structural measurements and other observations)
UL460 Location + thin section
UL250 Location + thin section used for phase equilibrium modeling

Fig. A.1.

A.2. Paragenesis overview of the thin sections

Sample	Main minerals							Accessory minerals							Nappe	Rock type
	Bt	Pl	Qtz	Grt	Kfs	Sil	Ky	Ms	Hbl	Chl	Cal	Zrn	Tur	Mnz	Rt	Spn	Opq	Ap	Ep/Aln/Zoi		
UL159	x		x	x	x		x	x				x	x		x		x			N	ky-grt-mica schist
UL230	x	x	x	x	x	x	x	x					x	x			x	x		Kå	sil/ky-grt-mica schist
UL232	x		x	x	x	x	x	x					x		x	x	x			Kå-N boundary	sil/ky-grt-mica schist
UL234a	x	x	x	x	x		x	x				x			x		x			Kå-N boundary	ky-grt-mica schist
UL234b	x	x	x	x	x				x			x				x		x	x	Kå-N boundary	grt-hbl-mica gneiss
UL236	x		x	x	x		x	x								x	x			N	quartzitic ky-grt-mica schist
UL237	x		x	x	x		x	x				x	x	x			x	x		N	ky-grt-mica schist
UL240	x	x	x	x	x			x	x	x		x	x			x			x	N	migmatized grt-hbl-mica gneiss
UL242	x	x	x	x	x			x				x					x			N	migmatized grt geniss
UL243	x	x	x	x	x					x			x		x		x		x	Kå	zoi-bt-grt schist
UL244	x	x	x	x					x		x	x			x		x		x	V-Kå boundary	cal-bt-hbl-grt schist
UL244b		x	x						x						x	x			x	V-Kå boundary	amphibolite
UL246	x	x	x	x	x			x				x					x		x	V	bt-ms-grt gneiss
UL247	x	x	x	x	x			x				x				x			x	V	bt-ms-grt gneiss
UL248	x	x	x	x	x			x				x			x	x	x	x	x	V	bt-ms-grt gneiss
UL248b	x	x	x	x	x			x								x			x	V	bt-ms-grt gneiss
UL249	x	x	x	x				x				x	x		x	x	x		x	K	quartzitic grt-mica schist
UL250	x	x	x	x	x			x				x			x	x	x	x	x	K	quartzitic grt-mica schist
UL279	x	x	x	x	x			x				x				x	x		x	N	migmatized grt-mica schist
UL297		x	x	x					x							x	x			K	amphibolite
UL300			x		x			x									x		x	K	meta-arkose
UL319	x	x	x	x				x		x		x			x	x	x	x	x	K	quartzitic grt-mica schist
UL340	x	x	x	x	x			x		x		x			x	x			x	V	quartzitic grt-mica schist
UL366	x	x	x	x				x		x		x	x			x	x		x	Kå	grt-mica schist
UL367	x	x	x	x				x					x			x	x			Kå	grt-mica schist
UL371	x	x	x	x	x							x			x	x	x		x	V-Kå boundary	quartzitic grt-mica schist
UL373	x	x	x						x		x					x	x		x	V	zoi-bt schist with calcite
UL378	x	x	x	x	x			x			x				x	x		x		K-V boundary	migmatitic zoi-grt-bt schist
UL460	x	x	x	x	x			x							x	x	x			K	quartzitic grt-mica schists
UL463	x	x	x					x		x		x		x	x					V	quartzitic mica schist
UL476	x	x	x	x	x			x				x				x	x			V	migmatitic grt gneiss

A.3. Additional Pseudosections

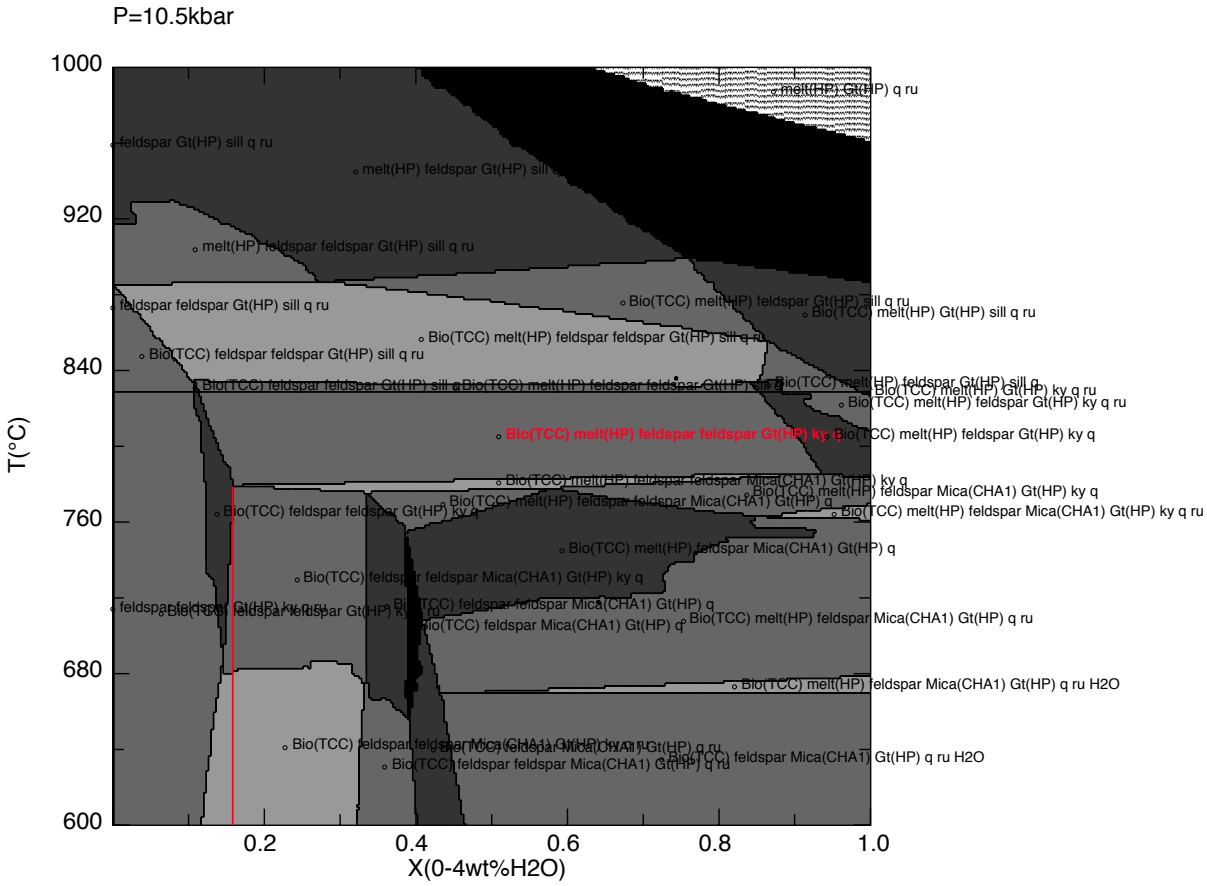

Fig. A.2.: The T-X section was calculated with a variable water-content from 0 to 4 wt% for a range of temperatures at a constant pressure of 10.5 kbar. This section was used to estimate the H_2O-content at the water-saturated solidus of the sample UL234a. A water content of 0.7 wt% was estimated correlating to the lowest melting temperature of the peak mineral assemblage in the T-X section.

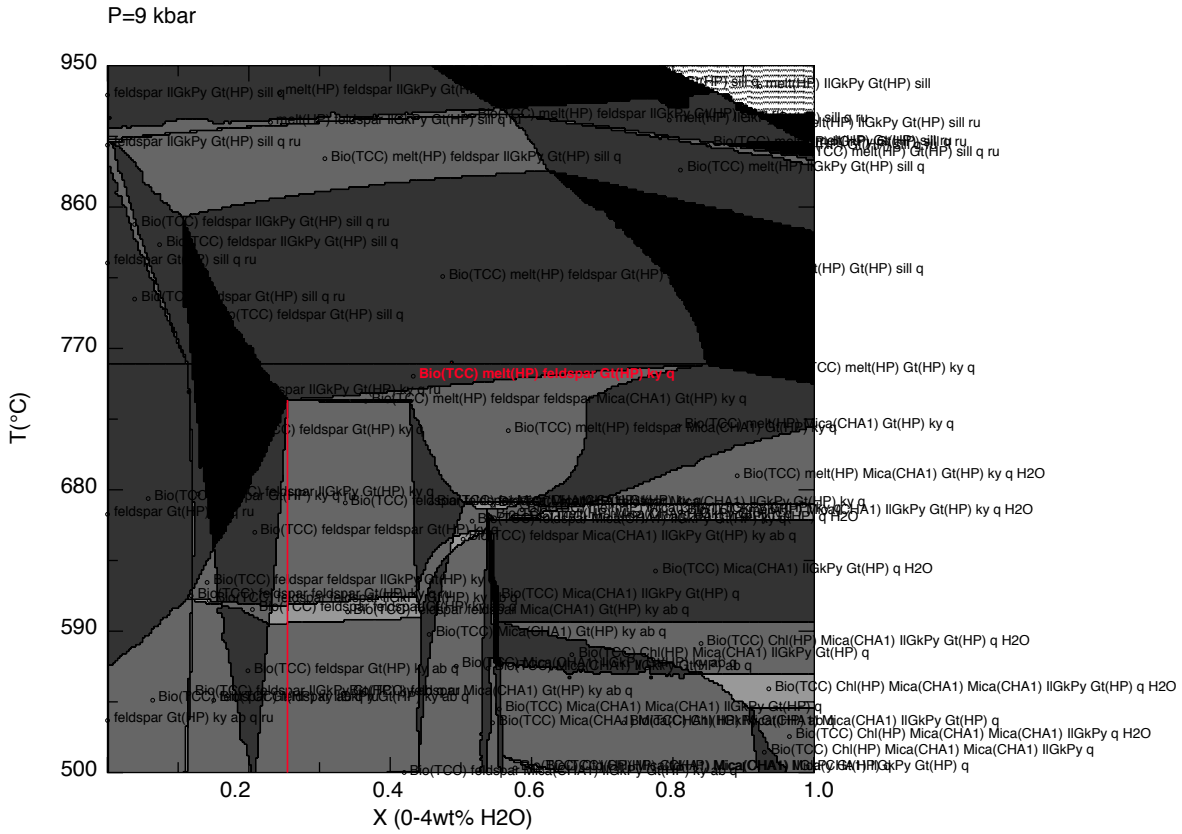

Fig. A.3.: The T-X section was calculated with a variable water-content from 0 to 4 wt% for a range of temperatures at a constant pressure of 9 kbar. This section was used to estimate the H_2O-content at the water-saturated solidus of the sample UL237. A water content of 1 wt% was estimated correlating to the lowest melting temperature of the peak mineral assemblage in the T-X section.

A.4. Microprobe data

A.4.1. Kalak Nappe Complex - Sample UL250

	grt 3 profile 1	grt 3 profile 2	grt 3 profile 3	grt 3 profile 4	grt 3 profile 5	grt 3 profile 6	grt 3 profile 7	grt 3 profile 8	grt 3 profile 10	grt 3 profile 11
Analysis No.	657	658	659	660	661	662	663	664	666	667
SiO2	37.77	37.74	37.88	37.73	37.80	37.59	37.76	37.74	37.77	37.70
TiO2	0.11	0.00	0.00	0.00	0.00	0.08	0.01	0.06	0.10	0.09
Cr2O3	0.00	0.00	0.00	0.00	0.00	0.00	0.00	0.00	0.00	0.00
Al2O3	21.55	21.58	21.64	21.60	21.64	21.68	21.65	21.52	21.60	21.56
FeO	28.33	28.22	28.41	28.04	27.04	26.78	25.95	27.70	26.66	27.67
MnO	0.94	0.99	1.31	2.46	2.84	2.75	2.55	1.89	2.30	2.32
NiO	0.00	0.00	0.00	0.00	0.00	0.00	0.00	0.00	0.00	0.00
MgO	1.70	1.70	1.74	1.83	1.75	1.73	1.67	1.67	1.60	1.70
CaO	10.34	9.97	9.74	8.92	9.35	9.68	11.11	9.58	11.10	9.32
Na2O	0.00	0.00	0.00	0.00	0.00	0.00	0.00	0.00	0.00	0.00
K2O	0.00	0.00	0.00	0.00	0.00	0.00	0.00	0.00	0.00	0.00
Total wt%	100.74	100.20	100.72	100.58	100.42	100.29	100.70	100.16	101.13	100.36
a.p.f.u. for 12 Oxygens										
Si	2.98	2.99	2.99	2.99	3.00	2.98	2.98	3.00	2.97	2.99
Ti	0.01	0.00	0.00	0.00	0.00	0.01	0.00	0.00	0.01	0.01
Cr	0.00	0.00	0.00	0.00	0.00	0.00	0.00	0.00	0.00	0.00
Al	2.01	2.02	2.01	2.02	2.02	2.03	2.01	2.02	2.00	2.02
Fe3+	0.02	0.00	0.00	0.01	0.00	0.00	0.04	0.00	0.05	0.00
Fe2+	1.85	1.87	1.88	1.85	1.79	1.77	1.67	1.84	1.70	1.84
Mn	0.06	0.07	0.09	0.17	0.19	0.18	0.17	0.13	0.15	0.16
Ni	0.00	0.00	0.00	0.00	0.00	0.00	0.00	0.00	0.00	0.00
Mg	0.20	0.20	0.20	0.22	0.21	0.20	0.20	0.20	0.19	0.20
Ca	0.87	0.85	0.82	0.76	0.79	0.82	0.94	0.82	0.93	0.79
Na	0.00	0.00	0.00	0.00	0.00	0.00	0.00	0.00	0.00	0.00
K	0.00	0.00	0.00	0.00	0.00	0.00	0.00	0.00	0.00	0.00
Total	8.00	8.00	8.00	8.00	8.00	8.00	8.00	8.00	8.00	8.00
xMg	0.10	0.10	0.10	0.10	0.10	0.10	0.10	0.10	0.10	0.10
Prp	0.07	0.07	0.07	0.07	0.07	0.07	0.06	0.07	0.06	0.07
Alm	0.61	0.62	0.62	0.61	0.60	0.59	0.55	0.61	0.55	0.61
Gross	0.29	0.28	0.27	0.25	0.26	0.27	0.31	0.27	0.30	0.26
Spes	0.02	0.02	0.03	0.05	0.06	0.06	0.06	0.04	0.05	0.05
Total Endmemembers	1.00	1.00	1.00	1.00	0.99	1.00	0.99	0.99	0.99	1.00

	grt 3 profile 12	grt 3 profile 13	grt 3 profile 14	grt 3 profile 15	grt 3 profile 16	grt 3 profile 19	grt 3 profile 20	grt 3 profile 21	grt 3 profile 22	grt 3 profile 23
Analysis No.	668	669	670	671	672	675	676	677	678	679
SiO2	37.76	37.67	37.68	37.49	37.45	37.87	37.42	37.62	37.77	37.57
TiO2	0.13	0.05	0.00	0.05	0.04	0.09	0.12	0.20	0.18	0.06
Cr2O3	0.00	0.00	0.00	0.00	0.00	0.00	0.00	0.00	0.00	0.00
Al2O3	21.41	21.69	21.38	21.53	21.51	21.60	21.36	21.35	21.59	21.51
FeO	27.27	25.42	24.30	23.67	25.37	24.17	24.75	24.70	25.73	26.19
MnO	2.47	3.35	5.19	5.99	3.55	4.77	4.23	3.51	3.20	3.66
NiO	0.00	0.00	0.00	0.00	0.00	0.00	0.00	0.00	0.00	0.00
MgO	1.77	1.51	1.34	1.16	1.54	1.40	1.50	1.52	1.58	1.60
CaO	8.85	10.90	10.35	10.37	10.60	10.88	10.50	11.16	10.56	9.87
Na2O	0.00	0.00	0.00	0.00	0.00	0.00	0.00	0.00	0.00	0.00
K2O	0.00	0.00	0.00	0.00	0.00	0.00	0.00	0.00	0.00	0.00
Total wt%	99.66	100.59	100.24	100.26	100.07	100.78	99.88	100.05	100.62	100.47
a.p.f.u. for 12 Oxygens										
Si	3.02	2.98	2.99	2.98	2.97	2.99	2.98	2.99	2.98	2.98
Ti	0.01	0.00	0.00	0.00	0.00	0.01	0.01	0.01	0.01	0.00
Cr	0.00	0.00	0.00	0.00	0.00	0.00	0.00	0.00	0.00	0.00
Al	2.02	2.02	2.00	2.02	2.01	2.01	2.01	2.00	2.01	2.01
Fe3+	0.00	0.02	0.01	0.01	0.03	0.00	0.02	0.01	0.00	0.03
Fe2+	1.82	1.65	1.60	1.56	1.65	1.59	1.63	1.63	1.70	1.71
Mn	0.17	0.22	0.35	0.40	0.24	0.32	0.29	0.24	0.21	0.25
Ni	0.00	0.00	0.00	0.00	0.00	0.00	0.00	0.00	0.00	0.00
Mg	0.21	0.18	0.16	0.14	0.18	0.16	0.18	0.18	0.19	0.19
Ca	0.76	0.92	0.88	0.88	0.90	0.92	0.90	0.95	0.89	0.84
Na	0.00	0.00	0.00	0.00	0.00	0.00	0.00	0.00	0.00	0.00
K	0.00	0.00	0.00	0.00	0.00	0.00	0.00	0.00	0.00	0.00
Total	8.00	8.00	8.00	8.00	8.00	8.00	8.00	8.00	8.00	8.00
xMg	0.10	0.10	0.09	0.08	0.10	0.09	0.10	0.10	0.10	0.10
Prp	0.07	0.06	0.05	0.05	0.06	0.05	0.06	0.06	0.06	0.06
Alm	0.59	0.54	0.53	0.52	0.54	0.53	0.54	0.54	0.56	0.56
Gross	0.24	0.30	0.29	0.29	0.30	0.31	0.29	0.31	0.30	0.27
Spes	0.05	0.07	0.12	0.13	0.08	0.11	0.09	0.08	0.07	0.08
Total Endmemembers	0.98	0.99	1.00	0.99	0.99	1.00	1.00	1.00	1.00	0.99

	grt 3 profile 24	grt 3 profile 25	grt 3 profile 26	grt 3 profile 27	grt 3 profile 28	grt 3 profile 29	grt 3 profile 30	grt 3 profile 31	grt 3 profile 32	grt 3 profile 33
Analysis No.	680	681	682	683	684	685	686	687	688	689
SiO2	37.60	37.69	37.86	37.95	37.39	37.71	37.58	37.86	37.71	38.00
TiO2	0.00	0.10	0.18	0.19	0.23	0.15	0.12	0.10	0.05	0.16
Cr2O3	0.00	0.00	0.00	0.00	0.00	0.00	0.00	0.00	0.00	0.00
Al2O3	21.40	21.42	21.56	21.29	21.41	21.55	21.38	21.34	21.54	21.49
FeO	24.87	23.97	25.14	24.92	24.34	24.17	23.62	23.46	22.61	22.75
MnO	4.36	4.61	4.56	4.00	4.61	4.74	5.23	5.25	6.44	6.71
NiO	0.00	0.00	0.00	0.00	0.00	0.00	0.00	0.00	0.00	0.00
MgO	1.58	1.54	1.50	1.63	1.44	1.52	1.36	1.38	1.21	1.15
CaO	10.25	10.59	10.07	10.55	10.41	10.53	10.60	10.47	10.79	10.88
Na2O	0.00	0.00	0.00	0.00	0.00	0.00	0.00	0.00	0.00	0.00
K2O	0.00	0.00	0.00	0.00	0.00	0.00	0.00	0.00	0.00	0.00
Total wt%	100.06	99.92	100.87	100.52	99.83	100.37	99.89	99.86	100.35	101.14
a.p.f.u. for 12 Oxygens										
Si	2.99	3.00	2.99	3.00	2.98	2.99	2.99	3.02	2.99	2.99
Ti	0.00	0.01	0.01	0.01	0.01	0.01	0.01	0.01	0.00	0.01
Cr	0.00	0.00	0.00	0.00	0.00	0.00	0.00	0.00	0.00	0.00
Al	2.01	2.01	2.01	1.99	2.01	2.01	2.01	2.00	2.01	2.00
Fe3+	0.02	0.00	0.00	0.00	0.00	0.00	0.00	0.00	0.00	0.00
Fe2+	1.64	1.59	1.66	1.65	1.62	1.60	1.57	1.56	1.50	1.50
Mn	0.29	0.31	0.30	0.27	0.31	0.32	0.35	0.35	0.43	0.45
Ni	0.00	0.00	0.00	0.00	0.00	0.00	0.00	0.00	0.00	0.00
Mg	0.19	0.18	0.18	0.19	0.17	0.18	0.16	0.16	0.14	0.13
Ca	0.87	0.90	0.85	0.89	0.89	0.89	0.90	0.89	0.92	0.92
Na	0.00	0.00	0.00	0.00	0.00	0.00	0.00	0.00	0.00	0.00
K	0.00	0.00	0.00	0.00	0.00	0.00	0.00	0.00	0.00	0.00
Total	8.00	8.00	8.00	8.00	8.00	8.00	8.00	8.00	8.00	8.00
xMg	0.10	0.10	0.10	0.10	0.10	0.10	0.09	0.09	0.09	0.08
Prp	0.06	0.06	0.06	0.06	0.06	0.06	0.05	0.05	0.05	0.04
Alm	0.54	0.53	0.55	0.54	0.54	0.53	0.52	0.51	0.50	0.50
Gross	0.29	0.30	0.28	0.29	0.29	0.30	0.30	0.29	0.31	0.30
Spes	0.10	0.10	0.10	0.09	0.10	0.11	0.12	0.11	0.14	0.15
Total Endmemembers	1.00	1.00	1.00	1.00	1.00	1.00	1.00	0.98	1.00	1.00

	grt 3 profile 34	grt 3 profile 35	grt 3 profile 36	grt 3 profile 37	grt 3 profile 38	grt 3 profile 39	grt 3 profile 40	grt 3 profile 41	grt 3 profile 42	grt 3 profile 43
Analysis No.	690	691	692	693	694	695	696	697	698	699
SiO2	37.81	37.52	37.84	37.67	37.73	37.85	37.55	37.55	37.93	37.81
TiO2	0.01	0.13	0.13	0.10	0.02	0.00	0.00	0.07	0.08	0.03
Cr2O3	0.00	0.00	0.00	0.00	0.00	0.00	0.00	0.00	0.00	0.00
Al2O3	21.37	21.29	21.48	21.46	21.52	21.55	21.66	21.59	21.51	21.57
FeO	23.05	24.48	24.10	25.42	25.34	25.42	26.68	25.02	24.23	23.61
MnO	5.90	4.83	4.70	3.82	3.65	3.60	3.19	4.08	5.18	5.86
NiO	0.00	0.00	0.00	0.00	0.00	0.00	0.00	0.00	0.00	0.00
MgO	1.27	1.48	1.46	1.62	1.56	1.55	1.66	1.50	1.37	1.25
CaO	10.65	10.37	10.70	10.12	10.48	10.55	9.57	10.68	10.58	10.54
Na2O	0.00	0.00	0.00	0.00	0.00	0.00	0.00	0.00	0.00	0.00
K2O	0.00	0.00	0.00	0.00	0.00	0.00	0.00	0.00	0.00	0.00
Total wt%	100.06	100.10	100.41	100.21	100.29	100.52	100.31	100.49	100.88	100.67
a.p.f.u. for 12 Oxygens										
Si	3.01	2.98	3.00	2.99	2.99	2.99	2.98	2.97	2.99	2.99
Ti	0.00	0.01	0.01	0.01	0.00	0.00	0.00	0.00	0.00	0.00
Cr	0.00	0.00	0.00	0.00	0.00	0.00	0.00	0.00	0.00	0.00
Al	2.00	2.00	2.00	2.01	2.01	2.01	2.03	2.01	2.00	2.01
Fe3+	0.00	0.02	0.00	0.00	0.01	0.00	0.01	0.04	0.00	0.00
Fe2+	1.53	1.61	1.60	1.69	1.67	1.68	1.76	1.62	1.60	1.56
Mn	0.40	0.33	0.32	0.26	0.25	0.24	0.21	0.27	0.35	0.39
Ni	0.00	0.00	0.00	0.00	0.00	0.00	0.00	0.00	0.00	0.00
Mg	0.15	0.18	0.17	0.19	0.18	0.18	0.20	0.18	0.16	0.15
Ca	0.91	0.88	0.91	0.86	0.89	0.89	0.81	0.91	0.89	0.89
Na	0.00	0.00	0.00	0.00	0.00	0.00	0.00	0.00	0.00	0.00
K	0.00	0.00	0.00	0.00	0.00	0.00	0.00	0.00	0.00	0.00
Total	8.00	8.00	8.00	8.00	8.00	8.00	8.00	8.00	8.00	8.00
xMg	0.09	0.10	0.10	0.10	0.10	0.10	0.10	0.10	0.09	0.09
Prp	0.05	0.06	0.06	0.06	0.06	0.06	0.06	0.06	0.05	0.05
Alm	0.51	0.53	0.53	0.56	0.56	0.56	0.58	0.53	0.53	0.52
Gross	0.30	0.29	0.30	0.29	0.30	0.30	0.27	0.30	0.30	0.30
Spes	0.13	0.11	0.10	0.09	0.08	0.08	0.07	0.09	0.12	0.13
Total Endmemembers	0.99	1.00	1.00	1.00	1.00	1.00	0.99	0.99	1.00	1.00

	grt 3 profile 44	grt 3 profile 45	grt 3 profile 46	grt 3 profile 47	grt 3 profile 48	grt 3 profile 49	grt 3 profile 50	grt 3 profile 51	grt 3 profile 52
Analysis No.	700	701	702	703	704	705	706	707	708
SiO2	37.86	37.40	37.56	37.85	37.30	37.50	37.52	37.69	37.66
TiO2	0.09	0.00	0.03	0.07	0.09	0.01	0.00	0.00	0.01
Cr2O3	0.00	0.00	0.00	0.00	0.00	0.00	0.00	0.00	0.00
Al2O3	21.63	21.52	21.40	21.78	21.53	21.63	21.42	21.56	21.61
FeO	23.91	24.82	25.21	25.59	25.31	26.18	26.32	27.69	27.93
MnO	5.31	4.32	4.46	4.27	3.91	3.39	2.97	2.79	2.46
NiO	0.00	0.00	0.00	0.00	0.00	0.00	0.00	0.00	0.00
MgO	1.37	1.43	1.54	1.56	1.68	1.71	1.67	1.79	1.80
CaO	10.60	10.36	9.81	9.57	9.88	9.86	10.11	8.84	8.93
Na2O	0.00	0.00	0.00	0.00	0.00	0.00	0.00	0.00	0.00
K2O	0.00	0.00	0.00	0.00	0.00	0.00	0.00	0.00	0.00
Total wt%	100.76	99.85	100.02	100.69	99.70	100.28	100.01	100.36	100.40
a.p.f.u. for 12 Oxygens									
Si	2.99	2.98	2.99	2.99	2.97	2.97	2.98	2.99	2.99
Ti	0.01	0.00	0.00	0.00	0.01	0.00	0.00	0.00	0.00
Cr	0.00	0.00	0.00	0.00	0.00	0.00	0.00	0.00	0.00
Al	2.01	2.02	2.01	2.03	2.02	2.02	2.01	2.02	2.02
Fe3+	0.00	0.02	0.01	0.00	0.02	0.03	0.03	0.00	0.00
Fe2+	1.58	1.63	1.67	1.69	1.67	1.71	1.72	1.84	1.85
Mn	0.36	0.29	0.30	0.29	0.26	0.23	0.20	0.19	0.17
Ni	0.00	0.00	0.00	0.00	0.00	0.00	0.00	0.00	0.00
Mg	0.16	0.17	0.18	0.18	0.20	0.20	0.20	0.21	0.21
Ca	0.90	0.88	0.84	0.81	0.84	0.84	0.86	0.75	0.76
Na	0.00	0.00	0.00	0.00	0.00	0.00	0.00	0.00	0.00
K	0.00	0.00	0.00	0.00	0.00	0.00	0.00	0.00	0.00
Total	8.00	8.00	8.00	8.00	8.00	8.00	8.00	8.00	8.00
xMg	0.09	0.09	0.10	0.10	0.11	0.10	0.10	0.10	0.10
Prp	0.05	0.06	0.06	0.06	0.07	0.07	0.07	0.07	0.07
Alm	0.52	0.54	0.55	0.56	0.55	0.56	0.57	0.61	0.62
Gross	0.30	0.29	0.28	0.27	0.28	0.28	0.28	0.25	0.25
Spes	0.12	0.10	0.10	0.10	0.09	0.07	0.07	0.06	0.06
Total Endmemembers	1.00	0.99	1.00	0.99	0.99	0.99	0.99	1.00	1.00

	bt inclusion	bt inclusion	bt inclusion	bt inclusion	bt 12 rim	bt 12 rim	bt 12 rim	bt 12 rim	bt 12 core	bt 12 core	bt 12 core	bt 12 core
Analysisi No.	719	720	721	722	723	724	725	726	727	728	729	730
SiO2	36.60	36.26	36.04	36.04	36.32	36.27	35.71	36.11	35.66	36.01	35.94	36.21
TiO2	2.21	2.00	1.96	3.86	1.92	2.15	1.88	1.88	2.02	2.18	2.19	1.88
Cr2O3	0.02	0.06	0.00	0.01	0.00	0.00	0.00	0.00	0.03	0.03	0.00	0.03
Al2O3	17.82	17.80	17.41	17.08	17.92	17.63	17.14	17.16	17.03	17.32	16.94	17.69
FeO	19.65	20.48	22.03	19.95	20.99	20.87	22.14	22.25	21.90	21.54	21.64	21.56
MnO	0.03	0.08	0.52	0.12	0.10	0.08	0.11	0.09	0.08	0.07	0.05	0.09
NiO	0.00	0.00	0.00	0.00	0.00	0.00	0.00	0.00	0.00	0.00	0.00	0.00
MgO	9.02	8.53	7.78	8.12	8.65	8.78	8.36	8.45	8.37	8.88	8.51	8.51
CaO	0.10	0.08	0.05	0.10	0.02	0.04	0.02	0.02	0.02	0.02	0.01	0.00
Na2O	0.18	0.21	0.15	0.26	0.16	0.13	0.11	0.11	0.13	0.15	0.11	0.09
K2O	9.41	9.40	9.20	9.39	9.22	9.25	9.28	9.56	9.34	9.19	9.39	9.14
Total	95.05	94.89	95.14	94.93	95.30	95.19	94.74	95.62	94.58	95.39	94.78	95.20
a.p.f.u. for 11 Oxygens												
Si	2.88	2.87	2.87	2.87	2.86	2.86	2.84	2.85	2.84	2.84	2.86	2.86
Ti	0.13	0.12	0.12	0.23	0.11	0.13	0.11	0.11	0.12	0.13	0.13	0.11
Cr	0.00	0.00	0.00	0.00	0.00	0.00	0.00	0.00	0.00	0.00	0.00	0.00
Al	1.65	1.66	1.63	1.60	1.66	1.64	1.61	1.60	1.60	1.61	1.59	1.65
Fe3+	0.00	0.00	0.00	0.00	0.00	0.00	0.00	0.00	0.00	0.00	0.00	0.00
Fe2+	1.29	1.35	1.47	1.33	1.38	1.38	1.47	1.47	1.46	1.42	1.44	1.43
Mn	0.00	0.01	0.04	0.01	0.01	0.01	0.01	0.01	0.01	0.00	0.00	0.01
Ni	0.00	0.00	0.00	0.00	0.00	0.00	0.00	0.00	0.00	0.00	0.00	0.00
Mg	1.06	1.01	0.92	0.96	1.02	1.03	0.99	0.99	0.99	1.04	1.01	1.00
Ca	0.01	0.01	0.00	0.01	0.00	0.00	0.00	0.00	0.00	0.00	0.00	0.00
Na	0.03	0.03	0.02	0.04	0.02	0.02	0.02	0.02	0.02	0.02	0.02	0.01
K	0.94	0.95	0.93	0.95	0.93	0.93	0.94	0.96	0.95	0.92	0.95	0.92
H	2.00	2.00	2.00	2.00	2.00	2.00	2.00	2.00	2.00	2.00	2.00	2.00
F	0.00	0.00	0.00	0.00	0.00	0.00	0.00	0.00	0.00	0.00	0.00	0.00
Cl	0.00	0.00	0.00	0.00	0.00	0.00	0.00	0.00	0.00	0.00	0.00	0.00
Total	8.00	8.00	8.00	8.00	8.00	8.00	8.00	8.00	8.00	8.00	8.00	8.00
xMg	0.45	0.43	0.39	0.42	0.42	0.43	0.40	0.40	0.41	0.42	0.41	0.41

	plag 5 core	plag 5 core	plag 5 core	plag 5 rim	plag 5 rim	plag 5 rim	plag 5 rim	plag 5 rim	plag 5 rim	plag 6 core	plag 6 rim	plag 7 rim
Analysisi No.	766	767	768	769	770	771	772	773	774	775	776	787
SiO2	62.60	62.20	61.88	61.31	62.69	63.34	62.93	62.41	62.68	63.02	62.62	62.55
TiO2	0.00	0.00	0.00	0.00	0.00	0.00	0.00	0.00	0.00	0.00	0.00	0.00
Cr2O3	0.00	0.00	0.00	0.00	0.00	0.00	0.00	0.00	0.00	0.00	0.00	0.00
Al2O3	23.31	23.67	23.87	23.89	23.41	22.61	22.92	23.37	23.50	22.84	23.46	23.02
FeO	0.09	0.03	0.03	0.03	0.07	0.16	0.07	0.01	0.03	0.11	0.21	0.14
MnO	0.00	0.00	0.00	0.00	0.00	0.00	0.00	0.00	0.00	0.00	0.00	0.00
NiO	0.00	0.00	0.00	0.00	0.00	0.00	0.00	0.00	0.00	0.00	0.00	0.00
MgO	0.00	0.00	0.00	0.00	0.00	0.00	0.00	0.00	0.00	0.00	0.00	0.00
CaO	4.39	4.72	4.83	5.07	4.51	3.91	3.93	4.42	4.41	3.98	4.32	4.35
Na2O	9.30	9.11	9.18	8.97	9.25	9.79	9.82	9.30	9.43	9.67	9.37	9.63
K2O	0.17	0.15	0.13	0.11	0.10	0.07	0.12	0.10	0.11	0.15	0.13	0.09
Total	99.85	99.88	99.92	99.38	100.03	99.88	99.79	99.61	100.16	99.77	100.11	99.77
a.p.f.u. for 8 Oxygens												
Si	2.77	2.75	2.73	2.73	2.77	2.79	2.77	2.76	2.76	2.78	2.76	2.76
Ti	0.00	0.00	0.00	0.00	0.00	0.00	0.00	0.00	0.00	0.00	0.00	0.00
Cr	0.00	0.00	0.00	0.00	0.00	0.00	0.00	0.00	0.00	0.00	0.00	0.00
Al	1.21	1.23	1.24	1.25	1.22	1.18	1.19	1.22	1.22	1.19	1.22	1.20
Fe3+	0.00	0.00	0.00	0.00	0.00	0.01	0.00	0.00	0.00	0.00	0.01	0.00
Fe2+	0.00	0.00	0.00	0.00	0.00	0.00	0.00	0.00	0.00	0.00	0.00	0.00
Mn	0.00	0.00	0.00	0.00	0.00	0.00	0.00	0.00	0.00	0.00	0.00	0.00
Ni	0.00	0.00	0.00	0.00	0.00	0.00	0.00	0.00	0.00	0.00	0.00	0.00
Mg	0.00	0.00	0.00	0.00	0.00	0.00	0.00	0.00	0.00	0.00	0.00	0.00
Ca	0.21	0.22	0.23	0.24	0.21	0.18	0.19	0.21	0.21	0.19	0.20	0.21
Na	0.80	0.78	0.79	0.77	0.79	0.84	0.84	0.80	0.80	0.83	0.80	0.82
K	0.01	0.01	0.01	0.01	0.01	0.00	0.01	0.01	0.01	0.01	0.01	0.00
Total	5.00	5.00	5.00	5.00	5.00	5.00	5.00	5.00	5.00	5.00	5.00	5.00
An	0.20	0.22	0.22	0.24	0.21	0.18	0.18	0.21	0.20	0.18	0.20	0.20
Alb	0.79	0.77	0.77	0.76	0.78	0.82	0.81	0.79	0.79	0.81	0.79	0.80
Or	0.01	0.01	0.01	0.01	0.01	0.00	0.01	0.01	0.01	0.01	0.01	0.00
Total Endmemembers	1.00	1.00	1.00	1.00	1.00	1.00	1.00	1.00	1.00	1.00	1.00	1.00

	mus 4 core	mus 3 core	mus 3 rim	mus 3 rim	mus 4 rim	mus 4 rim	mus 4 core	mus 4 core	mus 5 rim	mus 5 core	mus 5 core	mus 4 rim	mus 5 rim
Analysis No.	732	733	734	735	736	737	738	739	782	783	784	785	786
SiO2	46.84	46.81	47.78	47.51	47.47	47.12	47.42	47.14	47.27	47.38	47.37	45.53	44.40
TiO2	0.87	0.95	0.80	0.78	0.73	0.71	0.91	0.89	0.77	0.85	0.83	0.91	0.54
Cr2O3	0.04	0.00	0.00	0.00	0.01	0.01	0.02	0.00	0.01	0.02	0.00	0.02	0.02
Al2O3	31.20	31.33	30.63	31.35	31.32	31.54	30.86	30.48	31.67	31.70	31.01	30.61	31.17
FeO	2.49	2.76	2.95	2.62	2.33	2.29	2.57	2.52	2.69	2.26	2.72	2.06	4.13
MnO	0.03	0.03	0.05	0.02	0.00	0.01	0.00	0.00	0.03	0.01	0.01	0.04	0.08
NiO	0.00	0.00	0.00	0.00	0.00	0.00	0.00	0.00	0.00	0.00	0.00	0.00	0.00
MgO	1.59	1.59	1.84	1.68	1.62	1.58	1.70	1.80	1.50	1.48	1.76	1.46	1.84
CaO	0.00	0.02	0.00	0.00	0.00	0.03	0.01	0.00	0.05	0.00	0.00	0.03	0.05
Na2O	0.51	0.51	0.47	0.48	0.50	0.52	0.54	0.47	0.50	0.47	0.49	0.48	0.37
K2O	10.64	10.78	10.75	10.74	10.71	10.84	10.55	10.69	10.45	10.73	10.79	10.15	10.64
Total	94.21	94.77	95.27	95.19	94.69	94.66	94.58	93.99	94.95	94.91	94.98	91.28	93.24
a.p.f.u. for 11 Oxygens													
Si	3.17	3.15	3.20	3.19	3.20	3.17	3.20	3.20	3.18	3.19	3.18	3.18	3.04
Ti	0.04	0.05	0.04	0.04	0.04	0.04	0.05	0.05	0.04	0.04	0.04	0.05	0.03
Cr	0.00	0.00	0.00	0.00	0.00	0.00	0.00	0.00	0.00	0.00	0.00	0.00	0.00
Al	2.49	2.49	2.42	2.48	2.49	2.50	2.46	2.44	2.51	2.51	2.46	2.52	2.52
Fe3+	0.06	0.10	0.07	0.05	0.03	0.08	0.03	0.06	0.01	0.01	0.08	0.00	0.24
Fe2+	0.08	0.05	0.10	0.09	0.10	0.05	0.12	0.09	0.14	0.12	0.07	0.12	0.00
Mn	0.00	0.00	0.00	0.00	0.00	0.00	0.00	0.00	0.00	0.00	0.00	0.00	0.00
Ni	0.00	0.00	0.00	0.00	0.00	0.00	0.00	0.00	0.00	0.00	0.00	0.00	0.00
Mg	0.16	0.16	0.18	0.17	0.16	0.16	0.17	0.18	0.15	0.15	0.18	0.15	0.19
Ca	0.00	0.00	0.00	0.00	0.00	0.00	0.00	0.00	0.00	0.00	0.00	0.00	0.00
Na	0.07	0.07	0.06	0.06	0.06	0.07	0.07	0.06	0.07	0.06	0.06	0.06	0.05
K	0.92	0.93	0.92	0.92	0.92	0.93	0.91	0.93	0.90	0.92	0.92	0.91	0.93
H	2.00	2.00	2.00	2.00	2.00	2.00	2.00	2.00	2.00	2.00	2.00	2.00	2.00
F	0.00	0.00	0.00	0.00	0.00	0.00	0.00	0.00	0.00	0.00	0.00	0.00	0.00
Cl	0.00	0.00	0.00	0.00	0.00	0.00	0.00	0.00	0.00	0.00	0.00	0.00	0.00
Total	7.00	7.00	7.00	7.00	7.00	7.00	7.00	7.00	7.00	7.00	7.00	7.00	7.00
xMg	0.53	0.51	0.53	0.53	0.55	0.55	0.54	0.56	0.50	0.54	0.54	0.56	0.44

A.4.2. Vaddas Nappe - Sample UL248

	grt 3 profile 1	grt 3 profile 2	grt 3 profile 3	grt 3 profile 4	grt 3 profile 5	grt 3 profile 6	grt 3 profile 7	grt 3 profile 8	grt 3 profile 9	grt 3 profile 10
Analysis No.	127	128	129	130	131	132	133	134	135	136
SiO2	38.12	38.01	38.00	37.95	37.78	38.13	37.83	37.93	37.62	37.63
TiO2	0.22	0.07	0.14	0.02	0.00	0.00	0.05	0.01	0.02	0.02
Cr2O3	0.00	0.00	0.00	0.00	0.00	0.00	0.00	0.00	0.00	0.00
Al2O3	21.42	21.41	21.46	21.81	21.49	21.33	21.70	21.60	21.48	21.23
FeO	24.11	24.70	25.21	26.09	25.43	24.53	27.88	27.84	27.86	27.59
MnO	1.42	1.66	2.20	2.94	2.97	2.90	4.19	4.79	5.08	5.38
NiO	0.00	0.00	0.00	0.00	0.00	0.00	0.00	0.00	0.00	0.00
MgO	1.34	1.38	1.49	1.52	1.48	1.49	1.91	1.96	2.00	2.10
CaO	13.84	13.46	11.91	10.76	11.23	11.59	7.50	7.00	6.46	6.22
Na2O	0.00	0.00	0.00	0.00	0.00	0.00	0.00	0.00	0.00	0.00
K2O	0.00	0.00	0.00	0.00	0.00	0.00	0.00	0.00	0.00	0.00
Total	100.47	100.69	100.41	101.09	100.38	99.97	101.06	101.13	100.52	100.17
a.p.f.u. 12 oxygens										
Si	3.00	2.99	3.00	2.98	2.99	3.02	2.99	3.00	3.00	3.01
Ti	0.01	0.00	0.01	0.00	0.00	0.00	0.00	0.00	0.00	0.00
Cr	0.00	0.00	0.00	0.00	0.00	0.00	0.00	0.00	0.00	0.00
Al	1.99	1.98	2.00	2.02	2.00	1.99	2.02	2.01	2.02	2.00
Fe3+	0.00	0.04	0.00	0.01	0.02	0.00	0.00	0.00	0.00	0.00
Fe2+	1.59	1.59	1.66	1.70	1.66	1.63	1.84	1.84	1.86	1.84
Mn	0.09	0.11	0.15	0.20	0.20	0.19	0.28	0.32	0.34	0.36
Ni	0.00	0.00	0.00	0.00	0.00	0.00	0.00	0.00	0.00	0.00
Mg	0.16	0.16	0.18	0.18	0.17	0.18	0.23	0.23	0.24	0.25
Ca	1.17	1.13	1.01	0.91	0.95	0.98	0.64	0.59	0.55	0.53
Na	0.00	0.00	0.00	0.00	0.00	0.00	0.00	0.00	0.00	0.00
K	0.00	0.00	0.00	0.00	0.00	0.00	0.00	0.00	0.00	0.00
Total	8.00	8.00	8.00	8.00	8.00	8.00	8.00	8.00	8.00	8.00
xMg	0.09	0.09	0.10	0.09	0.09	0.10	0.11	0.11	0.11	0.12
Prp	0.05	0.05	0.06	0.06	0.06	0.06	0.07	0.08	0.08	0.08
Alm	0.52	0.52	0.55	0.56	0.55	0.52	0.61	0.61	0.62	0.61
Grs	0.38	0.37	0.33	0.30	0.31	0.32	0.21	0.20	0.18	0.18
Sps	0.03	0.04	0.05	0.06	0.07	0.06	0.09	0.11	0.11	0.12
Total Endmemembers	1.00	1.00	1.00	0.99	1.00	0.99	0.99	1.00	1.00	0.99

	grt 3 profile 11	grt 3 profile 12	grt 3 profile 13	grt 3 profile 14	grt 3 profile 15	grt 3 profile 16	grt 3 profile 17	grt 3 profile 18	grt 3 profile 19	grt 3 profile 20
Analysis No.	137	138	139	140	141	142	143	144	145	146
SiO2	37.74	37.71	37.84	37.76	37.75	37.51	37.66	37.55	37.65	37.60
TiO2	0.09	0.00	0.00	0.00	0.00	0.01	0.06	0.15	0.02	0.06
Cr2O3	0.00	0.00	0.00	0.00	0.00	0.00	0.00	0.00	0.00	0.00
Al2O3	21.39	21.66	21.59	21.60	21.43	21.41	21.48	21.43	21.50	21.51
FeO	27.16	26.75	26.81	27.00	28.17	27.81	28.77	28.75	28.50	28.31
MnO	5.57	5.42	5.34	5.43	5.85	6.06	6.05	6.22	6.15	6.25
NiO	0.00	0.00	0.00	0.00	0.00	0.00	0.00	0.00	0.00	0.00
MgO	2.01	2.00	1.92	1.92	2.07	2.21	2.19	2.24	2.25	2.28
CaO	6.79	6.73	7.57	7.34	5.74	5.19	4.94	4.55	4.60	4.44
Na2O	0.00	0.00	0.00	0.00	0.00	0.00	0.00	0.00	0.00	0.00
K2O	0.00	0.00	0.00	0.00	0.00	0.00	0.00	0.00	0.00	0.00
Total	100.75	100.27	101.07	101.05	101.01	100.20	101.15	100.89	100.67	100.45
a.p.f.u. 12 oxygens										
Si	3.00	3.01	2.99	2.99	3.00	3.00	2.99	2.99	3.00	3.00
Ti	0.01	0.00	0.00	0.00	0.00	0.00	0.00	0.01	0.00	0.00
Cr	0.00	0.00	0.00	0.00	0.00	0.00	0.00	0.00	0.00	0.00
Al	2.00	2.03	2.01	2.01	2.01	2.02	2.01	2.01	2.02	2.03
Fe3+	0.00	0.00	0.01	0.01	0.00	0.00	0.00	0.00	0.00	0.00
Fe2+	1.80	1.78	1.77	1.77	1.87	1.86	1.91	1.91	1.90	1.89
Mn	0.37	0.37	0.36	0.36	0.39	0.41	0.41	0.42	0.42	0.42
Ni	0.00	0.00	0.00	0.00	0.00	0.00	0.00	0.00	0.00	0.00
Mg	0.24	0.24	0.23	0.23	0.24	0.26	0.26	0.27	0.27	0.27
Ca	0.58	0.57	0.64	0.62	0.49	0.44	0.42	0.39	0.39	0.38
Na	0.00	0.00	0.00	0.00	0.00	0.00	0.00	0.00	0.00	0.00
K	0.00	0.00	0.00	0.00	0.00	0.00	0.00	0.00	0.00	0.00
Total	8.00	8.00	8.00	8.00	8.00	8.00	8.00	8.00	8.00	8.00
xMg	0.12	0.12	0.11	0.11	0.12	0.12	0.12	0.12	0.12	0.13
Prp	0.08	0.08	0.08	0.08	0.08	0.09	0.09	0.09	0.09	0.09
Alm	0.60	0.59	0.59	0.59	0.62	0.62	0.63	0.64	0.63	0.62
Grs	0.19	0.19	0.21	0.21	0.16	0.15	0.14	0.13	0.13	0.13
Sps	0.12	0.12	0.12	0.12	0.13	0.14	0.14	0.14	0.14	0.14
Total Endmemembers	1.00	0.99	1.00	1.00	1.00	0.99	1.00	1.00	0.99	0.99

	grt 3 profile 21	grt 3 profile 22	grt 3 profile 23	grt 3 profile 24	grt 3 profile 25	grt 3 profile 26	grt 3 profile 27	grt 3 profile 28	grt 3 profile 29	grt 3 profile 30
Analysis No.	147	148	149	150	151	152	153	154	155	156
SiO2	37.63	37.77	37.53	37.51	37.43	37.73	37.77	37.70	37.95	37.98
TiO2	0.00	0.01	0.02	0.05	0.02	0.09	0.00	0.00	0.11	0.01
Cr2O3	0.00	0.00	0.00	0.00	0.00	0.00	0.00	0.00	0.00	0.00
Al2O3	21.64	21.72	21.60	21.58	21.63	21.61	21.53	21.79	21.77	21.68
FeO	28.74	29.23	29.03	29.07	29.08	28.51	27.04	28.17	27.06	26.56
MnO	6.25	6.25	6.33	6.26	6.01	5.68	5.11	3.53	3.69	4.20
NiO	0.00	0.00	0.00	0.00	0.00	0.00	0.00	0.00	0.00	0.00
MgO	2.24	2.32	2.33	2.27	2.30	2.16	2.01	1.83	1.81	1.89
CaO	4.52	4.23	4.40	4.72	4.27	5.28	6.82	7.70	8.49	8.27
Na2O	0.00	0.00	0.00	0.00	0.00	0.00	0.00	0.00	0.00	0.00
K2O	0.00	0.00	0.00	0.00	0.00	0.00	0.00	0.00	0.00	0.00
Total	101.02	101.53	101.24	101.46	100.74	101.06	100.28	100.72	100.88	100.59
a.p.f.u. 12 oxygens										
Si	2.99	2.99	2.98	2.97	2.98	2.99	3.01	2.99	3.00	3.01
Ti	0.00	0.00	0.00	0.00	0.00	0.01	0.00	0.00	0.01	0.00
Cr	0.00	0.00	0.00	0.00	0.00	0.00	0.00	0.00	0.00	0.00
Al	2.03	2.03	2.02	2.01	2.03	2.02	2.02	2.04	2.03	2.02
Fe3+	0.00	0.00	0.02	0.04	0.00	0.00	0.00	0.00	0.00	0.00
Fe2+	1.91	1.93	1.90	1.88	1.94	1.89	1.80	1.87	1.79	1.76
Mn	0.42	0.42	0.43	0.42	0.41	0.38	0.34	0.24	0.25	0.28
Ni	0.00	0.00	0.00	0.00	0.00	0.00	0.00	0.00	0.00	0.00
Mg	0.27	0.27	0.28	0.27	0.27	0.26	0.24	0.22	0.21	0.22
Ca	0.38	0.36	0.37	0.40	0.36	0.45	0.58	0.65	0.72	0.70
Na	0.00	0.00	0.00	0.00	0.00	0.00	0.00	0.00	0.00	0.00
K	0.00	0.00	0.00	0.00	0.00	0.00	0.00	0.00	0.00	0.00
Total	8.00	8.00	8.00	8.00	8.00	8.00	8.00	8.00	8.00	8.00
xMg	0.12	0.12	0.13	0.12	0.12	0.12	0.12	0.10	0.11	0.11
Prp	0.09	0.09	0.09	0.09	0.09	0.08	0.08	0.07	0.07	0.07
Alm	0.64	0.64	0.63	0.61	0.65	0.63	0.59	0.62	0.59	0.58
Grs	0.13	0.12	0.12	0.13	0.12	0.15	0.19	0.22	0.24	0.23
Sps	0.14	0.14	0.14	0.14	0.14	0.13	0.11	0.08	0.08	0.09
Total Endmemembers	0.99	0.99	0.99	0.99	0.99	0.99	0.99	0.99	0.99	0.99

	grt 3 profile 31	grt 3 profile 32	grt 3 profile 33	grt 3 profile 34	grt 3 profile 35	grt 3 profile 26	grt 3 profile 37	grt 3 profile 38	grt 3 profile 39
Analysis No.	157	158	159	160	161	162	163	164	165
SiO2	37.66	38.36	38.18	37.41	37.95	38.41	38.21	38.29	38.23
TiO2	0.05	0.02	0.11	0.23	0.12	0.07	0.03	0.14	0.04
Cr2O3	0.00	0.00	0.00	0.00	0.00	0.00	0.00	0.00	0.00
Al2O3	21.49	21.60	21.44	21.14	21.56	21.79	21.59	21.55	21.49
FeO	26.44	25.77	25.54	25.81	24.60	24.25	24.20	24.14	24.64
MnO	4.25	3.04	2.40	1.98	2.05	1.79	1.65	1.51	1.48
NiO	0.00	0.00	0.00	0.00	0.00	0.00	0.00	0.00	0.00
MgO	1.91	1.71	1.43	2.09	1.42	1.36	1.38	1.31	1.32
CaO	8.40	10.43	11.89	11.15	12.69	13.41	13.69	14.11	13.57
Na2O	0.00	0.00	0.00	0.00	0.00	0.00	0.00	0.00	0.00
K2O	0.00	0.00	0.00	0.00	0.00	0.00	0.00	0.00	0.00
Total	100.20	100.93	100.99	99.81	100.39	101.08	100.74	101.05	100.77
a.p.f.u. 12 oxygens									
Si	3.00	3.02	3.00	2.97	2.99	3.00	3.00	2.99	3.00
Ti	0.00	0.00	0.01	0.01	0.01	0.00	0.00	0.01	0.00
Cr	0.00	0.00	0.00	0.00	0.00	0.00	0.00	0.00	0.00
Al	2.01	2.00	1.99	1.98	2.00	2.01	2.00	1.99	1.99
Fe3+	0.00	0.00	0.00	0.06	0.00	0.00	0.01	0.01	0.01
Fe2+	1.76	1.70	1.68	1.65	1.62	1.59	1.58	1.57	1.61
Mn	0.29	0.20	0.16	0.13	0.14	0.12	0.11	0.10	0.10
Ni	0.00	0.00	0.00	0.00	0.00	0.00	0.00	0.00	0.00
Mg	0.23	0.20	0.17	0.25	0.17	0.16	0.16	0.15	0.15
Ca	0.72	0.88	1.00	0.95	1.07	1.12	1.15	1.18	1.14
Na	0.00	0.00	0.00	0.00	0.00	0.00	0.00	0.00	0.00
K	0.00	0.00	0.00	0.00	0.00	0.00	0.00	0.00	0.00
Total	8.00	8.00	8.00	8.00	8.00	8.00	8.00	8.00	8.00
xMg	0.11	0.11	0.09	0.13	0.09	0.09	0.09	0.09	0.09
Prp	0.08	0.07	0.06	0.08	0.06	0.05	0.05	0.05	0.05
Alm	0.59	0.55	0.55	0.53	0.54	0.52	0.52	0.52	0.53
Grs	0.24	0.29	0.33	0.30	0.36	0.37	0.38	0.39	0.38
Sps	0.10	0.07	0.05	0.04	0.05	0.04	0.04	0.03	0.03
Total Endmemembers	1.00	0.99	1.00	0.99	1.00	0.99	1.00	1.00	1.00

	bt inclusion	bt 3 core	bt 3 rim	bt 3 core	bt inclusion	bt inclusion	bt 4 rim	bt 4 core	bt inclusion
Analysis No.	175	176	177	178	179	180	181	182	183
SiO2	36.46	36.29	36.54	36.60	36.49	36.07	35.55	36.36	36.61
TiO2	2.82	2.95	2.83	2.71	2.79	3.18	1.99	2.21	3.67
Cr2O3	0.05	0.01	0.02	0.00	0.05	0.00	0.02	0.00	0.00
Al2O3	17.31	16.94	17.31	17.20	18.25	17.03	17.39	17.15	18.46
FeO	21.03	21.26	21.22	22.16	20.41	20.39	22.85	21.87	18.16
MnO	0.17	0.22	0.14	0.17	0.12	0.15	0.17	0.18	0.20
NiO	0.00	0.00	0.00	0.00	0.00	0.00	0.00	0.00	0.00
MgO	7.46	7.81	7.63	7.44	7.67	8.31	7.88	8.09	8.52
CaO	0.00	0.00	0.00	0.01	0.01	0.04	0.01	0.00	0.00
Na2O	0.08	0.07	0.03	0.05	0.10	0.09	0.03	0.03	0.20
K2O	10.06	10.16	10.11	10.26	10.29	10.04	9.82	10.19	10.15
Total	95.44	95.70	95.83	96.61	96.18	95.30	95.71	96.07	95.97
a.p.f.u. 11 oxygens									
Si	2.89	2.87	2.89	2.87	2.86	2.85	2.81	2.86	2.86
Ti	0.17	0.18	0.17	0.16	0.16	0.19	0.12	0.13	0.22
Cr	0.00	0.00	0.00	0.00	0.00	0.00	0.00	0.00	0.00
Al	1.62	1.58	1.61	1.59	1.69	1.59	1.62	1.59	1.70
Fe3+	0.00	0.00	0.00	0.00	0.00	0.00	0.00	0.00	0.00
Fe2+	1.39	1.41	1.40	1.46	1.34	1.35	1.51	1.44	1.18
Mn	0.01	0.01	0.01	0.01	0.01	0.01	0.01	0.01	0.01
Ni	0.00	0.00	0.00	0.00	0.00	0.00	0.00	0.00	0.00
Mg	0.88	0.92	0.90	0.87	0.90	0.98	0.93	0.95	0.99
Ca	0.00	0.00	0.00	0.00	0.00	0.00	0.00	0.00	0.00
Na	0.01	0.01	0.01	0.01	0.01	0.01	0.01	0.00	0.03
K	1.02	1.02	1.02	1.03	1.03	1.01	0.99	1.02	1.01
H	2.00	2.00	2.00	2.00	2.00	2.00	2.00	2.00	2.00
F	0.00	0.00	0.00	0.00	0.00	0.00	0.00	0.00	0.00
Cl	0.00	0.00	0.00	0.00	0.00	0.00	0.00	0.00	0.00
Total	8.00	8.00	8.00	8.00	8.00	8.00	8.00	8.00	8.00
xMg	0.39	0.40	0.39	0.37	0.40	0.42	0.38	0.40	0.46

	kfs 1 core	kfs 1 rim	kfs 1 core	plag 1 core	plag 1 rim	plag 2 core	plag 2 rim	plag 3 core	plag 3 rim
Analysis No.	121	122	123	184	185	186	187	194	195
SiO2	64.13	64.18	63.94	60.84	61.97	60.29	60.63	62.61	62.16
TiO2	0.00	0.00	0.00	0.00	0.00	0.00	0.00	0.00	0.00
Cr2O3	0.00	0.00	0.00	0.00	0.00	0.00	0.00	0.00	0.00
Al2O3	18.45	18.60	18.59	24.67	23.00	24.75	24.72	23.45	23.59
FeO	0.17	0.09	0.22	0.00	0.18	0.07	0.03	0.02	0.00
MnO	0.00	0.00	0.00	0.00	0.00	0.00	0.00	0.00	0.00
NiO	0.00	0.00	0.00	0.00	0.00	0.00	0.00	0.00	0.00
MgO	0.00	0.00	0.00	0.00	0.00	0.00	0.00	0.00	0.00
CaO	0.00	0.00	0.00	6.05	4.66	6.18	5.93	4.57	4.87
Na2O	0.66	0.59	0.62	8.25	9.05	8.17	8.48	9.19	9.06
K2O	16.54	16.49	16.62	0.31	0.28	0.29	0.25	0.16	0.17
Total	99.95	99.95	99.99	100.12	99.14	99.75	100.04	100.00	99.85
a.p.f.u. 8 oxygens									
Si	2.96	2.96	2.95	2.70	2.76	2.68	2.68	2.77	2.75
Ti	0.00	0.00	0.00	0.00	0.00	0.00	0.00	0.00	0.00
Cr	0.00	0.00	0.00	0.00	0.00	0.00	0.00	0.00	0.00
Al	1.00	1.01	1.01	1.29	1.21	1.30	1.29	1.22	1.23
Fe3+	0.01	0.00	0.01	0.00	0.01	0.00	0.00	0.00	0.00
Fe2+	0.00	0.00	0.00	0.00	0.00	0.00	0.00	0.00	0.00
Mn	0.00	0.00	0.00	0.00	0.00	0.00	0.00	0.00	0.00
Ni	0.00	0.00	0.00	0.00	0.00	0.00	0.00	0.00	0.00
Mg	0.00	0.00	0.00	0.00	0.00	0.00	0.00	0.00	0.00
Ca	0.00	0.00	0.00	0.29	0.22	0.29	0.28	0.22	0.23
Na	0.06	0.05	0.06	0.71	0.78	0.70	0.73	0.79	0.78
K	0.97	0.97	0.98	0.02	0.02	0.02	0.01	0.01	0.01
Total	5.00	5.00	5.00	5.00	5.00	5.00	5.00	5.00	5.00
An	0.00	0.00	0.00	0.28	0.22	0.29	0.27	0.21	0.23
Alb	0.06	0.05	0.05	0.70	0.77	0.69	0.71	0.78	0.76
Or	0.94	0.95	0.95	0.02	0.02	0.02	0.01	0.01	0.01
Total Endmemembers	1.00	1.00	1.00	1.00	1.00	1.00	1.00	1.00	1.00

	mus 3 core	mus 3 core	mus 3 core	mus 3 rim	mus 3 rim	mus 3 rim	mus 3 rim	mus 4 core	mus 4 core	mus 4 core	mus 4 rim	mus 4 rim
Analysis No.	206	207	208	209	210	211	212	213	214	215	216	217
SiO2	46.08	46.32	46.19	47.67	46.84	48.17	48.26	46.77	46.89	47.44	46.95	47.70
TiO2	0.72	1.08	0.75	1.30	1.42	0.98	1.00	1.44	1.33	1.51	1.64	1.32
Cr2O3	0.02	0.03	0.01	0.00	0.06	0.03	0.03	0.00	0.02	0.00	0.00	0.00
Al2O3	33.37	33.27	33.61	30.53	30.94	30.62	30.78	30.88	30.88	30.60	30.79	30.43
FeO	2.46	2.41	2.54	2.73	2.69	2.84	2.59	2.78	2.82	2.81	2.50	2.65
MnO	0.01	0.02	0.05	0.00	0.07	0.01	0.05	0.02	0.03	0.04	0.03	0.04
NiO	0.00	0.00	0.00	0.00	0.00	0.00	0.00	0.00	0.00	0.00	0.00	0.00
MgO	1.03	1.09	1.01	1.65	1.55	1.66	1.76	1.42	1.47	1.51	1.47	1.66
CaO	0.00	0.00	0.00	0.01	0.00	0.00	0.00	0.00	0.00	0.00	0.00	0.00
Na2O	0.38	0.36	0.41	0.28	0.28	0.24	0.25	0.33	0.29	0.30	0.30	0.20
K2O	11.26	11.25	11.11	11.46	11.24	11.55	11.30	11.30	11.21	11.29	11.31	11.46
Total	95.33	95.81	95.67	95.64	95.08	96.10	96.02	94.93	94.93	95.50	94.98	95.46
a.p.f.u. 11 oxygens												
Si	3.08	3.09	3.08	3.19	3.16	3.21	3.22	3.16	3.16	3.18	3.17	3.20
Ti	0.04	0.05	0.04	0.07	0.07	0.05	0.05	0.07	0.07	0.08	0.08	0.07
Cr	0.00	0.00	0.00	0.00	0.00	0.00	0.00	0.00	0.00	0.00	0.00	0.00
Al	2.63	2.61	2.64	2.41	2.46	2.40	2.42	2.46	2.46	2.42	2.45	2.41
Fe3+	0.14	0.11	0.12	0.09	0.09	0.09	0.04	0.10	0.08	0.06	0.07	0.06
Fe2+	0.00	0.03	0.02	0.06	0.06	0.07	0.10	0.05	0.08	0.09	0.08	0.09
Mn	0.00	0.00	0.00	0.00	0.00	0.00	0.00	0.00	0.00	0.00	0.00	0.00
Ni	0.00	0.00	0.00	0.00	0.00	0.00	0.00	0.00	0.00	0.00	0.00	0.00
Mg	0.10	0.11	0.10	0.17	0.16	0.16	0.17	0.14	0.15	0.15	0.15	0.17
Ca	0.00	0.00	0.00	0.00	0.00	0.00	0.00	0.00	0.00	0.00	0.00	0.00
Na	0.05	0.05	0.05	0.04	0.04	0.03	0.03	0.04	0.04	0.04	0.04	0.03
K	0.96	0.96	0.94	0.98	0.97	0.98	0.96	0.97	0.96	0.97	0.97	0.98
H	2.00	2.00	2.00	2.00	2.00	2.00	2.00	2.00	2.00	2.00	2.00	2.00
F	0.00	0.00	0.00	0.00	0.00	0.00	0.00	0.00	0.00	0.00	0.00	0.00
Cl	0.00	0.00	0.00	0.00	0.00	0.00	0.00	0.00	0.00	0.00	0.00	0.00
Total	7.00	7.00	7.00	7.00	7.00	7.00	7.00	7.00	7.00	7.00	7.00	7.00
xMg	0.43	0.45	0.42	0.52	0.51	0.51	0.55	0.48	0.48	0.49	0.51	0.53

A.4.3. Kåfjord Nappe - UL230

	grt 1 profile 1	grt 1 profile 2	grt 1 profile 3	grt 1 profile 5	grt 1 profile 6	grt 1 profile 7	grt 1 profile 8	grt 1 profile 9	grt 1 profile 10	grt 1 profile 11
Analysis No.	315	316	317	319	320	321	322	323	324	325
SiO2	38.10	38.42	37.96	38.10	38.19	38.01	38.33	38.40	38.23	38.10
TiO2	0.03	0.00	0.00	0.00	0.00	0.00	0.07	0.01	0.07	0.01
Cr2O3	0.00	0.00	0.00	0.00	0.00	0.00	0.00	0.00	0.00	0.00
Al2O3	21.79	22.08	21.76	21.78	21.81	21.87	22.16	21.94	22.02	21.85
FeO	32.62	32.37	32.35	32.33	32.12	31.53	31.39	32.47	31.87	32.61
MnO	0.99	0.94	1.00	0.90	0.89	0.87	0.97	0.93	0.90	0.89
NiO	0.00	0.00	0.00	0.00	0.00	0.00	0.00	0.00	0.00	0.00
MgO	4.41	4.43	4.61	4.49	4.51	4.53	4.52	4.48	4.29	4.25
CaO	3.29	3.25	3.32	3.31	3.41	3.28	3.44	3.49	3.41	3.30
Na2O	0.00	0.00	0.00	0.00	0.00	0.00	0.00	0.00	0.00	0.00
K2O	0.00	0.00	0.00	0.00	0.00	0.00	0.00	0.00	0.00	0.00
Total	101.23	101.49	101.00	100.91	100.93	100.09	100.87	101.72	100.79	101.01
a.p.f.u. 12 oxygens										
Si	2.99	3.00	2.98	2.99	3.00	3.01	3.01	2.99	3.01	3.00
Ti	0.00	0.00	0.00	0.00	0.00	0.00	0.00	0.00	0.00	0.00
Cr	0.00	0.00	0.00	0.00	0.00	0.00	0.00	0.00	0.00	0.00
Al	2.01	2.03	2.01	2.02	2.02	2.04	2.05	2.02	2.04	2.03
Fe3+	0.01	0.00	0.03	0.00	0.00	0.00	0.00	0.00	0.00	0.00
Fe2+	2.13	2.12	2.09	2.12	2.11	2.09	2.06	2.12	2.10	2.14
Mn	0.07	0.06	0.07	0.06	0.06	0.06	0.06	0.06	0.06	0.06
Ni	0.00	0.00	0.00	0.00	0.00	0.00	0.00	0.00	0.00	0.00
Mg	0.52	0.52	0.54	0.53	0.53	0.53	0.53	0.52	0.50	0.50
Ca	0.28	0.27	0.28	0.28	0.29	0.28	0.29	0.29	0.29	0.28
Na	0.00	0.00	0.00	0.00	0.00	0.00	0.00	0.00	0.00	0.00
K	0.00	0.00	0.00	0.00	0.00	0.00	0.00	0.00	0.00	0.00
Total	8.00	8.00	8.00	8.00	8.00	8.00	8.00	8.00	8.00	8.00
xMg	0.19	0.20	0.20	0.20	0.20	0.20	0.20	0.20	0.19	0.19
Prp	0.17	0.17	0.18	0.18	0.18	0.18	0.17	0.17	0.17	0.17
Alm	0.71	0.70	0.69	0.71	0.70	0.69	0.68	0.71	0.69	0.71
Grs	0.09	0.09	0.09	0.09	0.10	0.09	0.10	0.10	0.09	0.09
Sps	0.02	0.02	0.02	0.02	0.02	0.02	0.02	0.02	0.02	0.02
Total Endmemembers	1.00	0.99	0.99	1.00	0.99	0.98	0.98	1.00	0.98	0.99

	grt 1 profile 12	grt 1 profile 13	grt 1 profile 14	grt 1 profile 15	grt 1 profile 16	grt 1 profile 17	grt 1 profile 18	grt 1 profile 19	grt 1 profile 20
Analysis No.	326	327	328	329	330	331	332	333	334
SiO2	38.08	38.27	38.40	37.87	38.48	37.93	38.04	38.18	38.10
TiO2	0.00	0.05	0.00	0.00	0.07	0.00	0.00	0.03	0.01
Cr2O3	0.00	0.00	0.00	0.00	0.00	0.00	0.00	0.00	0.00
Al2O3	21.80	21.92	21.81	21.81	21.81	21.80	21.94	21.88	21.88
FeO	32.32	32.31	32.53	32.26	32.36	32.21	32.08	32.39	31.35
MnO	0.93	0.96	0.93	0.92	0.97	0.96	0.90	0.86	0.92
NiO	0.00	0.00	0.00	0.00	0.00	0.00	0.00	0.00	0.00
MgO	4.22	4.20	4.22	4.51	4.38	4.64	4.39	4.47	4.29
CaO	3.44	3.39	3.50	3.41	3.48	3.35	3.50	3.47	3.49
Na2O	0.00	0.00	0.00	0.00	0.00	0.00	0.00	0.00	0.00
K2O	0.00	0.00	0.00	0.00	0.00	0.00	0.00	0.00	0.00
Total	100.79	101.10	101.39	100.78	101.55	100.89	100.85	101.27	100.04
a.p.f.u. 12 oxygens									
Si	3.00	3.01	3.01	2.98	3.01	2.98	2.99	2.99	3.02
Ti	0.00	0.00	0.00	0.00	0.00	0.00	0.00	0.00	0.00
Cr	0.00	0.00	0.00	0.00	0.00	0.00	0.00	0.00	0.00
Al	2.02	2.03	2.01	2.02	2.01	2.02	2.03	2.02	2.04
Fe3+	0.00	0.00	0.00	0.02	0.00	0.03	0.00	0.00	0.00
Fe2+	2.13	2.12	2.13	2.10	2.11	2.09	2.11	2.12	2.08
Mn	0.06	0.06	0.06	0.06	0.06	0.06	0.06	0.06	0.06
Ni	0.00	0.00	0.00	0.00	0.00	0.00	0.00	0.00	0.00
Mg	0.50	0.49	0.49	0.53	0.51	0.54	0.51	0.52	0.51
Ca	0.29	0.29	0.29	0.29	0.29	0.28	0.30	0.29	0.30
Na	0.00	0.00	0.00	0.00	0.00	0.00	0.00	0.00	0.00
K	0.00	0.00	0.00	0.00	0.00	0.00	0.00	0.00	0.00
Total	8.00	8.00	8.00	8.00	8.00	8.00	8.00	8.00	8.00
xMg	0.19	0.19	0.19	0.20	0.19	0.20	0.20	0.20	0.20
Prp	0.17	0.16	0.16	0.17	0.17	0.18	0.17	0.17	0.17
Alm	0.71	0.70	0.70	0.69	0.69	0.69	0.70	0.71	0.68
Grs	0.10	0.09	0.10	0.10	0.10	0.09	0.10	0.10	0.10
Sps	0.02	0.02	0.02	0.02	0.02	0.02	0.02	0.02	0.02
Total Endmemembers	0.99	0.99	0.99	0.99	0.99	0.99	0.99	1.00	0.97

	bt 1 inclusion	bt 1 inclusion	bt 1 inclusion	bt 2 rim	bt 2 core	bt 2 core	bt 3 rim	bt 3 rim	bt 3 core	bt 3 core	bt 4 rim	bt 4 core	bt 5
Analysis No.	346	347	348	349	350	351	352	353	354	355	356	357	358
SiO2	37.23	37.50	37.05	36.64	36.94	36.63	37.12	37.07	36.77	36.74	36.33	36.58	36.56
TiO2	3.49	3.59	3.52	3.88	3.81	3.84	3.70	3.45	4.01	3.32	3.06	3.49	4.15
Cr2O3	0.00	0.07	0.06	0.04	0.08	0.01	0.00	0.01	0.02	0.03	0.04	0.03	0.03
Al2O3	18.49	18.87	18.55	18.23	18.18	17.74	18.81	17.87	17.90	18.84	18.39	18.18	18.81
FeO	15.82	14.74	15.24	17.23	16.52	17.15	15.97	16.57	16.27	15.11	17.10	16.05	15.96
MnO	0.02	0.02	0.05	0.03	0.03	0.03	0.01	0.00	0.03	0.06	0.02	0.03	0.05
NiO	0.00	0.00	0.00	0.00	0.00	0.00	0.00	0.00	0.00	0.00	0.00	0.00	0.00
MgO	11.23	10.87	11.06	10.44	10.40	10.42	9.96	10.40	10.53	10.27	9.89	10.47	9.37
CaO	0.00	0.00	0.00	0.00	0.00	0.00	0.01	0.00	0.00	0.00	0.07	0.00	0.00
Na2O	0.10	0.06	0.10	0.09	0.10	0.06	0.10	0.08	0.10	0.10	0.07	0.07	0.10
K2O	10.23	10.21	10.34	10.13	10.29	10.22	10.18	10.22	10.26	10.33	9.69	10.01	10.20
Total	96.61	95.93	95.97	96.71	96.35	96.10	95.86	95.67	95.89	94.79	94.66	94.91	95.22
a.p.f.u. 11 oxygens													
Si	2.84	2.88	2.84	2.81	2.84	2.83	2.87	2.87	2.84	2.86	2.85	2.85	2.86
Ti	0.20	0.21	0.20	0.22	0.22	0.22	0.22	0.20	0.23	0.19	0.18	0.20	0.24
Cr	0.00	0.00	0.00	0.00	0.00	0.00	0.00	0.00	0.00	0.00	0.00	0.00	0.00
Al	1.66	1.71	1.68	1.65	1.65	1.62	1.71	1.63	1.63	1.73	1.70	1.67	1.73
Fe3+	0.00	0.00	0.00	0.00	0.00	0.00	0.00	0.00	0.00	0.00	0.00	0.00	0.00
Fe2+	1.01	0.95	0.98	1.11	1.06	1.11	1.03	1.07	1.05	0.98	1.12	1.05	1.04
Mn	0.00	0.00	0.00	0.00	0.00	0.00	0.00	0.00	0.00	0.00	0.00	0.00	0.00
Ni	0.00	0.00	0.00	0.00	0.00	0.00	0.00	0.00	0.00	0.00	0.00	0.00	0.00
Mg	1.28	1.24	1.26	1.20	1.19	1.20	1.15	1.20	1.21	1.19	1.16	1.22	1.09
Ca	0.00	0.00	0.00	0.00	0.00	0.00	0.00	0.00	0.00	0.00	0.01	0.00	0.00
Na	0.02	0.01	0.01	0.01	0.02	0.01	0.01	0.01	0.02	0.01	0.01	0.01	0.01
K	1.00	1.00	1.01	0.99	1.01	1.01	1.00	1.01	1.01	1.03	0.97	1.00	1.02
H	2.00	2.00	2.00	2.00	2.00	2.00	2.00	2.00	2.00	2.00	2.00	2.00	2.00
F	0.00	0.00	0.00	0.00	0.00	0.00	0.00	0.00	0.00	0.00	0.00	0.00	0.00
Cl	0.00	0.00	0.00	0.00	0.00	0.00	0.00	0.00	0.00	0.00	0.00	0.00	0.00
Total	8.00	8.00	8.00	8.00	8.00	8.00	8.00	8.00	8.00	8.00	8.00	8.00	8.00
xMg	0.56	0.57	0.56	0.52	0.53	0.52	0.53	0.53	0.54	0.55	0.51	0.54	0.51

	plag 1 rim	plag 1 core	plag 2 core	plag 2 core	kfs 1 core	kfs 1 core	plag 3 core	plag 3 core	plag 3 rim	plag 3 rim	plag 4 core	plag 4 core
Analysis No.	395	396	397	398	399	400	424	425	426	427	428	429
SiO2	60.69	61.71	61.94	61.59	64.64	64.34	61.33	61.77	61.47	62.27	61.44	60.84
TiO2	0.00	0.00	0.00	0.00	0.00	0.00	0.00	0.00	0.00	0.00	0.00	0.00
Cr2O3	0.00	0.00	0.00	0.00	0.00	0.00	0.00	0.00	0.00	0.00	0.00	0.00
Al2O3	24.77	24.27	24.23	24.46	18.55	18.72	24.47	24.51	24.43	23.73	24.41	24.51
FeO	0.16	0.17	0.14	0.09	0.29	0.48	0.23	0.19	0.22	0.23	0.23	0.10
MnO	0.00	0.00	0.00	0.00	0.00	0.00	0.00	0.00	0.00	0.00	0.00	0.00
NiO	0.00	0.00	0.00	0.00	0.00	0.00	0.00	0.00	0.00	0.00	0.00	0.00
MgO	0.00	0.00	0.00	0.00	0.00	0.00	0.00	0.00	0.00	0.00	0.00	0.00
CaO	6.08	5.67	5.35	5.66	0.03	0.03	5.80	5.75	5.81	5.04	5.75	6.08
Na2O	8.35	8.77	9.03	8.60	1.20	1.13	8.47	8.56	8.48	8.82	8.54	8.38
K2O	0.15	0.14	0.11	0.11	15.60	15.88	0.16	0.14	0.14	0.18	0.14	0.18
Total	100.20	100.73	100.80	100.51	100.31	100.57	100.46	100.92	100.55	100.26	100.51	100.09
a.p.f.u. 8 oxygens												
Si	2.69	2.71	2.72	2.72	2.96	2.94	2.71	2.72	2.71	2.75	2.71	2.70
Ti	0.00	0.00	0.00	0.00	0.00	0.00	0.00	0.00	0.00	0.00	0.00	0.00
Cr	0.00	0.00	0.00	0.00	0.00	0.00	0.00	0.00	0.00	0.00	0.00	0.00
Al	1.29	1.26	1.25	1.27	1.00	1.01	1.27	1.27	1.27	1.24	1.27	1.28
Fe3+	0.01	0.01	0.01	0.00	0.01	0.02	0.01	0.01	0.01	0.01	0.01	0.00
Fe2+	0.00	0.00	0.00	0.00	0.00	0.00	0.00	0.00	0.00	0.00	0.00	0.00
Mn	0.00	0.00	0.00	0.00	0.00	0.00	0.00	0.00	0.00	0.00	0.00	0.00
Ni	0.00	0.00	0.00	0.00	0.00	0.00	0.00	0.00	0.00	0.00	0.00	0.00
Mg	0.00	0.00	0.00	0.00	0.00	0.00	0.00	0.00	0.00	0.00	0.00	0.00
Ca	0.29	0.27	0.25	0.27	0.00	0.00	0.27	0.27	0.27	0.24	0.27	0.29
Na	0.72	0.75	0.77	0.74	0.11	0.10	0.73	0.73	0.73	0.76	0.73	0.72
K	0.01	0.01	0.01	0.01	0.91	0.93	0.01	0.01	0.01	0.01	0.01	0.01
Total	5.00	5.00	5.00	5.00	5.00	5.00	5.00	5.00	5.00	5.00	5.00	5.00
An	0.28	0.26	0.25	0.27	0.00	0.00	0.27	0.27	0.27	0.24	0.27	0.28
Alv	0.71	0.73	0.75	0.73	0.10	0.10	0.72	0.72	0.72	0.75	0.72	0.71
Or	0.01	0.01	0.01	0.01	0.89	0.90	0.01	0.01	0.01	0.01	0.01	0.01
Total Endmemembers	1.00	1.00	1.00	1.00	1.00	1.00	1.00	1.00	1.00	1.00	1.00	1.00

	mus 1 rim	mus 1 core	mus 1 rim	mus 1 rim	mus 2 core	mus 2 core	mus 2 core	mus 2 rim	mus 2 rim
Analysis No.	382	383	384	385	386	387	388	389	390
SiO2	47.82	46.86	47.80	47.15	47.51	47.77	47.63	45.95	47.01
TiO2	1.25	1.74	1.70	1.61	1.43	1.46	1.70	1.63	1.45
Cr2O3	0.05	0.06	0.00	0.01	0.00	0.01	0.03	0.06	0.05
Al2O3	33.62	33.73	33.37	33.70	32.76	33.64	33.78	32.91	33.39
FeO	0.95	1.01	1.19	0.98	1.27	1.09	1.00	1.49	1.07
MnO	0.00	0.00	0.01	0.00	0.04	0.04	0.03	0.00	0.01
NiO	0.00	0.00	0.00	0.00	0.00	0.00	0.00	0.00	0.00
MgO	1.18	1.05	1.25	1.14	1.34	1.19	1.19	1.22	1.21
CaO	0.00	0.02	0.02	0.05	0.00	0.00	0.00	0.00	0.03
Na2O	0.34	0.35	0.32	0.31	0.33	0.35	0.38	0.37	0.44
K2O	11.27	11.21	11.23	11.21	11.18	11.25	11.15	11.01	10.89
Total	96.47	96.03	96.88	96.16	95.86	96.79	96.90	94.64	95.55
a.p.f.u. 11 oxygens	Cations								
Si	3.16	3.11	3.15	3.13	3.16	3.15	3.13	3.10	3.13
Ti	0.06	0.09	0.08	0.08	0.07	0.07	0.08	0.08	0.07
Cr	0.00	0.00	0.00	0.00	0.00	0.00	0.00	0.00	0.00
Al	2.62	2.64	2.59	2.63	2.57	2.61	2.62	2.62	2.62
Fe3+	0.00	0.00	0.00	0.00	0.00	0.00	0.00	0.02	0.00
Fe2+	0.05	0.06	0.07	0.05	0.07	0.06	0.05	0.07	0.06
Mn	0.00	0.00	0.00	0.00	0.00	0.00	0.00	0.00	0.00
Ni	0.00	0.00	0.00	0.00	0.00	0.00	0.00	0.00	0.00
Mg	0.12	0.10	0.12	0.11	0.13	0.12	0.12	0.12	0.12
Ca	0.00	0.00	0.00	0.00	0.00	0.00	0.00	0.00	0.00
Na	0.04	0.05	0.04	0.04	0.04	0.04	0.05	0.05	0.06
K	0.95	0.95	0.94	0.95	0.95	0.95	0.94	0.95	0.93
H	2.00	2.00	2.00	2.00	2.00	2.00	2.00	2.00	2.00
F	0.00	0.00	0.00	0.00	0.00	0.00	0.00	0.00	0.00
Cl	0.00	0.00	0.00	0.00	0.00	0.00	0.00	0.00	0.00
Total	7.00	7.00	7.00	7.00	7.00	7.00	7.00	7.00	7.00
xMg	0.69	0.65	0.65	0.67	0.65	0.66	0.68	0.59	0.67

A.4.4. Kåfjord with Nordmannvik Nappe Boundary - UL234a

	grt 1 profile 1	grt 1 profile 2	grt 1 profile 3	grt 1 profile 4	grt 1 profile 5	grt 1 profile 6	grt 1 profile 7	grt 1 profile 8	grt 1 profile 9	grt 1 profile 10
Analysis No.	38	39	40	41	42	43	44	45	46	47
SiO2	37.84	38.20	38.00	37.85	38.07	38.05	38.13	38.48	38.34	38.36
TiO2	0.03	0.05	0.02	0.00	0.00	0.00	0.00	0.00	0.00	0.00
Cr2O3	0.00	0.00	0.00	0.00	0.00	0.00	0.00	0.00	0.00	0.00
Al2O3	21.86	21.85	21.84	21.88	21.83	21.81	21.88	21.79	21.99	21.85
FeO	32.37	31.75	32.25	31.47	32.03	31.54	31.90	31.27	31.89	31.92
MnO	0.99	0.91	0.90	0.85	0.98	0.98	0.85	0.95	1.07	0.99
NiO	0.00	0.00	0.00	0.00	0.00	0.00	0.00	0.00	0.00	0.00
MgO	4.29	4.44	4.82	4.62	4.81	4.79	4.62	4.75	4.73	4.73
CaO	3.53	3.27	2.95	3.48	3.27	3.33	3.42	3.32	3.28	3.34
Na2O	0.00	0.00	0.00	0.00	0.00	0.00	0.00	0.00	0.00	0.00
K2O	0.00	0.00	0.00	0.00	0.00	0.00	0.00	0.00	0.00	0.00
Total	100.90	100.47	100.79	100.15	100.99	100.50	100.80	100.56	101.30	101.19
a.p.f.u. 12 oxygens										
Si	2.98	3.01	2.99	2.99	2.98	2.99	2.99	3.03	3.00	3.00
Ti	0.00	0.00	0.00	0.00	0.00	0.00	0.00	0.00	0.00	0.00
Cr	0.00	0.00	0.00	0.00	0.00	0.00	0.00	0.00	0.00	0.00
Al	2.03	2.03	2.02	2.04	2.02	2.02	2.03	2.02	2.03	2.01
Fe3+	0.02	0.00	0.00	0.00	0.02	0.00	0.00	0.00	0.00	0.00
Fe2+	2.11	2.09	2.11	2.08	2.08	2.08	2.09	2.06	2.08	2.09
Mn	0.07	0.06	0.06	0.06	0.06	0.07	0.06	0.06	0.07	0.07
Ni	0.00	0.00	0.00	0.00	0.00	0.00	0.00	0.00	0.00	0.00
Mg	0.50	0.52	0.56	0.54	0.56	0.56	0.54	0.56	0.55	0.55
Ca	0.30	0.28	0.25	0.29	0.27	0.28	0.29	0.28	0.27	0.28
Na	0.00	0.00	0.00	0.00	0.00	0.00	0.00	0.00	0.00	0.00
K	0.00	0.00	0.00	0.00	0.00	0.00	0.00	0.00	0.00	0.00
Total	8.00	8.00	8.00	8.00	8.00	8.00	8.00	8.00	8.00	8.00
xMg	0.19	0.20	0.21	0.21	0.21	0.21	0.21	0.21	0.21	0.21
Prp	0.17	0.17	0.19	0.18	0.19	0.19	0.18	0.18	0.18	0.18
Alm	0.70	0.68	0.70	0.69	0.69	0.69	0.70	0.66	0.69	0.70
Grs	0.10	0.09	0.08	0.10	0.09	0.09	0.10	0.09	0.09	0.09
Sps	0.02	0.02	0.02	0.02	0.02	0.02	0.02	0.02	0.02	0.02
Total Endmemembers	0.99	0.98	1.00	0.99	0.99	0.99	0.99	0.98	0.99	0.99

	grt 1 profile 11	grt 1 profile 12	grt 1 profile 13	grt 1 profile 14	grt 1 profile 15	grt 1 profile 16	grt 1 profile 17	grt 1 profile 18	grt 1 profile 19	grt 1 profile 20
Analysis No.	48	49	50	51	52	53	54	55	56	57
SiO2	37.92	38.32	38.38	38.31	37.97	38.23	38.27	38.41	38.25	38.18
TiO2	0.06	0.09	0.05	0.04	0.06	0.02	0.04	0.00	0.01	0.00
Cr2O3	0.00	0.00	0.00	0.00	0.00	0.00	0.00	0.00	0.00	0.00
Al2O3	21.66	21.74	21.86	21.66	21.77	21.71	21.94	21.96	21.82	21.91
FeO	31.74	31.82	31.05	32.21	31.60	31.87	31.09	31.91	31.57	31.37
MnO	1.04	0.96	1.01	0.91	1.04	1.08	1.02	0.99	1.04	0.99
NiO	0.00	0.00	0.00	0.00	0.00	0.00	0.00	0.00	0.00	0.00
MgO	4.80	4.60	4.66	4.77	4.73	4.70	4.70	4.74	4.74	4.85
CaO	3.29	3.39	3.50	3.38	3.43	3.49	3.51	3.52	3.44	3.41
Na2O	0.00	0.00	0.00	0.00	0.00	0.00	0.00	0.00	0.00	0.00
K2O	0.00	0.00	0.00	0.00	0.00	0.00	0.00	0.00	0.00	0.00
Total	100.51	100.92	100.51	101.28	100.60	101.10	100.57	101.53	100.87	100.71
a.p.f.u. 12 oxygens										
Si	2.99	3.01	3.02	3.00	2.99	2.99	3.01	2.99	3.00	3.00
Ti	0.00	0.01	0.00	0.00	0.00	0.00	0.00	0.00	0.00	0.00
Cr	0.00	0.00	0.00	0.00	0.00	0.00	0.00	0.00	0.00	0.00
Al	2.01	2.01	2.03	2.00	2.02	2.00	2.03	2.02	2.02	2.03
Fe3+	0.01	0.00	0.00	0.01	0.00	0.00	0.00	0.00	0.00	0.00
Fe2+	2.08	2.09	2.04	2.10	2.08	2.08	2.04	2.08	2.07	2.06
Mn	0.07	0.06	0.07	0.06	0.07	0.07	0.07	0.07	0.07	0.07
Ni	0.00	0.00	0.00	0.00	0.00	0.00	0.00	0.00	0.00	0.00
Mg	0.56	0.54	0.55	0.56	0.55	0.55	0.55	0.55	0.55	0.57
Ca	0.28	0.29	0.29	0.28	0.29	0.29	0.30	0.29	0.29	0.29
Na	0.00	0.00	0.00	0.00	0.00	0.00	0.00	0.00	0.00	0.00
K	0.00	0.00	0.00	0.00	0.00	0.00	0.00	0.00	0.00	0.00
Total	8.00	8.00	8.00	8.00	8.00	8.00	8.00	8.00	8.00	8.00
xMg	0.21	0.20	0.21	0.21	0.21	0.21	0.21	0.21	0.21	0.22
Prp	0.19	0.18	0.18	0.18	0.18	0.18	0.18	0.18	0.18	0.19
Alm	0.69	0.68	0.66	0.70	0.69	0.69	0.67	0.69	0.69	0.69
Grs	0.09	0.09	0.10	0.09	0.10	0.10	0.10	0.10	0.10	0.10
Sps	0.02	0.02	0.02	0.02	0.02	0.02	0.02	0.02	0.02	0.02
Total Endmemembers	1.00	0.99	0.98	1.00	1.00	1.00	0.98	1.00	0.99	0.99

	grt 1 profile 21	grt 1 profile 22	grt 1 profile 23	grt 1 profile 24	grt 1 profile 25	grt 1 profile 26	grt 1 profile 27
Analysis No.	58	59	60	61	62	63	64
SiO2	38.05	38.33	38.26	38.22	37.93	38.21	38.26
TiO2	0.00	0.01	0.00	0.08	0.05	0.02	0.09
Cr2O3	0.00	0.00	0.00	0.00	0.00	0.00	0.00
Al2O3	21.74	21.82	21.87	21.85	21.74	21.69	21.87
FeO	31.71	32.26	31.58	32.01	31.34	31.88	31.90
MnO	0.97	0.96	1.02	0.94	0.99	1.01	0.86
NiO	0.00	0.00	0.00	0.00	0.00	0.00	0.00
MgO	4.78	4.80	4.91	4.94	4.75	4.75	4.49
CaO	3.51	3.12	3.24	2.91	3.17	3.07	3.47
Na2O	0.00	0.00	0.00	0.00	0.00	0.00	0.00
K2O	0.00	0.00	0.00	0.00	0.00	0.00	0.00
Total	100.76	101.30	100.88	100.95	99.96	100.62	100.93
a.p.f.u. 12 oxygens							
Si	2.99	3.00	3.00	3.00	3.00	3.01	3.00
Ti	0.00	0.00	0.00	0.00	0.00	0.00	0.01
Cr	0.00	0.00	0.00	0.00	0.00	0.00	0.00
Al	2.01	2.01	2.02	2.02	2.03	2.01	2.02
Fe3+	0.01	0.00	0.00	0.00	0.00	0.00	0.00
Fe2+	2.07	2.11	2.07	2.10	2.07	2.10	2.09
Mn	0.06	0.06	0.07	0.06	0.07	0.07	0.06
Ni	0.00	0.00	0.00	0.00	0.00	0.00	0.00
Mg	0.56	0.56	0.57	0.58	0.56	0.56	0.53
Ca	0.30	0.26	0.27	0.24	0.27	0.26	0.29
Na	0.00	0.00	0.00	0.00	0.00	0.00	0.00
K	0.00	0.00	0.00	0.00	0.00	0.00	0.00
Total	8.00	8.00	8.00	8.00	8.00	8.00	8.00
xMg	0.21	0.21	0.22	0.22	0.21	0.21	0.20
Prp	0.19	0.19	0.19	0.19	0.19	0.18	0.17
Alm	0.68	0.70	0.69	0.70	0.69	0.69	0.69
Grs	0.10	0.09	0.09	0.08	0.09	0.09	0.10
Sps	0.02	0.02	0.02	0.02	0.02	0.02	0.02
Total Endmememembers	1.00	1.00	0.99	0.99	0.99	0.99	0.99

Analysis No.	inclusion 90	inclusion 91	inclusion 92	inclusion 93	bt 1 rim 94	bt 1 rim 95	bt 1 rim 96	bt 1 core 97	bt 1 core 98	bt 1 core 99	bt 2 rim 105	bt 2 core 106
SiO2	37.06	36.93	37.16	36.92	36.74	37.11	36.81	36.46	36.70	36.58	36.42	36.38
TiO2	3.44	3.94	3.92	3.43	2.86	2.67	2.48	2.51	2.70	2.73	3.45	3.41
Cr2O3	0.06	0.01	0.07	0.05	0.04	0.02	0.04	0.08	0.06	0.07	0.03	0.03
Al2O3	18.78	18.62	19.08	19.10	18.83	18.87	19.68	19.17	19.22	18.91	18.22	18.56
FeO	13.68	13.15	13.59	14.24	16.09	16.64	15.25	15.96	15.97	16.06	16.07	15.96
MnO	0.04	0.05	0.03	0.02	0.09	0.08	0.06	0.02	0.05	0.06	0.04	0.00
NiO	0.00	0.00	0.00	0.00	0.00	0.00	0.00	0.00	0.00	0.00	0.00	0.00
MgO	11.80	12.27	11.52	11.36	11.04	10.94	11.36	11.17	11.04	10.82	10.40	10.51
CaO	0.02	0.00	0.00	0.02	0.00	0.01	0.00	0.00	0.00	0.00	0.00	0.01
Na2O	0.12	0.14	0.18	0.13	0.14	0.13	0.19	0.13	0.11	0.14	0.09	0.11
K2O	9.99	10.02	9.99	10.05	10.14	10.04	10.23	10.02	10.11	10.01	10.23	10.02
Total	94.98	95.13	95.54	95.32	95.97	96.52	96.10	95.52	95.96	95.38	94.94	94.98
a.p.f.u. 11 oxygens												
Si	2.85	2.83	2.85	2.84	2.82	2.83	2.80	2.80	2.81	2.82	2.84	2.83
Ti	0.20	0.23	0.23	0.20	0.16	0.15	0.14	0.15	0.16	0.16	0.20	0.20
Cr	0.00	0.00	0.00	0.00	0.00	0.00	0.00	0.00	0.00	0.00	0.00	0.00
Al	1.70	1.68	1.72	1.73	1.70	1.70	1.77	1.74	1.74	1.72	1.67	1.70
Fe3+	0.00	0.00	0.00	0.00	0.00	0.00	0.00	0.00	0.00	0.00	0.00	0.00
Fe2+	0.88	0.84	0.87	0.92	1.03	1.06	0.97	1.03	1.02	1.04	1.05	1.04
Mn	0.00	0.00	0.00	0.00	0.01	0.00	0.00	0.00	0.00	0.00	0.00	0.00
Ni	0.00	0.00	0.00	0.00	0.00	0.00	0.00	0.00	0.00	0.00	0.00	0.00
Mg	1.35	1.40	1.32	1.30	1.26	1.25	1.29	1.28	1.26	1.25	1.21	1.22
Ca	0.00	0.00	0.00	0.00	0.00	0.00	0.00	0.00	0.00	0.00	0.00	0.00
Na	0.02	0.02	0.03	0.02	0.02	0.02	0.03	0.02	0.02	0.02	0.01	0.02
K	0.98	0.98	0.98	0.99	0.99	0.98	0.99	0.98	0.99	0.99	1.02	0.99
H	2.00	2.00	2.00	2.00	2.00	2.00	2.00	2.00	2.00	2.00	2.00	2.00
F	0.00	0.00	0.00	0.00	0.00	0.00	0.00	0.00	0.00	0.00	0.00	0.00
Cl	0.00	0.00	0.00	0.00	0.00	0.00	0.00	0.00	0.00	0.00	0.00	0.00
Total	8.00	8.00	8.00	8.00	8.00	8.00	8.00	8.00	8.00	8.00	8.00	8.00
xMg	0.61	0.62	0.60	0.59	0.55	0.54	0.57	0.56	0.55	0.55	0.54	0.54

	plag 1 core	plag 1 core	plag 1 rim	plag 1 rim	plag 1 rim	plag 2 core	plag 2 core	plag 2 core	plag 2 core	plag 2 rim	plag 2 rim
Analysis No.	114	115	116	117	118	209	210	211	212	213	214
SiO2	59.51	59.19	60.45	60.39	60.16	60.38	60.09	60.44	60.30	60.17	60.61
TiO2	0.00	0.00	0.00	0.00	0.00	0.00	0.00	0.00	0.00	0.00	0.00
Cr2O3	0.00	0.00	0.00	0.00	0.00	0.00	0.00	0.00	0.00	0.00	0.00
Al2O3	25.31	25.36	24.59	24.80	24.56	24.82	24.54	24.43	24.68	24.55	24.54
FeO	0.06	0.00	0.02	0.06	0.09	0.11	0.10	0.00	0.06	0.14	0.14
MnO	0.00	0.00	0.00	0.00	0.00	0.00	0.00	0.00	0.00	0.00	0.00
NiO	0.00	0.00	0.00	0.00	0.00	0.00	0.00	0.00	0.00	0.00	0.00
MgO	0.00	0.00	0.00	0.00	0.00	0.00	0.00	0.00	0.00	0.00	0.00
CaO	6.83	7.20	6.14	6.33	6.29	6.26	6.19	6.14	6.37	6.15	6.04
Na2O	8.01	7.69	8.33	8.21	8.20	8.07	8.16	8.30	8.07	8.32	8.38
K2O	0.23	0.23	0.24	0.20	0.19	0.19	0.19	0.15	0.19	0.18	0.16
Total	99.95	99.67	99.76	99.99	99.49	99.82	99.26	99.46	99.67	99.51	99.87
a.p.f.u. 8 oxygens											
Si	2.64	2.64	2.69	2.68	2.68	2.69	2.69	2.70	2.69	2.68	2.69
Ti	0.00	0.00	0.00	0.00	0.00	0.00	0.00	0.00	0.00	0.00	0.00
Cr	0.00	0.00	0.00	0.00	0.00	0.00	0.00	0.00	0.00	0.00	0.00
Al	1.33	1.33	1.29	1.30	1.29	1.30	1.29	1.28	1.30	1.29	1.28
Fe3+	0.00	0.00	0.00	0.00	0.00	0.00	0.00	0.00	0.00	0.01	0.01
Fe2+	0.00	0.00	0.00	0.00	0.00	0.00	0.00	0.00	0.00	0.00	0.00
Mn	0.00	0.00	0.00	0.00	0.00	0.00	0.00	0.00	0.00	0.00	0.00
Ni	0.00	0.00	0.00	0.00	0.00	0.00	0.00	0.00	0.00	0.00	0.00
Mg	0.00	0.00	0.00	0.00	0.00	0.00	0.00	0.00	0.00	0.00	0.00
Ca	0.33	0.34	0.29	0.30	0.30	0.30	0.30	0.29	0.30	0.29	0.29
Na	0.69	0.67	0.72	0.71	0.71	0.70	0.71	0.72	0.70	0.72	0.72
K	0.01	0.01	0.01	0.01	0.01	0.01	0.01	0.01	0.01	0.01	0.01
Total	5.00	5.00	5.00	5.00	5.00	5.00	5.00	5.00	5.00	5.00	5.00
An	0.32	0.34	0.29	0.30	0.29	0.30	0.29	0.29	0.30	0.29	0.28
Alb	0.67	0.65	0.70	0.69	0.69	0.69	0.70	0.70	0.69	0.70	0.71
Or	0.01	0.01	0.01	0.01	0.01	0.01	0.01	0.01	0.01	0.01	0.01
Total Endmemembers	1.00	1.00	1.00	1.00	1.00	1.00	1.00	1.00	1.00	1.00	1.00

	mus 1 core	mus 1 core	mus 1 core	mus 1 rim	mus 1 rim	mus 1 rim	mus 1 core	mus 1 core	mus 2 core	mus 2 core	mus 2 core	mus 2 rim
Analysis No.	181	182	183	184	185	186	187	188	189	190	191	192
SiO2	46.93	46.67	46.80	46.75	46.95	46.34	47.12	46.97	47.18	46.95	46.39	46.86
TiO2	1.69	1.59	1.53	1.67	1.84	1.54	1.64	1.51	1.56	1.55	1.66	1.52
Cr2O3	0.03	0.04	0.00	0.05	0.05	0.04	0.00	0.00	0.00	0.06	0.05	0.01
Al2O3	33.35	33.60	33.52	32.98	32.85	33.38	33.21	33.18	32.10	32.75	32.97	33.15
FeO	1.15	1.16	1.05	1.49	1.19	1.07	1.22	1.23	1.45	1.40	1.17	1.19
MnO	0.02	0.06	0.02	0.03	0.00	0.02	0.02	0.02	0.02	0.02	0.04	0.00
NiO	0.00	0.00	0.00	0.00	0.00	0.00	0.00	0.00	0.00	0.00	0.00	0.00
MgO	1.17	1.08	1.18	1.34	1.27	1.13	1.24	1.25	1.50	1.39	1.18	1.23
CaO	0.00	0.00	0.01	0.00	0.00	0.00	0.00	0.00	0.00	0.00	0.02	0.00
Na2O	0.35	0.34	0.42	0.28	0.35	0.35	0.35	0.38	0.34	0.38	0.34	0.33
K2O	11.09	10.91	11.03	11.15	11.22	11.01	11.35	11.16	11.31	11.15	10.99	11.34
Total	95.78	95.45	95.55	95.72	95.73	94.88	96.15	95.69	95.45	95.65	94.80	95.63
a.p.f.u. 11 oxygens												
Si	3.13	3.12	3.12	3.12	3.13	3.11	3.13	3.13	3.15	3.13	3.12	3.12
Ti	0.08	0.08	0.08	0.08	0.09	0.08	0.08	0.08	0.08	0.08	0.08	0.08
Cr	0.00	0.00	0.00	0.00	0.00	0.00	0.00	0.00	0.00	0.00	0.00	0.00
Al	2.62	2.65	2.63	2.59	2.58	2.64	2.60	2.61	2.53	2.57	2.62	2.60
Fe3+	0.00	0.00	0.00	0.00	0.00	0.00	0.00	0.00	0.02	0.00	0.00	0.00
Fe2+	0.06	0.07	0.06	0.08	0.07	0.06	0.07	0.07	0.06	0.08	0.07	0.06
Mn	0.00	0.00	0.00	0.00	0.00	0.00	0.00	0.00	0.00	0.00	0.00	0.00
Ni	0.00	0.00	0.00	0.00	0.00	0.00	0.00	0.00	0.00	0.00	0.00	0.00
Mg	0.12	0.11	0.12	0.13	0.13	0.11	0.12	0.12	0.15	0.14	0.12	0.12
Ca	0.00	0.00	0.00	0.00	0.00	0.00	0.00	0.00	0.00	0.00	0.00	0.00
Na	0.04	0.04	0.05	0.04	0.05	0.05	0.05	0.05	0.04	0.05	0.04	0.04
K	0.94	0.93	0.94	0.95	0.95	0.94	0.96	0.95	0.96	0.95	0.94	0.96
H	2.00	2.00	2.00	2.00	2.00	2.00	2.00	2.00	2.00	2.00	2.00	2.00
F	0.00	0.00	0.00	0.00	0.00	0.00	0.00	0.00	0.00	0.00	0.00	0.00
Cl	0.00	0.00	0.00	0.00	0.00	0.00	0.00	0.00	0.00	0.00	0.00	0.00
Total	7.00	7.00	7.00	7.00	7.00	7.00	7.00	7.00	7.00	7.00	7.00	7.00
xMg	0.65	0.62	0.67	0.62	0.66	0.65	0.65	0.64	0.65	0.64	0.64	0.65

A.4.5. Nordmannvik Nappe - UL237

	grt 2 profile 1	grt 2 profile 2	grt 2 profile 3	grt 2 profile 4	grt 2 profile 5	grt 2 profile 6	grt 2 profile 7	grt 2 profile 8	grt 2 profile 9	grt 2 profile 10
Analysis No.	319	320	321	322	323	324	325	326	327	328
SiO2	37.82	37.72	37.99	37.88	37.46	37.92	37.68	37.88	37.87	38.02
TiO2	0.04	0.03	0.00	0.00	0.01	0.00	0.03	0.00	0.00	0.00
Cr2O3	0.00	0.00	0.00	0.00	0.00	0.00	0.00	0.00	0.00	0.00
Al2O3	21.72	21.64	21.73	21.78	21.68	21.68	21.57	21.67	21.83	21.68
FeO	35.99	35.27	35.49	36.26	35.14	35.36	34.86	35.70	35.46	35.39
MnO	0.67	0.62	0.65	0.61	0.62	0.63	0.70	0.59	0.56	0.63
NiO	0.00	0.00	0.00	0.00	0.00	0.00	0.00	0.00	0.00	0.00
MgO	3.94	4.18	4.35	4.41	4.45	4.51	4.40	4.45	4.46	4.60
CaO	0.79	0.77	0.67	0.67	0.77	0.71	0.67	0.63	0.66	0.68
Na2O	0.00	0.00	0.00	0.00	0.00	0.00	0.00	0.00	0.00	0.00
K2O	0.00	0.00	0.00	0.00	0.00	0.00	0.00	0.00	0.00	0.00
Total	100.97	100.23	100.88	101.61	100.13	100.81	99.91	100.93	100.84	101.00
a.p.f.u. 12 oxygens										
Si	3.00	3.01	3.01	2.98	2.99	3.00	3.01	3.00	3.00	3.00
Ti	0.00	0.00	0.00	0.00	0.00	0.00	0.00	0.00	0.00	0.00
Cr	0.00	0.00	0.00	0.00	0.00	0.00	0.00	0.00	0.00	0.00
Al	2.03	2.03	2.03	2.02	2.04	2.02	2.03	2.02	2.04	2.02
Fe3+	0.00	0.00	0.00	0.02	0.00	0.00	0.00	0.00	0.00	0.00
Fe2+	2.39	2.35	2.35	2.37	2.34	2.34	2.33	2.36	2.35	2.34
Mn	0.05	0.04	0.04	0.04	0.04	0.04	0.05	0.04	0.04	0.04
Ni	0.00	0.00	0.00	0.00	0.00	0.00	0.00	0.00	0.00	0.00
Mg	0.47	0.50	0.51	0.52	0.53	0.53	0.52	0.52	0.53	0.54
Ca	0.07	0.07	0.06	0.06	0.07	0.06	0.06	0.05	0.06	0.06
Na	0.00	0.00	0.00	0.00	0.00	0.00	0.00	0.00	0.00	0.00
K	0.00	0.00	0.00	0.00	0.00	0.00	0.00	0.00	0.00	0.00
Total	8.00	8.00	8.00	8.00	8.00	8.00	8.00	8.00	8.00	8.00
xMg	0.16	0.17	0.18	0.18	0.18	0.19	0.18	0.18	0.18	0.19
Prp	0.15	0.16	0.17	0.17	0.18	0.18	0.17	0.17	0.18	0.18
Alm	0.79	0.77	0.77	0.78	0.78	0.78	0.76	0.79	0.78	0.78
Grs	0.02	0.02	0.02	0.02	0.02	0.02	0.02	0.02	0.02	0.02
Sps	0.01	0.01	0.01	0.01	0.01	0.01	0.02	0.01	0.01	0.01
Total Endmemembers	0.99	0.98	0.99	0.99	0.99	0.99	0.98	0.99	0.99	0.99

	grt 2 profile 11	grt 2 profile 12	grt 2 profile 13	grt 2 profile 14	grt 2 profile 15	grt 2 profile 16	grt 2 profile 17	grt 2 profile 18	grt 2 profile 19	grt 2 profile 20
Analysis No.	329	330	331	332	333	334	335	336	337	338
SiO2	37.60	37.73	37.81	37.71	37.66	37.45	37.83	37.73	37.62	37.64
TiO2	0.05	0.02	0.02	0.06	0.07	0.00	0.07	0.00	0.07	0.03
Cr2O3	0.00	0.00	0.00	0.00	0.00	0.00	0.00	0.00	0.00	0.00
Al2O3	21.83	21.57	21.66	21.45	21.70	21.52	21.68	21.72	21.80	21.81
FeO	35.26	35.63	35.75	35.28	35.35	35.67	35.37	35.46	36.03	35.85
MnO	0.68	0.63	0.60	0.59	0.61	0.55	0.62	0.64	0.60	0.58
NiO	0.00	0.00	0.00	0.00	0.00	0.00	0.00	0.00	0.00	0.00
MgO	4.43	4.35	4.43	4.36	4.41	4.38	4.37	4.54	4.48	4.33
CaO	0.73	0.68	0.75	0.65	0.69	0.70	0.76	0.69	0.77	0.75
Na2O	0.00	0.00	0.00	0.00	0.00	0.00	0.00	0.00	0.00	0.00
K2O	0.00	0.00	0.00	0.00	0.00	0.00	0.00	0.00	0.00	0.00
Total	100.58	100.61	101.02	100.10	100.49	100.27	100.70	100.78	101.37	100.99
a.p.f.u. 12 oxygens										
Si	2.98	3.00	2.99	3.01	2.99	2.98	3.00	2.99	2.97	2.98
Ti	0.00	0.00	0.00	0.00	0.00	0.00	0.00	0.00	0.00	0.00
Cr	0.00	0.00	0.00	0.00	0.00	0.00	0.00	0.00	0.00	0.00
Al	2.04	2.02	2.02	2.02	2.03	2.02	2.03	2.03	2.03	2.03
Fe3+	0.00	0.00	0.00	0.00	0.00	0.01	0.00	0.00	0.04	0.01
Fe2+	2.34	2.37	2.36	2.35	2.35	2.37	2.35	2.35	2.34	2.37
Mn	0.05	0.04	0.04	0.04	0.04	0.04	0.04	0.04	0.04	0.04
Ni	0.00	0.00	0.00	0.00	0.00	0.00	0.00	0.00	0.00	0.00
Mg	0.52	0.52	0.52	0.52	0.52	0.52	0.52	0.54	0.53	0.51
Ca	0.06	0.06	0.06	0.06	0.06	0.06	0.06	0.06	0.06	0.06
Na	0.00	0.00	0.00	0.00	0.00	0.00	0.00	0.00	0.00	0.00
K	0.00	0.00	0.00	0.00	0.00	0.00	0.00	0.00	0.00	0.00
Total	8.00	8.00	8.00	8.00	8.00	8.00	8.00	8.00	8.00	8.00
xMg	0.18	0.18	0.18	0.18	0.18	0.18	0.18	0.19	0.18	0.18
Prp	0.17	0.17	0.17	0.17	0.17	0.17	0.17	0.18	0.17	0.17
Alm	0.78	0.79	0.79	0.77	0.78	0.79	0.78	0.78	0.76	0.79
Grs	0.02	0.02	0.02	0.02	0.02	0.02	0.02	0.02	0.02	0.02
Sps	0.02	0.01	0.01	0.01	0.01	0.01	0.01	0.01	0.01	0.01
Total Endmemembers	0.99	0.99	1.00	0.99	0.99	0.99	0.99	1.00	0.99	0.99

	grt 2 profile 21	grt 2 profile 22	grt 2 profile 23	grt 2 profile 24
Analysis No.	339	340	341	342
SiO2	37.55	37.76	37.38	37.38
TiO2	0.00	0.00	0.01	0.00
Cr2O3	0.00	0.00	0.00	0.00
Al2O3	21.61	21.68	21.61	21.45
FeO	35.68	35.60	35.13	36.57
MnO	0.68	0.62	0.70	0.71
NiO	0.00	0.00	0.00	0.00
MgO	4.39	4.43	3.96	3.60
CaO	0.71	0.76	0.82	0.74
Na2O	0.00	0.00	0.00	0.00
K2O	0.00	0.00	0.00	0.00
Total	100.62	100.85	99.61	100.44
a.p.f.u. 12 oxygens				
Si	2.98	2.99	3.00	2.99
Ti	0.00	0.00	0.00	0.00
Cr	0.00	0.00	0.00	0.00
Al	2.02	2.02	2.05	2.02
Fe3+	0.01	0.00	0.00	0.00
Fe2+	2.36	2.36	2.36	2.45
Mn	0.05	0.04	0.05	0.05
Ni	0.00	0.00	0.00	0.00
Mg	0.52	0.52	0.47	0.43
Ca	0.06	0.06	0.07	0.06
Na	0.00	0.00	0.00	0.00
K	0.00	0.00	0.00	0.00
Total	8.00	8.00	8.00	8.00
xMg	0.18	0.18	0.17	0.15
Prp	0.17	0.17	0.16	0.14
Alm	0.78	0.79	0.78	0.82
Grs	0.02	0.02	0.02	0.02
Sps	0.02	0.01	0.02	0.02
Total Endmemembers	0.99	1.00	0.98	1.00

	bt 6 core	bt 7 core	bt 7 core	bt 7 core	bt 7 rim	bt 7 rim	bt 7 rim	inclusion	inclusion	inclusion
Analysis No.	354	359	360	361	362	363	364	410	411	412
SiO2	35.91	36.00	36.07	36.01	37.10	35.87	36.08	36.69	36.29	36.64
TiO2	3.23	3.24	3.05	3.58	2.51	2.38	3.58	3.29	3.58	3.46
Cr2O3	0.05	0.03	0.02	0.04	0.02	0.01	0.00	0.04	0.03	0.04
Al2O3	17.96	18.23	18.46	17.96	18.90	18.32	17.86	19.80	19.78	19.64
FeO	19.11	18.64	17.81	18.75	17.01	18.43	18.98	15.44	15.35	14.93
MnO	0.03	0.05	0.06	0.07	0.01	0.02	0.03	0.05	0.04	0.06
NiO	0.00	0.00	0.00	0.00	0.00	0.00	0.00	0.00	0.00	0.00
MgO	9.80	9.43	9.38	9.35	9.61	10.24	9.18	10.24	10.14	11.15
CaO	0.00	0.00	0.00	0.00	0.01	0.00	0.00	0.05	0.02	0.00
Na2O	0.14	0.08	0.13	0.10	0.11	0.10	0.12	0.23	0.18	0.24
K2O	10.04	10.10	10.08	10.10	10.11	10.21	10.16	10.20	10.30	10.26
Total	96.26	95.80	95.07	95.96	95.39	95.58	95.99	96.03	95.71	96.42
a.p.f.u. 11 oxygens										
Si	2.78	2.81	2.82	2.81	2.88	2.78	2.81	2.82	2.80	2.79
Ti	0.19	0.19	0.18	0.21	0.15	0.14	0.21	0.19	0.21	0.20
Cr	0.00	0.00	0.00	0.00	0.00	0.00	0.00	0.00	0.00	0.00
Al	1.64	1.67	1.70	1.65	1.73	1.67	1.64	1.79	1.80	1.76
Fe3+	0.00	0.00	0.00	0.00	0.00	0.00	0.00	0.00	0.00	0.00
Fe2+	1.24	1.21	1.17	1.22	1.11	1.19	1.24	0.99	0.99	0.95
Mn	0.00	0.00	0.00	0.00	0.00	0.00	0.00	0.00	0.00	0.00
Ni	0.00	0.00	0.00	0.00	0.00	0.00	0.00	0.00	0.00	0.00
Mg	1.13	1.10	1.09	1.09	1.11	1.18	1.07	1.17	1.16	1.26
Ca	0.00	0.00	0.00	0.00	0.00	0.00	0.00	0.00	0.00	0.00
Na	0.02	0.01	0.02	0.01	0.02	0.02	0.02	0.03	0.03	0.04
K	0.99	1.00	1.01	1.00	1.00	1.01	1.01	1.00	1.01	1.00
H	2.00	2.00	2.00	2.00	2.00	2.00	2.00	2.00	2.00	2.00
F	0.00	0.00	0.00	0.00	0.00	0.00	0.00	0.00	0.00	0.00
Cl	0.00	0.00	0.00	0.00	0.00	0.00	0.00	0.00	0.00	0.00
Total	8.00	8.00	8.00	8.00	8.00	8.00	8.00	8.00	8.00	8.00
xMg	0.48	0.47	0.48	0.47	0.50	0.50	0.46	0.54	0.54	0.57

	kfs 1 core	kfs 1 core	kfs 1 core	kfs 1 rim	kfs 1 rim	kfs 1 rim	kfs 1 rim	kfs 1 rim
Analysis No.	468	469	470	471	472	473	474	475
SiO2	64.47	64.06	64.53	64.40	64.32	64.46	64.12	64.31
TiO2	0.00	0.00	0.00	0.00	0.00	0.00	0.00	0.00
Cr2O3	0.00	0.00	0.00	0.00	0.00	0.00	0.00	0.00
Al2O3	18.81	18.71	18.84	19.06	18.83	18.82	18.54	18.71
FeO	0.05	0.00	0.03	0.00	0.04	0.03	0.00	0.00
MnO	0.00	0.00	0.00	0.00	0.00	0.00	0.00	0.00
NiO	0.00	0.00	0.00	0.00	0.00	0.00	0.00	0.00
MgO	0.00	0.00	0.00	0.00	0.00	0.00	0.00	0.00
CaO	0.00	0.01	0.02	0.00	0.00	0.00	0.01	0.00
Na2O	1.29	1.45	1.81	1.36	1.29	1.74	1.22	1.56
K2O	15.76	15.50	15.06	15.67	15.72	14.92	15.73	15.61
Total	100.39	99.73	100.28	100.49	100.20	99.97	99.62	100.19
a.p.f.u. 8 oxygens								
Si	2.95	2.95	2.95	2.94	2.95	2.95	2.96	2.94
Ti	0.00	0.00	0.00	0.00	0.00	0.00	0.00	0.00
Cr	0.00	0.00	0.00	0.00	0.00	0.00	0.00	0.00
Al	1.01	1.01	1.01	1.03	1.02	1.02	1.01	1.01
Fe3+	0.00	0.00	0.00	0.00	0.00	0.00	0.00	0.00
Fe2+	0.00	0.00	0.00	0.00	0.00	0.00	0.00	0.00
Mn	0.00	0.00	0.00	0.00	0.00	0.00	0.00	0.00
Ni	0.00	0.00	0.00	0.00	0.00	0.00	0.00	0.00
Mg	0.00	0.00	0.00	0.00	0.00	0.00	0.00	0.00
Ca	0.00	0.00	0.00	0.00	0.00	0.00	0.00	0.00
Na	0.11	0.13	0.16	0.12	0.11	0.15	0.11	0.14
K	0.92	0.91	0.88	0.91	0.92	0.87	0.93	0.91
Total	5.00	5.00	5.00	5.00	5.00	5.00	5.00	5.00
An	0.00	0.00	0.00	0.00	0.00	0.00	0.00	0.00
Alb	0.11	0.12	0.15	0.12	0.11	0.15	0.11	0.13
Or	0.89	0.88	0.84	0.88	0.89	0.85	0.89	0.87
Total Endmemembers	1.00	1.00	1.00	1.00	1.00	1.00	1.00	1.00

	mus 2 core	mus 2 core	mus 2 rim	mus 2 rim	mus 2 rim	mus 2 rim	mus 2 rim	mus 3 core	mus 3 core	mus 3 rim	mus 3 rim
Analysis No.	299	300	301	302	303	304	305	355	356	357	358
SiO2	46.25	46.52	46.47	47.26	46.48	46.76	46.56	46.59	46.33	45.75	46.71
TiO2	1.03	0.98	1.16	1.16	1.03	1.03	1.13	1.06	0.97	1.08	1.01
Cr2O3	0.06	0.05	0.04	0.03	0.03	0.01	0.03	0.02	0.00	0.00	0.05
Al2O3	33.65	33.63	33.49	33.76	33.32	34.04	33.75	33.49	33.22	33.50	34.10
FeO	1.41	1.43	1.52	1.46	1.43	1.35	1.34	1.37	1.31	1.06	1.15
MnO	0.00	0.01	0.02	0.06	0.05	0.03	0.00	0.00	0.03	0.03	0.00
NiO	0.00	0.00	0.00	0.00	0.00	0.00	0.00	0.00	0.00	0.00	0.00
MgO	1.18	1.10	1.15	1.14	1.10	1.11	1.14	1.12	1.07	0.93	1.00
CaO	0.00	0.00	0.00	0.00	0.00	0.00	0.00	0.00	0.01	0.00	0.00
Na2O	0.64	0.58	0.46	0.46	0.62	0.62	0.54	0.38	0.41	0.49	0.47
K2O	10.83	11.02	10.93	10.88	10.78	10.79	11.05	11.38	10.87	10.92	10.98
Total	95.06	95.32	95.24	96.21	94.84	95.74	95.53	95.41	94.22	93.75	95.46
a.p.f.u. 12 oxygens											
Si	3.09	3.10	3.11	3.13	3.12	3.10	3.10	3.11	3.13	3.10	3.11
Ti	0.05	0.05	0.06	0.06	0.05	0.05	0.06	0.05	0.05	0.06	0.05
Cr	0.00	0.00	0.00	0.00	0.00	0.00	0.00	0.00	0.00	0.00	0.00
Al	2.65	2.64	2.64	2.64	2.63	2.66	2.65	2.63	2.65	2.68	2.68
Fe3+	0.07	0.06	0.02	0.00	0.03	0.02	0.05	0.06	0.00	0.02	0.00
Fe2+	0.01	0.02	0.07	0.08	0.05	0.06	0.03	0.02	0.07	0.04	0.06
Mn	0.00	0.00	0.00	0.00	0.00	0.00	0.00	0.00	0.00	0.00	0.00
Ni	0.00	0.00	0.00	0.00	0.00	0.00	0.00	0.00	0.00	0.00	0.00
Mg	0.12	0.11	0.11	0.11	0.11	0.11	0.11	0.11	0.11	0.09	0.10
Ca	0.00	0.00	0.00	0.00	0.00	0.00	0.00	0.00	0.00	0.00	0.00
Na	0.08	0.07	0.06	0.06	0.08	0.08	0.07	0.05	0.05	0.06	0.06
K	0.92	0.94	0.93	0.92	0.92	0.91	0.94	0.97	0.94	0.94	0.93
H	2.00	2.00	2.00	2.00	2.00	2.00	2.00	2.00	2.00	2.00	2.00
F	0.00	0.00	0.00	0.00	0.00	0.00	0.00	0.00	0.00	0.00	0.00
Cl	0.00	0.00	0.00	0.00	0.00	0.00	0.00	0.00	0.00	0.00	0.00
Total	7.00	7.00	7.00	7.00	7.00	7.00	7.00	7.00	7.00	7.00	7.00
xMg	0.60	0.58	0.57	0.58	0.58	0.59	0.60	0.59	0.59	0.61	0.61